AUTOMATIC DETECTION OF EXUDATE BASED ON DIABETIC RETINOPATHY FUNDUS IMAGE

SYNA SRENG

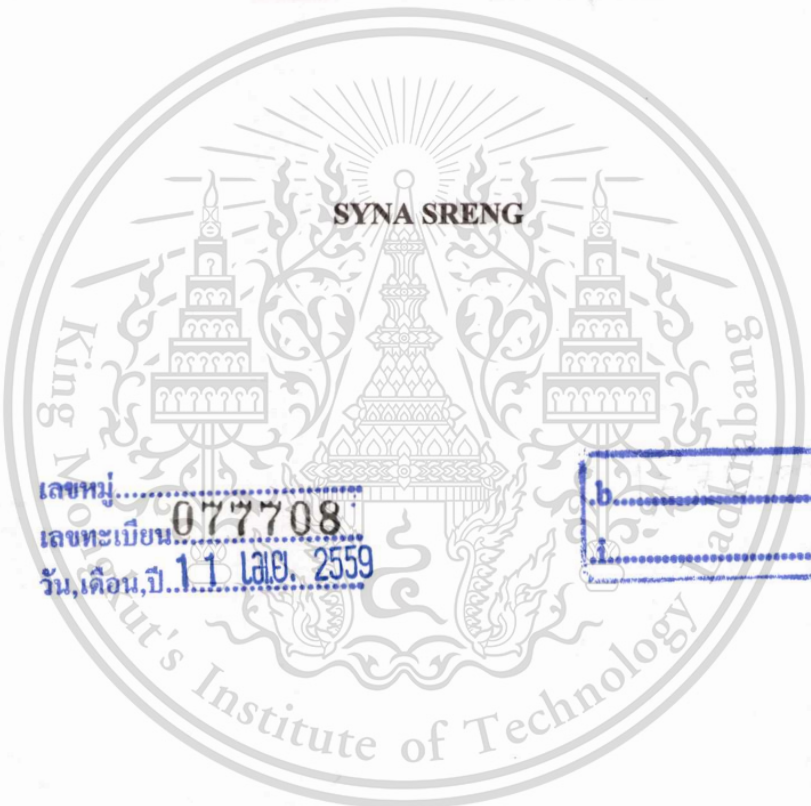

A THESIS SUBMITTED IN PARTIAL FULFILLMENT

OF THE REQUIREMENT FOR THE DEGREE OF

MASTER OF ENGINEERING IN COMPUTER ENGINEERING

INTERNATIONAL COLLEGE

KING MONGKUT'S INSTITUTE OF TECHNOLOGY LADKRABANG

2013

KMITL - 2013 - IC - M - 006 – 004

Thesis Title	Automatic Detection of Exudate based on Diabetic Retinopathy Fundus Image
Student	Mr. Syna Sreng
Student I.D	54601152
Degree	Master of Engineering
Program	Computer Engineering
Year	2013
Thesis Advisor	Asst. Prof. Dr. Noppadol Maneerat
Co-advisor	Prof. Dr. Jun-ichi Takada

ABSTRACT

Currently, the research in automatic fundus image analysis has become increasingly important in ophthalmology due to the offered value such as low-cost and wider reach. Image processing, analysis and computer vision techniques using medical images are vitals outcome of application for the analysis of the fundus images. Diabetic Retinopathy (DR) is a visual complication of diabetes which has become the most common cause of visual loss and blindness in diabetic patients, but early detection and timely treatment can prevent this problem. Exudates have been found to be one of the sign and serious DR anomalies so the proper detection of these lesions and treatment should be done immediately to prevent loss of vision. On the research work leading to automatic analysis of exudate detection, the knowledge of Optic Disk (OD) location is very useful. Therefore, an efficient algorithm is presented to detect the OD and exudate for early detection of diabetic retinopathy.

The aim of this thesis is to automatically detect exudates in fundus images. To achieve the goal, the proposed method first preprocesses to improve the quality of fundus image, and then OD is detected and eliminated to prevent the interference to the result of exudate detection. Next, exudates are detected by filtering out the bright pixels from the result of OD region eliminated. Since the result contains some noises which appear randomly so the post processing is applied to improve the result of false positive. Finally, exudates are extracted by using Morphological Reconstruction (MR).

The proposed technique has been tested on 1579 images from a hospital. Experimental results show that the best performance is 85 % of exudate detection correctly.

ACKNOWLEDGEMENTS

First of all, I am really grateful to my family for their unconditional supports especially my mother, who is always so supportive in every step in my life.

I would like to express my sincere gratitude to my advisor, Asst. Prof. Dr. Noppadol Maneerat for his continuous supervision and guidance as well as advice during my Master's study. He brought me to the ophthalmology imaging field that I found to have great interest. I would not be able to work in this challenging and interesting topic without his suggestion and I could also not have come this far without his support.

I would also like to express my thoughtful gratitude to Prof. Dr. Jun-ichi Takada (Tokyo Institute of Technology, Japan) who is my co-advisor for his guidance, advice, and comments on my papers and my thesis.

I would also like to express my sincere thanks to Dr. Don Isarakorn for giving me this project for doing research, and helping me to collect the database from Bhumibol Adulyadej Hospital.

I would also like to express my sincere thanks to Dr. Ronakorn Panjaphongse (M.D) for helping to verify the final result of Exudate detection.

My gratefully acknowledge goes also to all professors, lecturers and supporting staffs in both International College and Department of Instrumentation and Control Engineering, who always help and give me a guideline during the whole period of my master's study here.

I wish to express my thoughtful gratitude to Bhumibol Adulyadej Hospital for providing me the fundus images for doing research and I also wish to express my sincere thanks to Coordinating Center for Thai Government Science and Technology Scholarship students (CSTS), and National Science and Technology Development Agency (NSTDA) for granting me for this research.

I wish to express my acknowledgement to ASEAN University Network/Southeast Asia Engineering Education Development Network (AUN/SEED-Net) for awarding me the scholarship with the financial support for master degree within 2 years. Furthermore, I also extend my sincere appreciation to KMITL for giving me the great opportunity to do research in a warmly and friendly environment.

Finally, I would like to recognize all friends, international students and Thai students for the enjoyable and stimulating atmosphere that they provide with their companion and friendship.

Bangkok, Thailand
October 14 2013

Syna Sreng

TABLE OF CONTENTS

LIST OF TABLES

Table **Page**

LIST OF FIGURES

Figure **Page**

CHAPTER 1

INTRODUCTION

This chapter presents an overview of the research in this thesis, mainly, its introduction, motivation, objectives, data set and finally, the structure of this thesis. All experiments in this thesis are done in MATLAB.

1.1 Introduction

This research is a part of a larger project investigating on diabetic retinopathy caused by two groups of objects to be diagnosis: main regions of the retina (optic disc, fovea, and blood vessels) and the lesions caused by certain diseases which can be automatically detected from color fundus images. These lesions include red lesions (hemorrhages and microaneurysms) and bright lesions (exudates and cotton-wool spots).

The project is divided into two research topics, and the research presented in this master thesis concerns the detection of exudate. The other research develops methods for detecting red lesions (hemorrhages and microaneurysms). The department of ophthalmology at the Bhumibol Adulyadej Hospital provides fundus images for this research study. When the methods are fully developed, they will be combined together into an automatic fundus image analysis system. The automatic system is meant to be used in hospital level screening and monitoring to provide alerts of possible findings for further medical treatment.

Diabetes is a group of diseases characterized as the chronic condition in which there is an excess of glucose circulating in the bloodstream [1]. Basically there are three types of diabetes, Type 1 Diabetes, is caused as a result of auto immune problem. The immune system of the body destroys the insulin producing beta cells in the pancreas leading to no or less production of the required insulin by the pancreas. Type 2 Diabetes is a result of malfunctioning of the beta cell itself. This malfunction includes non-production of insulin or a situation known as insulin resistance. In insulin resistance, the muscles, fat and other cells do not respond to the insulin produced. Type 3 Diabetes is known as the gestational diabetes and only occurs during pregnancy. During this stage, the body resists the effect of insulin produced.

The effect of diabetes on the eye is called Diabetic Retinopathy (DR). DR clinical signs include microaneurysms, hemorrhages, cotton-wool spots and exudates. Exudates have been found to be one of the sign and serious DR anomalies so the proper detection of these lesions and treatment should be done immediately to prevent loss of vision. It appears as bright lesions with the random yellowish deposits of varying size, shapes and location in retinal images. On the research work leading to automatic analysis of exudate detection, the knowledge of Optic Disc (OD) location is very useful. OD is known as the bright circular region which appears with similar features as exudates. So, in order to prevent the result of exudate detection from the interference of OD, it should be removed out first. Therefore, an efficient algorithm is presented to detect the OD and exudate for early detection of diabetic retinopathy.

Digital image processing is the technology of applying a number of computer algorithms to process digital images. The outcomes of this process can be either images or a set of representative characteristics or properties of the original images. The application of digital image processing have been commonly found in robotics, intelligent system, medical imaging, biometric system, image analysis, satellite imaging, remote sensing, industry and so on.

Medical imaging was primarily seen as the use of non-invasive techniques to create internal images of the human body for clinical or medical purposes. The medical imaging rapidly evolves the field of medicine originated in the first decade of the 19th century, when Wilhelm Röntgen, a professor of physics at Würzburg University in Germany, discovered electromagnetic radiation. After that the development of computer technology has triggered an amazing revolution in medical imaging techniques [2]. The benefit of an automation analysis tasks can produce very interesting results such as less time spent by specialists, decrease of intra-and inter-observer differences, as well as in educational systems.

Medical imaging techniques approaches in literature were categories into three generations [3].

The first generation techniques are those techniques which are based on intrinsic image information, without any a priori information. They include:

- Threshold: Algorithms belonging to this type are assumed that the searched structures are related to clearly quantifiable features as image intensity and gradient.
- Region growing: From an initial seed located in the image, adjacent pixels are checked against a set of predefined homogeneity criteria. Pixels that meet the criteria are included in the region.

- Edge tracing: After the application of an edge detection algorithm, the edge pixels with adjacent neighbor connectivity are followed sequentially and collected into a list to represent an object boundary.

The second generation is composed of algorithms using image models, optimization methods, and uncertainty models, and includes:

- Pattern recognition and clustering: Certain structures in medical images can be treated as patterns, segmentation algorithms that combine pattern recognition techniques have been proposed to extract the searched structures.
- Deformable models: The curve evolution is used to perform segmentation. A moving equation should be defined to drive the initial curves to the right structure boundaries.
- Graph search: Image pixels are used to form nodes in a graph and the nodes are interconnected to neighbors, mapping the corresponding pixel associations in the image. Costs are assigned for each interconnection. Algorithms from combinatorial optimization are used to obtain minimum-cost solutions.
- Multiresolution methods: Multiresolution or multiscale analysis refers to the use of scale reduction to group pixels into image objects. A stack of images is formed by recursively reducing the scale of the original image by blurring followed by down sampling. The main idea for this category is that there may be scales that are more suited for processing some image features.

The third generation is characterized by algorithms that are capable of incorporating knowledge, such as:

- Shape and appearance models: Active Shape Model (ASM) was inspired by deformable models with the added intention of limiting the extent of model deformation. A statistical representation of an object is formed by identifying a set of landmark points on an object boundary and analyzing the variation of each across a set of training images.
- Atlas-based: It is a generic technique for automatic delineation of structures in volumetric images, which starts by registering an anatomical image from an atlas with a target image to be segmented. A critical underlying assumption is that it is possible to find a deformation that aligns the atlas with the target image in such a way that label propagation lines up the objects of interest.

- Rule-based: Image primitives are usually derived from first-generation and second generation algorithms and then interpreted using anatomical and image knowledge applied as a set of rules.

1.2 Motivations

Recently, medical images have become an important field of research due to the advances in their acquisition, storage and management in a wide range of applications. Regarding the medical domain, a great effort has been devoted to develop tools and applications related with disease diagnosis, bone reconstruction, identification of anatomical structures, etc. Particularly, automatic retinal image analysis plays an important role as the medical tools for automatically detection of DR. DR is a visual complication of diabetes, which becomes the most common cause of blindness but early detection and timely treatment can prevent the problem. For this reason, all diabetic patients should get their both eyes examined often at least once every year. Ophthalmologists play a most important role to help diabetic patients for an eye examination. However, the number of ophthalmologists is limited in many countries including Thailand. The study of Thailand diabetic project shows that about one thousand ophthalmologists have to work with six million diabetic patients. Among all of them about 30 percent of patients are effected by DR [4]. Therefore, automatic fundus image analysis is very useful to help ophthalmologists in detection and diagnoses of DR.

1.3 Objectives

The main objective of this research is to develop reliable and accurate image processing methods for automatic fundus image analysis. The main focus is on accurate and reliable detection of OD and exudate which can be analysis from color fundus images. To achieve the goal, this thesis proposes new algorithms to detect based on category of thresholding methods. The proposed method does not require any training sets which can make common issues with human segmentation inconsistencies. In addition, training sets method requires large amounts of data and training process. Therefore it takes long time for processing and can be difficult to obtain in the practical use. We based our work on thresholding methods because it does not require high computing power and take short time to be processed. Computing power and processing time are

very important for application in rural area in developing country where both expert ophthalmologists and high performance computers are rarely available.

1.4 Data Set

In this thesis, all algorithms were run on 100 fundus images with variable color, brightness and quality. The images were obtained from Bhumibol Adulyadej Hospital with the resolution of 3872 x 2592 pixels in 24 bit JPEG format. These images contain all lesions related to DR (microaneurysms, hemorrhages, cotton-wool spots, exudate, and so on) and healthy images.

1.5 Thesis Structure

The thesis is organized in seven chapters and is briefly summarized as follows.

Chapter 1 presents an overview of the research in this thesis, mainly, its introduction, motivation, objectives, data set and finally, the thesis structure.

Chapter 2 gives a brief introduction on the eye structure in Section 2.1 and shows some background information of DR in Section 2.2. In Section 2.3, we discuss the different types of fundus image screening as well as the automatic fundus image analysis. Finally some literatures reviews are introduced in Section 2.4.

Chapter 3 presents concepts and digital techniques for processing and analyzing images after they have been generated or digitized. It corresponds to basic knowledge of digital image processing, and the process of its applications.

In chapter 4, a simple, fast and robust optic disc detection method is presented. We propose methods that can detect the optic disc based on category of thresholding methods. The proposed method is composed of 5 steps. Preprocessing step is used to discuss on the problem of variable intensity in fundus image. It is discussed on section 4.1. Two differences methods are applied in section 4.2 to convert the image to binary image. After binarization the obtained object are all bright pixels which include all noises, OD and Exudates. Therefore in section 4.3 Region Of Interest (ROI) based segmentation is used to select only the interesting object which is known as OD. The result from ROI based segmentation cannot detect all ODs correctly when the level of thresholding is too big or too small so the area of OD is estimated in section 4.4. Finally the area of OD detection is extracted in section 4.5.

In chapter 5, the proposed method is composed of four main steps. Preprocessing step is discussed in section 5.1. Section 5.2, exudate segmentation is analyzed on two suitable methods based on category of thresholding. After exudate segmentation, the results still contain some noises in some fundus images which we can consider as poor quality images. There are two kinds of quality problems in the fundus images used in this research: The first is noise pixels whose colors are distorted. The second is noise from cotton wool spots, and artifacts in the papillary region that are characterized by the high gray-level intensity. To solve the problems, two methods are proposed in section 5.3. Finally exudates are extracted in section 5.4.

In chapter 6, the performance of proposed algorithms result is demonstrated.

Chapter 7 offers the conclusion of the thesis by reviewing and highlighting its contributions which have been presented in this thesis. The recommendations for future works related to this research are given as well.

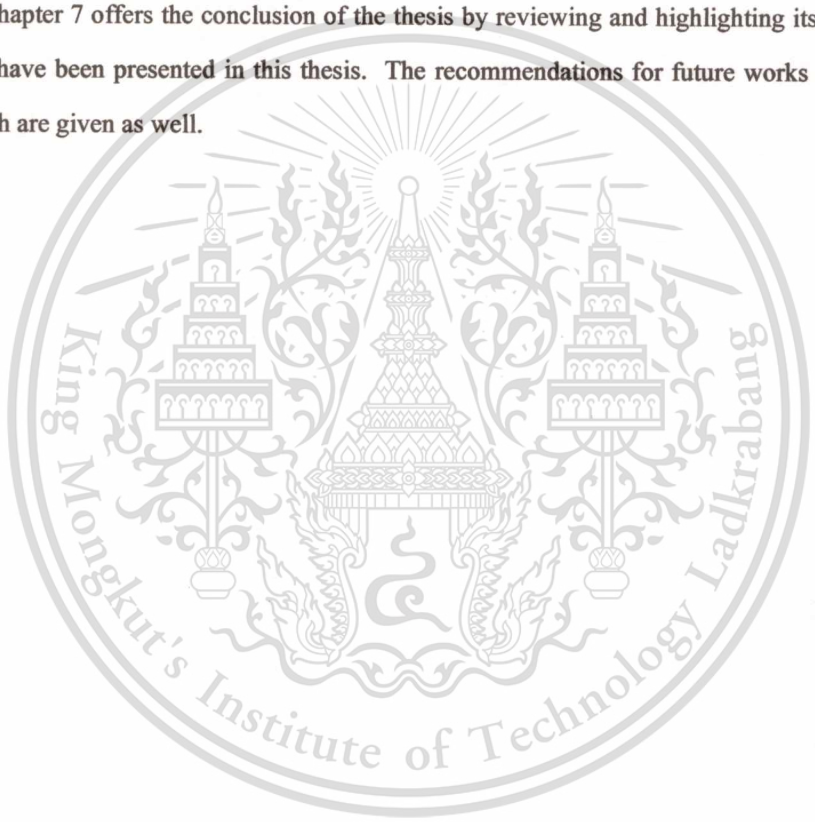

CHAPTER 2

BACKGROUND OF DIABETIC RETINOPAHTY

This chapter gives a brief introduction on the eye structure in Section 2.1 and shows some background information of DR in Section 2.2. In Section 2.3, we discuss the different types of retinal image screening as well as the automatic fundus image analysis. Finally, we introduce some literatures review in Section 2.4.

2.1 Eye Structure

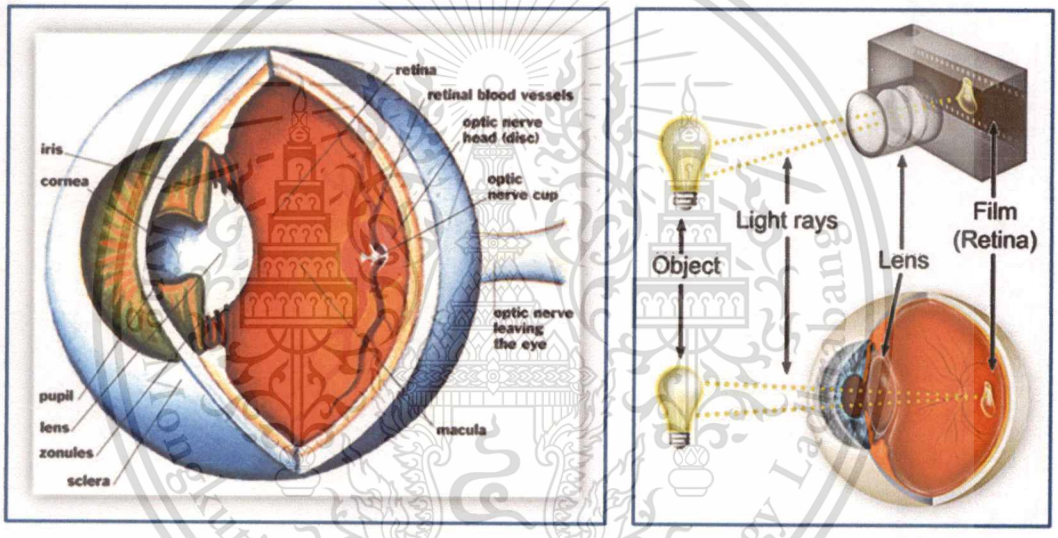

(a) Cross-section of the eye

(b) Comparison between the function of eye and camera [5]

Figure 2.1 Eye structure.

Fig. 2.1 (a) shows a cross-section of the eye and the structures involved in the image formation. Actually the eye can see any objects by the reflection of light from that object going into the eyes. Light entering the eye is first refracted when it passes through the cornea. It then passes through the pupil and is further refracted by the lens. Finally, it reaches the retina and is converted to electrical signals by photosensitive photoreceptor. The electrical signals are transmitted to the brain along the optic nerve [6].

The eye, shown in Fig. 2.2, is optically equivalent to the usual photographic camera. It has a lens system, a variable aperture system (the pupil), and a retina that corresponds to the film. Light reflected from an object is focused on the retina after passing through the cornea, pupil and lens, which is similar to light passing through the camera optics to the film or a sensor. In the retina, the incoming information is received by the photoreceptor cells dedicated for detecting light. From the retina, the information is further transmitted to the brain via the optic nerve, where the sensation of sight is produced. During the transmission, the information is processed in the retinal layers. In the eye behind the transparent cornea, the colored iris regulates the amount of light entering the eye by changing the size of the pupil [7]. In the dark, the pupil is large allowing the maximum amount of light to enter, and in the bright the pupil is small preventing the eye to receive an excess amount of light. In the same way, the camera regulates the amount of light entering the camera with the aperture. The eyes can focus on objects at different distances because of the ciliary muscle reshapes the elastic lens through the zonular fibres. For objects in short distances, the ciliary muscle contracts, zonular fibres loosen, and the lens thickens into orb shaped which results high refractive power. When the ciliary muscle is relaxed, the zonular fibres stretch the lens into thin shaped and the distant objects are in focus. This corresponds to the function of focal length, i.e. the distance between the lens and sensor, when focusing the camera. If the eye is properly focused, the light passes through the vitreous gel to the camera sensor of the eye, which is the retina.

Retina is the sensory layer of the eye. It contains photosensitive cells which convert incident light into signals which is then carried to the brain by the optic nerve. The brain then processes the signal and which finally allows us to 'see' and interpret the object in front of our eyes. The retina contains three important components; optic disc, macula, and blood vessel. The optic disc is responsible for transferring signal from retina to the brain to be interpreted. Optic disc abnormalities could be a marker for several diseases such as glaucoma and astigmatism [8]. In the middle of the macula is the fovea which is responsible for central photo-pic and high resolution vision [9]. Because of this, any abnormality occurring within this region may lead to blindness. The blood vessel is not only responsible for supplying blood to the retina, but also shares similar anatomical and physiological characteristics with the cerebral and coronary circulations [10]. Therefore, changes in other parts of the body will affect the blood vessel in retina.

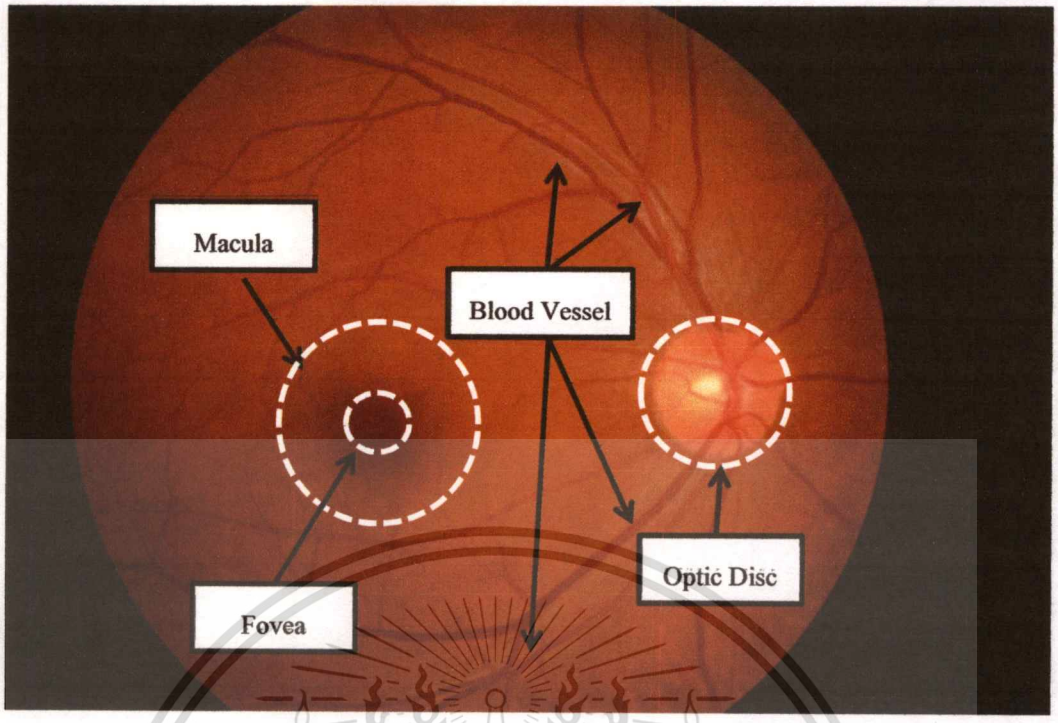

Figure 2.2 Normal physiological parts of the fundus image.

2.2 Diabetic Retinopathy

Diabetic Retinopathy is the effect of diabetes mellitus on the eye. It is a visual complication of diabetes mellitus, which becomes the most common cause of blindness. Early detection and timely treatment can prevent the problem. Recently, there has been significant effort towards building screening solutions for DR using color fundus image mainly due to the offered value such as low-cost and wider reach. These solutions focus on developing methods for automatically detecting the presence of lesions related to DR. There are different kinds of abnormal lesions caused by DR in a diabetic's eye. In this thesis, the following lesion types are briefly described: microaneurysms, hemorrhages, hard exudates, and soft exudates, and shown in Fig. 2.3.

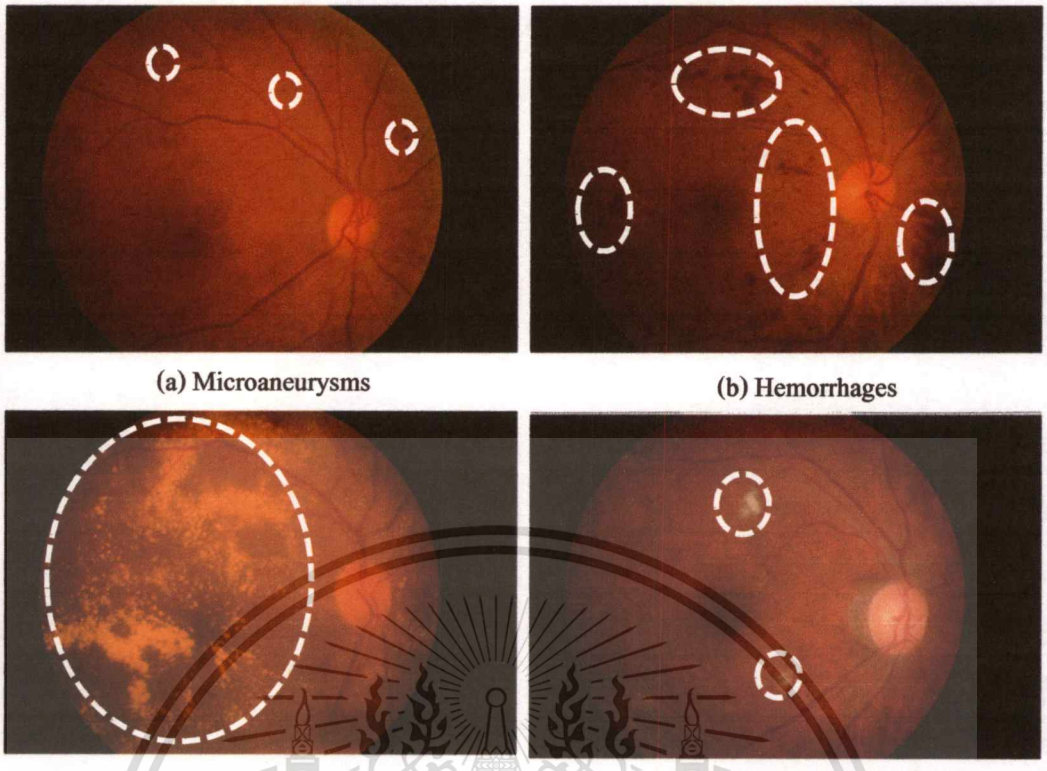

(a) Microaneurysms (b) Hemorrhages

(c) Exudates (d) Cotton-wool spots

Figure 2.3 Abnormalities belonging to diabetic retinopathy.

The diabetic retinopathy typically begins as small changes in the retinal capillaries. The smallest detectable abnormalities which are called microaneurysms as show in Fig. 2.4(a). They appear as small red dots in the retina and are local distensions of the weakened retinal capillary. Due to these damaged capillary walls, the small blood vessels may rupture and cause intraretinal hemorrhages. In Fig. 2.4(b), the hemorrhages appear either as small red dots indistinguishable from microaneurysms or larger round-shaped blots with irregular outline. The diabetic retinopathy also increases the permeability of the capillary walls which results in retinal edema and exudates. The exudates are lipid formations leaking from the weakened blood vessels and appear as random yellowish deposits of varying size, shapes and location in retinal images as shown in Fig. 2.4(c). If the local capillary circulation and oxygen support fail due to obstructed blood vessels, pale areas with indistinct margins appear in the retina. These areas are small micro-infarcts known as soft exudates Fig. 2.4(d). The retinal abnormalities caused by diabetic retinopathy are shown in Table 2.1.

Table 2.1 Abnormal lesion types in diabetic retinopathy.

Lesion type	Size	Color	Shape	Other
Microaneurysm	Very small	Dark red	Round-shaped	
Hemorrhage	From small to large	Dark red	Dot or flame-shaped	
Exudate	From small to large	Yellow	Not regular	Clear edges
Cotton-wool spot	From small to medium	Whitish	Usually oval-shape	Blurry edges

2.3 Screening for Diabetic Retinopathy

Screening of diabetic retinopathy is based on clinical eye examination and eye fundus photography [11]. The ophthalmoscope is an instrument through which an observer can look into another person's eye and see the retina with clarity [12]. Ophthalmoscopy may be undertaken by either the direct method (used by most doctors in everyday practice) or by the indirect method, used mainly by doctors in more specialist practice and by optometrists/opticians. A direct ophthalmoscope is a hand held apparatus through which a medical expert can observe the patient's eye. The apparatus consists of the illumination source and corrective lenses which the light beams are reflected into to the patient's eye using a mirror or prism. In the indirect ophthalmoscopy, the patient's eye is examined from an arm's length by focusing high intensity light through a hand-held condensing lens to the patient's eye and examining the reflected light (stereoscopic image) with the binocular lenses.

The fundus photographs are taken with a fundus camera during mass screening. The patient is required to seat in front of the fundus camera and the head is positioned into the instrument's head rest. A flash lamp produced light is emitted into patient's eye using optical mirrors and lenses and the reflected light is captured by the camera sensor. The captured images are typically color images. Fundus imaging allows patients' images to be stored, which makes disease monitoring easier. Patients, who stay in rural area where experts are not available, can be diagnosed by having their retinal photographs taken and sent to experts in the city or other countries for analysis. In contrast to traditional ophthalmoscopy, it allows to record diagnostic data and enable the expert consultation afterwards, and more importantly the eye fundus photography results in a better sensitivity rate, that is a better detection rate of abnormal eye. Due

to the rapid development of digital imaging, the eye fundus cameras also provide easy to file images in portable format that enable automatic diagnosis of diabetic retinopathy using image analysis algorithms [7].

Recently, there has been significant effort towards building screening solutions for DR using color fundus image mainly due to the offered value such as low-cost and wider reach. These solutions focus on developing methods for automatically detecting the presence of lesions related to DR. Exudates are visually, the most significant indicators of DR in color fundus image. Therefore, this thesis proposes new methods for automatically detection of these lesions.

2.4 Literatures Review

The effect of diabetes on the eye is called Diabetic Retinopathy. Early detection of DR is crucial for prevention of visual loss. Exudates have been found to be one of the signs and serious DR anomalies so the proper detection of these lesions and treatment should be done immediately to prevent loss of vision. In clinical environment, abnormality detection in retinal image is very complicated with the differences in luminosity, brightness and contrast inside retinal images. Therefore there have been many researchers try to propose new ideas to detect this type of lesions. The approaches for exudate detection presented in the literature can be roughly divided into different categories. Thresholding methods base on intensity levels and color image [13-15]. A global threshold is set manually for each image, whereas a local threshold is used for different regions, which are selected by the user. A local dynamic thresholding algorithm is proposed based on the histogram shape. The gray level variation of the exudates using mathematical morphology is also exploited for exudates detection [16]. A combination of region growing and edge detection based on the homogeneity of the exudates illumination [17, 18]. These techniques have the drawback of being computationally intensive. The classification methods build a feature vector for each pixel classification by using a naive Bayes classifier [19] and color images clustering [20], as well as a neural network classifier was used in [21].

On the research work leading to automatic analysis of exudate detection, the knowledge of Optic Disk (OD) location is very useful to prevent the result of exudate detection from its interference so many researchers try to report different techniques to remove it out first as you can see some in [22-24]. Sopharak et al. [22] apply entropy filtering operator and Otsu's binarization algorithm to separate the complex regions from the smooth regions, and then they use

compactness measurement and binary dilation to detect the OD. Next Naive Bayes classifier was employed to select the features of exudates. Wisaeng *et al.* [23] combine mathematical morphology and Otsu's algorithms to eliminate OD first and then use Fuzzy C-Means (FCM) clustering and morphological methods to extract exudates. Venkatalakshmi *et al.* [24] detect OD by applying perfect blob measurement, and then AND operation is performed to remove all false positive such as OD to detect exudates. Therefore, in this thesis an efficient algorithm is presented to detect the OD and exudate for early detection of diabetic retinopathy.

CHAPTER 3

BASIC TECHNIQUES FOR APPLICATIONS OF DIGITAL IMAGE PROCESSING

This chapter presents concepts and digital techniques for processing and analyzing images after they have been generated or digitized. It is organized into following sections that correspond to basic knowledge of digital image processing, and the process of its applications. For further reading and more information, the reader can refer to the books about medical imaging processing and analysis [25], an introduction to digital image processing with MATLAB [26], and digital image processing [27].

3.1 Images and Digital Images [26]

A digital image is a 2D signal in essence, and is the digital version of the 2D manifestation of the real-world 3D scene. Although the words picture and image are quite synonymous, we have to clear that the picture is the analog version of the image. For the moment, to make things easy we suppose the image is monochromatic (that is, shades of grey only), so no color. We may consider this image as a function of two real variables x and y, for example $f(x,y)$ with f as the brightness of the image at the given point (x,y) and its values can be the real numbers in the range 0 (black) to 1 (white), as shown in Fig. 3.1. The ranges of x and y will clearly depend on the image, but they can take all real values between their minima and maxima.

A digital image $f[m,n]$ described in a 2D discrete space is derived from an analog image $f(x,y)$ in 2D continuous space which its x, y and $f(x,y)$ values are obtained through a sampling and quantization process. Each sample of the image is called a pixel.

The 2D continuous image $f(x,y)$ is divided into N rows and M columns. The intersection of a row and columns is termed a pixel. The value assigned to the integer coordinates $[m,n]$ with $\{m = 0,1,2,\dots,M-1\}$ and $\{n = 0,1,2,\dots,N-1\}$ is $f[m,n]$. Image can be of various sizes; however, there are standard values for the various parameters encountered in digital image processing. The values occur due to the hardware constraints caused by the imaging source and/or by certain standards of imaging protocols are used. Similarly, the grayscale values of each pixel are also subjected to the constraints imposed by quantizing hardware that converts the analog

picture value into its digital equivalent. The number of bits is constrained for grayscale values is a power of 2, that $G = 2^B$, where B is the number of bits in the binary representation of the brightness levels. When $B > 1$, we call a gray-level image; when $B = 1$, we call a binary image. In binary image, there are just two levels, black (0) and white (1). A neighborhood can be characterized by its shape in the same way as a matrix: we can speak, for example, of a 3 x 3 neighborhood, or of a 7 x 7 neighborhood. Except in very special circumstances, neighborhoods have odd numbers of rows and columns. This ensures that the current pixel is in the center of the neighborhood. An example of a neighborhood is given in Fig. 3.2.

Figure 3.1 An image as a function.

48	219	168	145	244	188	120	58
49	218	87	94	133	35	17	148
174	151	74	179	224	3	252	194
77	127	87	139	44	228	149	135
138	229	136	113	250	51	108	163
38	210	185	177	69	76	131	53
178	164	79	158	64	169	85	97
96	209	214	203	223	73	110	200

Current pixel

3 x 5 neighborhoods

Figure 3.2 Pixels, with a neighborhood.

3.2 Digital Image Processing Applications

Since the 1960s, the field of image processing has grown vigorously. The areas of application of digital image processing are widely used in robotics, intelligent system, medical imaging, biometric system, image analysis, satellite imaging, remote sensing, industry and so on.

The general phases of applications using digital image processing are shown in Fig. 3.3. First, an image is captured by some types of camera (still camera, video camera, spectral camera, etc.). Then the acquired image is enhanced that the quality of the image is increased. After image preprocessing is segmented so the interesting objects are separated from the background. Then the separated objects are sometimes used directly to obtain as the final result, but in some applications the separated objects are needed to be quantified. Therefore the image quantification is needed.

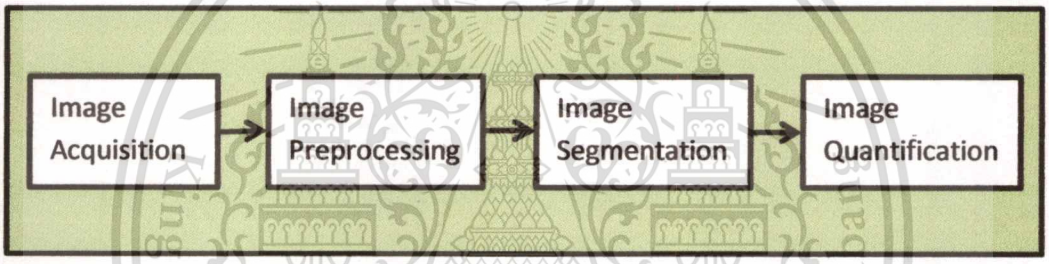

Figure 3.3 Phases of applications using digital image processing.

3.2.1 Image Preprocessing

Image preprocessing is used to reduce image noise and improve the contrast, so that desired image features become easier to perceive for the human visual system or more likely to be detected by automated image analysis system. Two typical techniques used in pre-processing are histogram processing, and filtering. The following subsections describe these techniques.

3.2.1.1 Histogram Preprocessing [27]

The histogram of a digital image with gray levels in the range $[0, L-1]$ is a discrete function $h(r_k) = n_k$, where r_k is the k^{th} gray level and n_k is the number of pixels in the image having gray level r_k. It is common practice to normalize a histogram by dividing each of its values by the total number of pixels in the image, denoted by n. Thus, a normalized histogram is given by $p(r_k) = \frac{n_k}{n}$, for $k = 0, 1, \ldots, L-1$. Loosely speaking, $p(r_k)$ gives an estimate of

the probability of occurrence of gray level r_k. Note that the sum of all components of a normalized histogram is equal to 1. Histograms are the basis for numerous spatial domain processing techniques. Histogram manipulation can be used effectively for image enhancement, as shown in this section.

Histogram equalization is one method for the contrast enhancement by transforming the values in an intensity image, so that the histogram of the output image approximately matches a specified histogram. Fig. 3.4 shows the original image and the result of histogram equalization with their histograms.

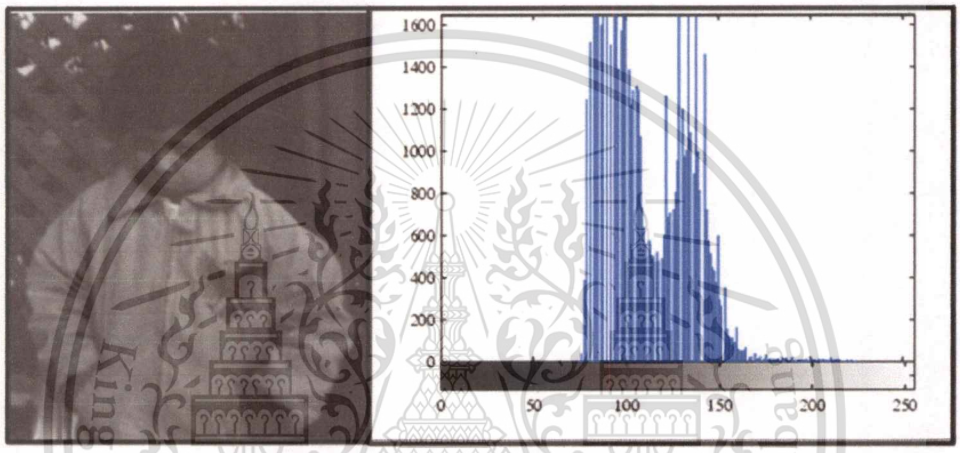

(a) Input image with its histogram

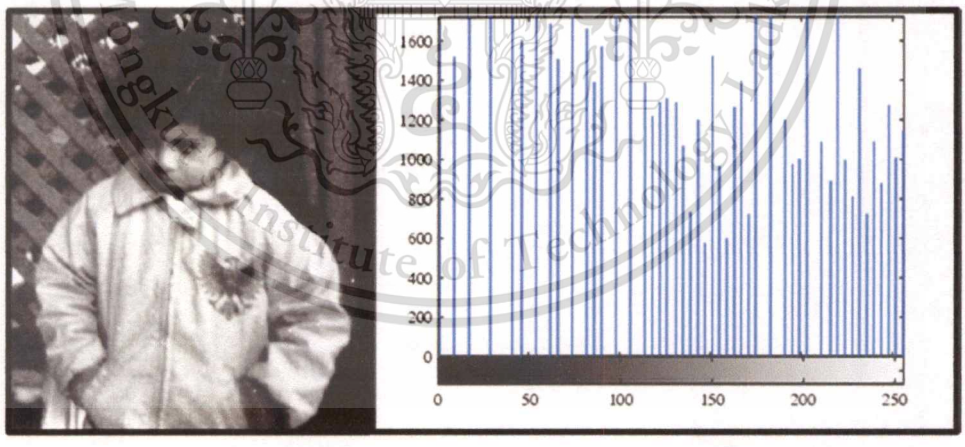

(b) Image after histogram equalization with its histogram

Figure 3.4 Result of histogram equalization.

Another technique for contrast enhancement is adaptive histogram equalization. It differs from ordinary histogram equalization in the respect that the adaptive method computes several

histograms, each corresponding to a distinct section of the image, and uses them to redistribute the lightness values of the image. It is therefore suitable for improving the local contrast of an image and bringing out more detail. However, adaptive histogram equalization has a tendency to over amplify noise in relatively homogeneous regions of an image. Therefore its contrast should be limited to prevent the over amplification of noise that adaptive histogram equalization can give the rise. This procedure is called Contrast Limited Adaptive Histogram Equalization (CLAHE). An example of CLAHE is illustrated in Fig. 3.5.

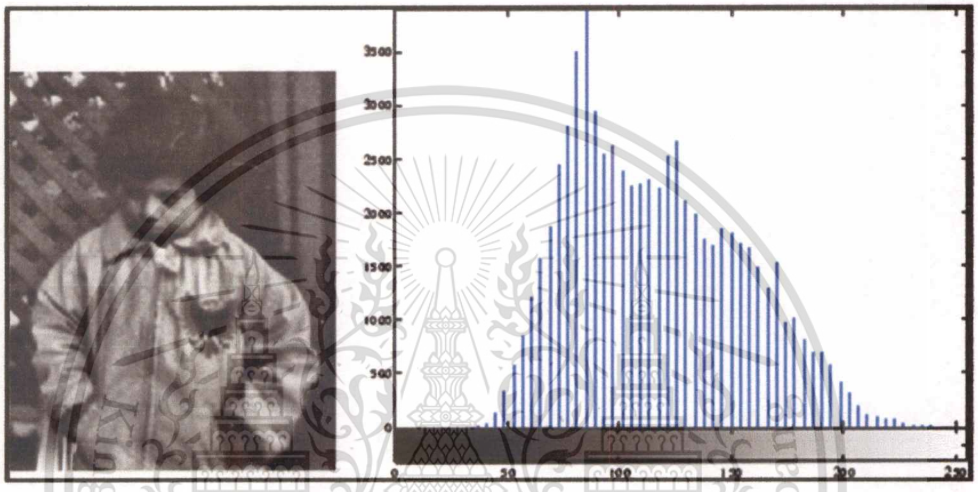

Figure 3.5 Image after CLAHE with its histogram.

3.2.1.2 Filtering [27]

In digital image processing, filtering is mainly used either for enhancing the quality of images or making them more suitable for further processing by smoothing the image, enhancing or detecting edges in the image. Image filtering can be performed either in the spatial or frequency domain. Spatial filtering operates directly on the image without transformations. In the frequency domain filtering, the image is first converted to the frequency domain which the filtering is performed. The conversion from the spatial to the frequency domain can be done using Fast Fourier Transform (FFT) type algorithm and then appropriate filtering is applied. Spatial filtering is based on a small mask that is simply moved from pixel to pixel in the image. At each pixel, the result of the filter is calculated using a preset rule. Fig. 3.6(a) shows a representation of a general 3 x 3 spatial filter mask where $w1, w2, \dots, w9$ are mask coefficients. In general, a filter mask can be size $m \times n$ where the width $m = 2a + 1$, height $n = 2b + 1$, and a and b

are non-negative integers. For linear spatial filtering, for example smoothing and sharpening, the result image g at each image pixel (x, y) can be calculated as a sum of the products of the filter coefficient w and the corresponding image pixels f as:

$$g(x,y) = \sum_{s=-b}^{b} \sum_{t=-a}^{a} w(t,s) f(x+t, y+s) \tag{3.1}$$

Note that the pixels near the edge of the image (closer than the a pixel in the horizontal direction or closer than the b pixel in the vertical direction) cannot be filtered since the location of a pixel in the equation should have non-negative integer. There are several ways to handle the pixels near the image edge: they can be omitted, causing the result image to be smaller than the original one, or those pixels can be set for example to 0's.

$w1$	$w2$	$w3$
$w4$	$w5$	$w6$
$w7$	$w8$	$w9$

(a) General 3 x 3 spatial filter

$\frac{1}{9}$	$\frac{1}{9}$	$\frac{1}{9}$
$\frac{1}{9}$	$\frac{1}{9}$	$\frac{1}{9}$
$\frac{1}{9}$	$\frac{1}{9}$	$\frac{1}{9}$

(b) 3 x 3 mean filter mask.

Figure 3.6 3 x 3 spatial filter masks.

Averaging or mean filtering is simply used to reduce the amount of intensity variation between one pixel and the next by replacing each pixel value in image with the mean value of its neighbors, including itself. Fig. 3.6(b) represents a simple 3 x 3 mask used in smoothing. In addition to the linear filters described above, order-statistics filters are also used. Order-statistics filter is nonlinear spatial filter whose response is based on ordering (ranking) the pixels contained in the image area encompassed by the filter, and then replacing the value of the center pixel with the value determined by the ranking result. The best-known example in this category is the median filter. Median filter is commonly used because they provide excellent noise reduction for certain random noise types and they do not blur images as heavily as linear filter. The median is calculated by first sorting all the pixel values from the surrounding neighborhood in numerical order and then replacing the pixel being considered with the middle pixel value. As an example of median filtering in Fig. 3.7, suppose that surrounding neighborhood pixels covered by a 3 x 3

filter mask have the gray-level values 100, 105, 103, 101, 153, 100, 102, 103, 105. The values are sorted as 100, 100, 101, 102, 103, 103, 105, 105, 153, where the median value is 103 since it is in the center of the sorted values.

100	105	103
101	153	100
102	103	105

→

---	---	---
---	103	---
---	---	---

Figure 3.7 3 x 3 filter mask and median result calculation.

Fig. 3.8 shows an example of comparison using mean and median filter. Fig. 3.8 (a) shows a gray level image that is heavily corrupted by salt-and-pepper noise. Fig. 3.8 (b) shows the results of 3 x 3 mean filtering where noise has been reduced but is still visible. Fig. 3.8 (c) represents the result of 3 x 3 median filtering where almost all noises have been removed, and thus, the quality of the image has appreciably increased.

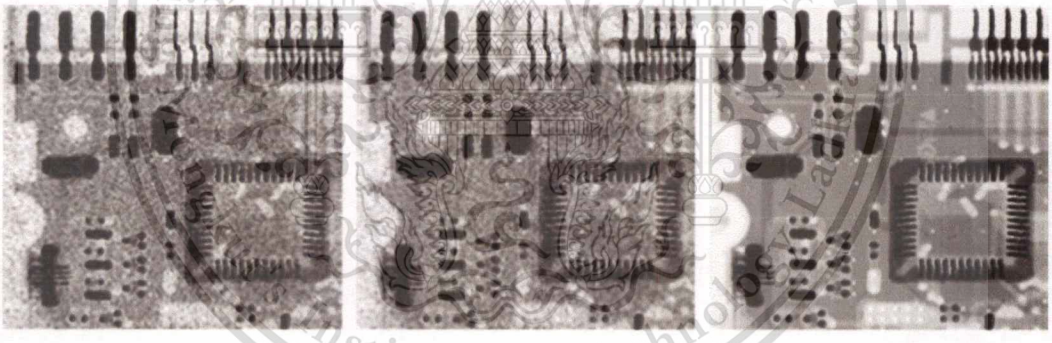

(a) X-ray image of circuit board corrupted by salt-and-pepper noise

(b) Noise reduction with a 3 x 3 mean filter

(c) Noise reduction with a 3 x 3 median filter

Figure 3.8 Example of spatial filtering.

3.2.2 Image Segmentation

In Sub-section 3.2.1 above we talked about some techniques used for preprocessing step so after the quality of images has already been improved, the next step is separating the objects of interest from the background. Segmentation is one of the most widely used steps in reducing

images to information [29]. Segmentation subdivides an image into regions or objects. The level of subdivision is carried depends on the problem being solved. It means that the segmentation of the image should stop when the objects of interest have been isolated.

Image segmentation algorithms generally are based on one of two basic properties of intensity values: discontinuity or similarity. In the discontinuity approach an image is partitioned on the basis of abrupt changes in intensity, such as edges, points, blobs, and lines in the image. In the similarity approach a set of pre-defined criteria is used for partitioning the image into regions that are similar according to the criterion set. Thresholding, region growing, and region splitting and merging are examples of similarity-based segmentation techniques.

In the next sub-sections thresholding, region growing, and edges detection are described with illustrative examples.

3.2.2.1 Thresholding [27]

In many applications of image processing, the gray levels of pixels belonging to the object are quite different from the gray levels of the pixels belonging to the background. Thresholding becomes then a simple and effective method to separate objects from the background.

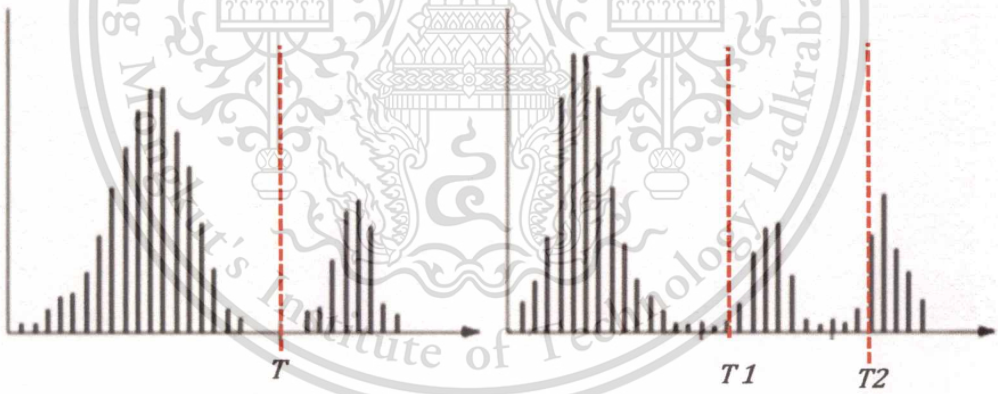

(a) A single threshold (b) Multiple thresholds

Figure 3.9 Gray-level histograms.

Suppose that the gray-level histogram shown in Fig. 3.9 (a) corresponds to an image, $f(x, y)$, composed of the pixels belong to object and background. One obvious way to extract the objects from the background is to select a threshold T that separates these modes. Then any points for which $f(x,y) > T$ is called an object point; otherwise, the point is called a background point.

Thresholding may be viewed as an operation that involves tests against a function T of the form $T = T[x, y, p(x, y), f(x, y)]$ where $f(x, y)$ is the gray level of point (x, y) and $p(x, y)$ denotes some local property of this point. A thresholded image $g(x, y)$ is defined as:

$$g(x,y) = \begin{cases} 1 \; if \; f(x,y) > T \\ 0 \; if \; f(x,y) \leq T \end{cases} \tag{3.2}$$

When T depends only on $f(x, y)$ (that is, only on gray level values) the threshold is called global. If T depends on both $f(x, y)$ and $p(x, y)$, the threshold is called local. If, in addition, T depends on the spatial coordinates x and y, the threshold is called dynamic or adaptive.

3.2.2.2 Global Thresholding [27]

Based on the histogram of an image on Fig. 3.9 (a), the simplest of all thresholding techniques is to partition the image histogram using a single global threshold T. The process of this work is done by scanning the image pixel by pixel labeling each pixel as object or background, depending on whether the gray level of that pixel is greater or less than the value of T.

(a) Original image (b) Image histogram (c) Result of global thresholding

Figure 3.10 Example of global thresholding.

The basic global threshold, T, is calculated as follows:

1. Select an initial estimate for T (typically the average grey level in the image).
2. Segment the image using T to produce two groups of pixels: G_1 consisting of pixels with grey levels $> T$ and G_2 consisting pixels with grey levels $\geq T$.
3. Compute the average grey levels of pixels in G_1 to give μ_1 and G_2 to give μ_2.

4. Compute a new threshold value: $T = \frac{\mu_1 + \mu_2}{2}$.
5. Repeat step 2 to 4 until the difference in T in successive iterations is less than a predefined limit T_{∞} .

This algorithm works very well for finding thresholds when the histogram is suitable. Figure 3.10 shows an example of this threshold.

3.2.2.3 Adaptive Thresholding [27]

An approach to handling situations in which single value thresholding is not work to divide an image into sub images and then utilizes a different threshold to segment each sub-image. Since the threshold used for each pixel depends on the location of the pixel in term of the sub-image, this type of thresholding is adaptive. Fig. 3.11 shows the result of global and adaptive thresholdings.

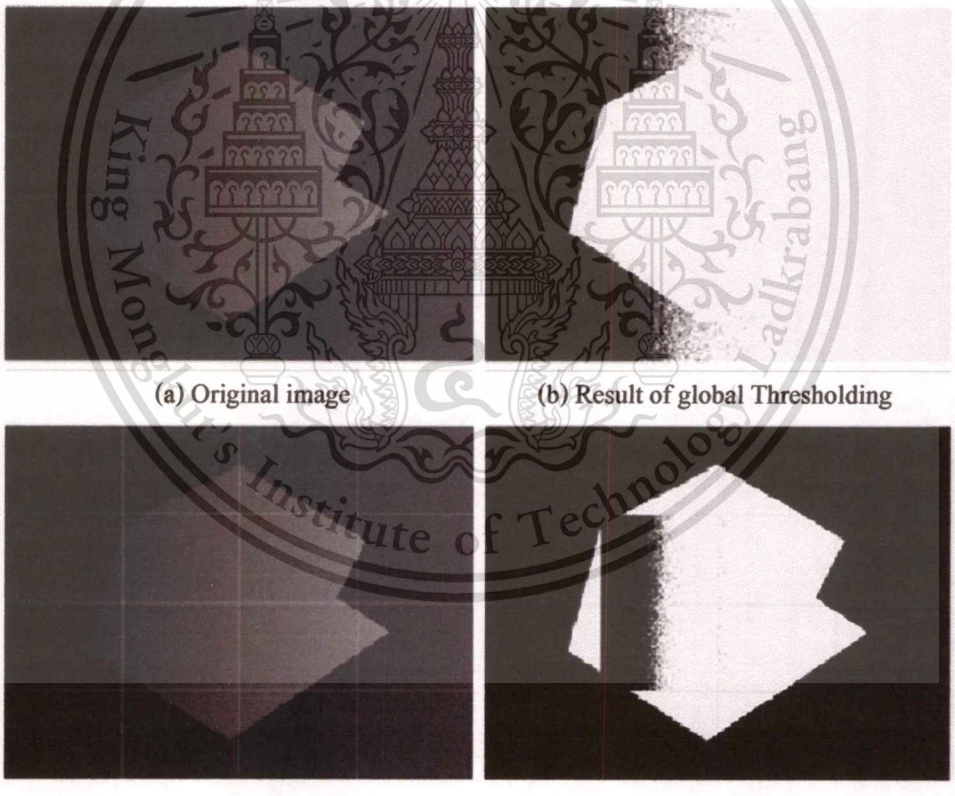

(a) Original image (b) Result of global Thresholding

(c) Image subdivided into individual subimages (d) Result of adaptive thresholding

Figure 3.11 Example of adaptive thresholding.

3.2.2.4 Local Thresholding [27]

A threshold that is calculated at each pixel characterizes this class of algorithms. The value of the threshold depends upon some local statistics such as mean intensity, variance, and surface fitting parameters or their logical combinations. A thresholding level can be adaptively set, for example, using the mean intensity of a local area. In general, thresholding based on moving averages works well when the objects of interest are small (or thin) with respect to the image size, a condition satisfied by images of typed or hand written text.

The moving average (mean intensity) at the k^{th} pixel can be expressed as:

$$m(k) = \frac{1}{n}\sum_{i=k+1-n}^{k} z_i = m(k-1) + \frac{1}{n}(z_k - z_{k-n}) \tag{3.3}$$

where n denotes the number of pixels used in computing the average.

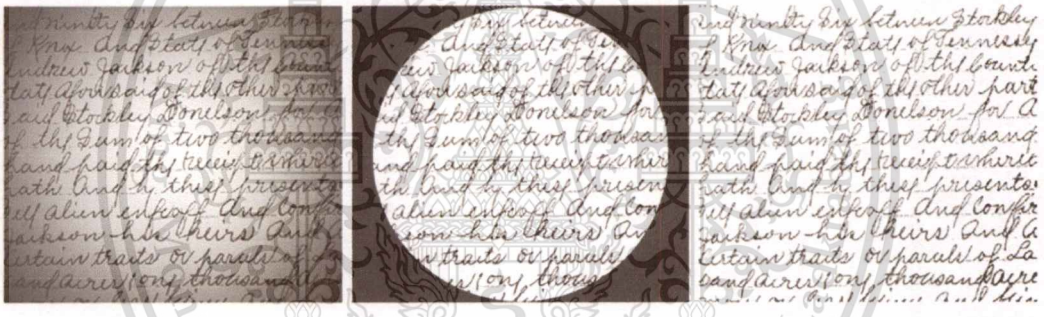

(a) Text image corrupted by spot shading (b) Result of global thresolding using Otsu's method (c) Result of local thresholding using moving averages

Figure 3.12 Example of local thresholding.

3.2.2.5 Region Growing [27]

Region growing is a procedure that groups' pixels or sub-regions become larger regions based on predefined criteria. The basic approach is to start with a set of seed points and from these grow regions by appending to each seed those neighboring pixels that have properties similar to the seed (such as specific ranges of gray level or color). Neighboring pixels are specified by a connectivity rule, for example 4-connectivity or 8-connectivity, where the neighboring pixels are located in four or eight positions. Another problem in region growing is the formulation of a stopping rule. Basically, growing a region should stop when no more pixels

satisfy the pre-defined criteria for example gray-level, texture, or color. Additional criteria that increase the power of region-growing algorithm utilize the concept of size, likeness between a candidate pixel and the region grown so far. An example of region growing is shown in Fig. 3.13. The first step is to determine the initial seed points which are known as the pixels of defective welds. Based on this information, we selected as starting points all pixels having values of 255. The points thus extracted from the original image are shown in Fig. 3.13 (b).

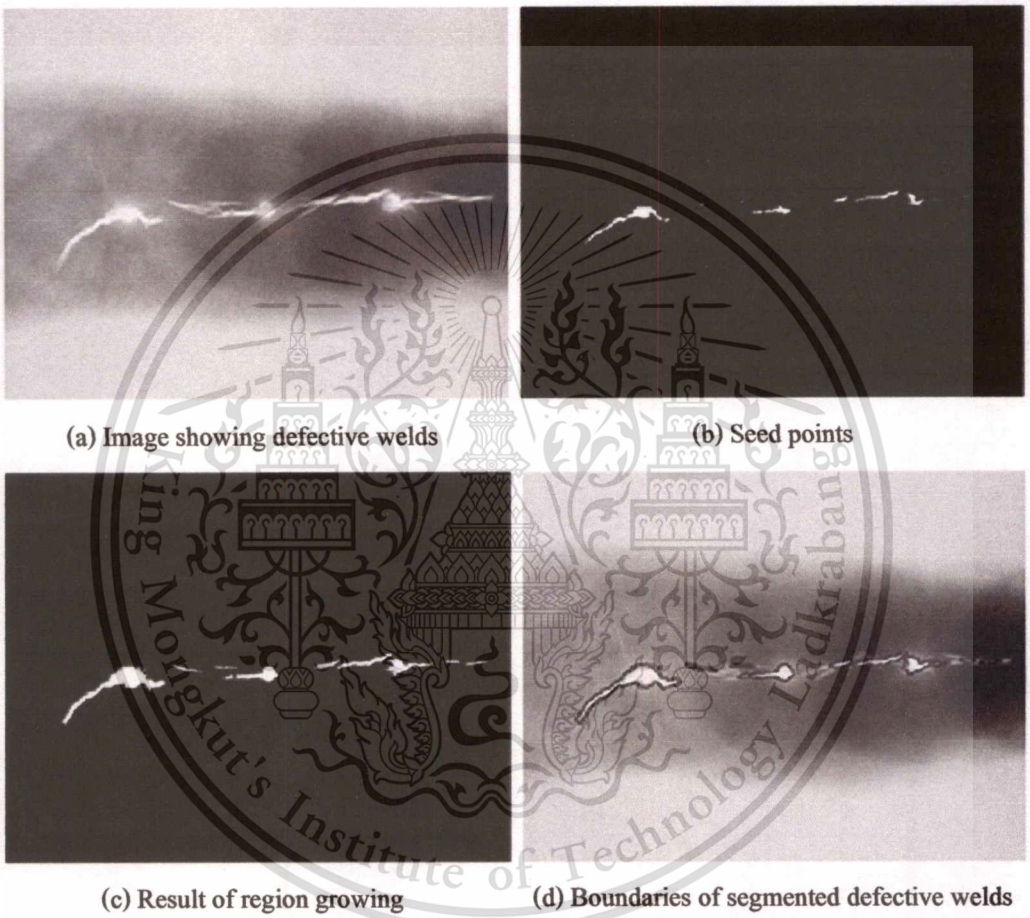

(a) Image showing defective welds (b) Seed points

(c) Result of region growing (d) Boundaries of segmented defective welds

Figure 3.13 Original image courtesy of X-TEK systems.

The next step is to choose criteria for region growing. Two criteria are chosen for a pixel to be annexed to a region:

Find all connected components in $s(x, y)$ and erode them to 1 pixel.

– Form image $f_q(x, y)$ =1 if $f(x, y)$ satisfies the predicate.

– Form image $g(x, y)$ =1 for all pixels in $f_q(x, y)$ that are 8-connected with to any seed point in $s(x, y)$.

– Label each connected component in $g(x, y)$ with a different label.

3.2.2.6 Edges Detection [26]

Edges contain some of the most useful information in an image. It may be used to measure the size of objects in an image, to isolate particular objects from their background, to recognize or classify objects. An edge can be defined as "a sudden change of intensity in an image." In binary images, an edge corresponds to a sudden change of intensity level to 1 from 0, and vice versa. This, essentially, represents high-frequency components in the image and thus extracting them would involve some procedures to extract high frequency from the image. Hence, edge detection is fundamentally a high-pass operation with thresholding added to it. This implies that once high-frequency components (i.e., edges) are found and they are thresholded to logic 1 in the image while all other pixels are set to zero. Too many edges represent a "rough" image, while too few would correspond to a relatively "smoother" image.

Fig. 3.14 shows an example of the edges detection. Two types of edges are illustrated here: a ramp edge, which the gray values change slowly, and a step edge, or an ideal edge, where the gray values change suddenly.

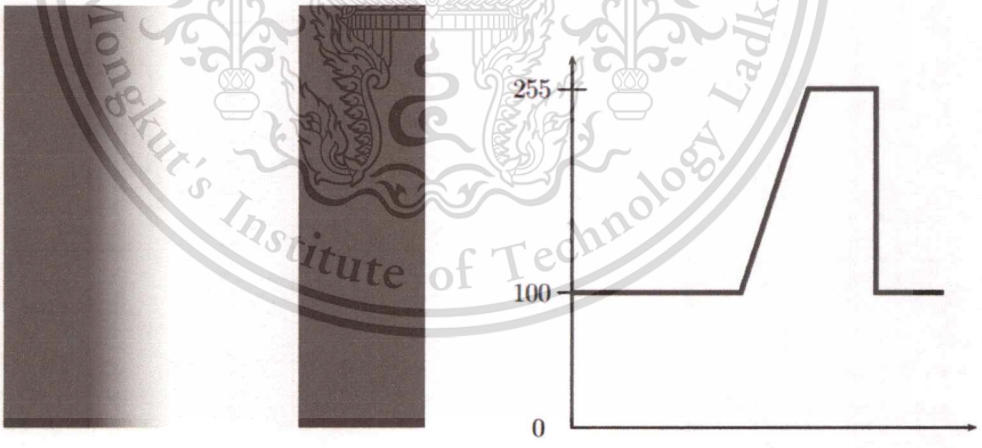

Figure 3.14 Edges and their profiles

Suppose the function which provides the profile in Fig. 3.14 is $f(x)$; then its derivative $f'(x)$ can be plotted, this is shown in Fig 3.15. The derivative, as expected, returns to zero for all

constant sections of the profile, and is non zero (in this example) only in those parts of the image in which difference occur.

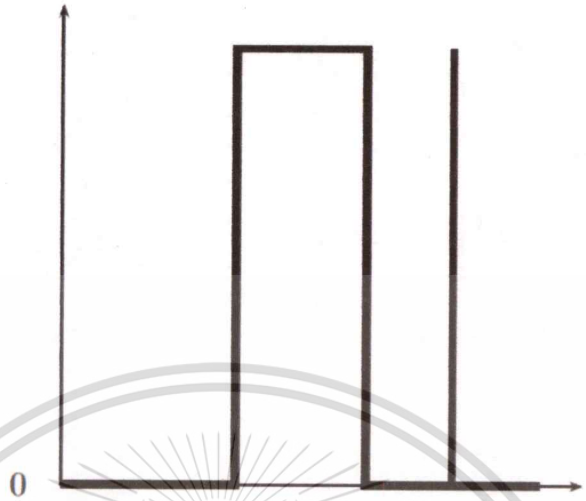

Figure 3.15 The derivative of the edge profile

The edge detection strategies usually correspond to high-pass filtering of the image to allow the high-frequency components to pass to the next stage. The typical filter implementation in images is through convolution kernels, so the edges detectors are also similar in nature. The commonly used edge detectors are Sobel, Prewitt, Robert, Robinson, LoG, zero-crossing, and Kirsch operators.

3.2.3 Image Quantification [25, 27]

After an image has been segmented into regions by methods such as those discussed in subsection 3.2.2, the result images are in the form of binary image. Basically representing a region involves two choices (the form of pixels along a boundary or pixels contained in a region). Although these data sometimes are used directly to obtain as the final result, the standard practice is to use schemes that compact the data into representations that are considerably more useful in the computation.

Shape and texture are two of the most informative visual cues in image interpretation for quantifying image with numerous automated techniques that address different aspects of data. Shape quantification techniques operate on three different ways; firstly are the compactness and

spatial moments which provide geometric and statistical computations to all pixels within a segmented region. Secondly are radial distance measures, chain codes, and Fourier descriptors that operate only on boundary pixels by using geometric, statistical, and spectral computations to provide mechanisms for encoding and representing a closed contour. When the structures of interest are elongated or branching, the essential shape information is contained in the media lines that can be obtained by thinning algorithms. Thirdly are texture quantification techniques which are used in three principal approached (statistical, structural and spectral approaches). Another technique use for image quantification is morphological image processing. In this chapter the example of shape quantification, which is known as compactness, and morphological image processing are shown. For the other techniques we do not explain because it is out of our scope.

3.2.3.1 Compactness Measurement [25]

Compactness is a common shape measurement which can be computed by using the following equation:

$$C = \frac{4\pi A}{P^2} \tag{3.13}$$

where C is the value of shape compactness, A is the shape area and P is the shape perimeter.

Compactness quantifies how close an object to the circle. The maximum value of compactness will be 1 if the region is a circle. This value will decrease depend on its shape for example elliptical-shaped regions, and irregular-shaped regions, as well as the other complicated boundaries regions.

3.2.3.2 Morphological Image Processing [27]

Mathematical morphology, usually performed for binary images, contains two fundamental operations: morphological dilation and erosion. Dilation expands and erosion shrinks objects marked in a binary image. Other morphological operations are for example morphological opening and closing which are based on dilation and erosion. Although morphology is often performed for binary images containing only 0's and 1's, morphology operations and algorithms can also be extended for gray-scale images. Morphological dilation and erosion are based on a certain mask called a structuring element. Both in dilation and erosion, a mask or a structuring element, is moved on an image.

In dilation, the center of the structuring element is checked on every pixel in the binary image. If the center pixel is marked with 1 in the image, all pixels specified by 1's in the structuring element are marked as 1's in the result image. Morphological dilation is expressed as $A \oplus B$, where A is the image being processed and B the structuring element. Morphological erosion is the opposite operation to dilation. Also in erosion the center of the structuring element is checked on every pixel in the image, but if the center pixel is marked with 0 in the image, all pixels specified by 1's in the structuring element are marked with 0's in the result image. Morphological erosion is marked as $A \ominus B$, where A is the image being processed and B the structuring element.

Morphological reconstruction is a part of morphological image processing which is a useful method for extracting meaningful information about shapes in an image. Reconstruction is a morphological transformation involving two images and a structuring element (instead of a single image and structuring element). One image, the marker, is the starting point for the transformation. The other image, the mask, constrains the transformation. The structuring element used defines connectivity. In this section we use 8-connectivity (the default), which implies that B in the following discussion is a 3 x 3 matrix of 1's, with the center defined at coordinates (2, 2).

Suppose G is the mask and F is the marker, the reconstruction of G from F, denoted $R_G(F)$, is defined by the following iterative procedure:

1. Initialize h_1 to be the marker image, F.
2. Create the structuring element: $B = ones(3)$.
3. Repeat: $h_{k+1} = (h_k \oplus B) \cap G$ until $h_{k+1} = h_k$.
4. $R_G(F) = h_{k+1}$.

Marker F must be a subset of G: $F \subseteq G$.

An example of this reconstruction, filling holes, is explained. Let I denotes a binary image, and supposes that we choose the marker image, F, to be 0 everywhere except on the image border, where it is set to $1 - I$:

$$F(x,y) = \begin{cases} I(x,y) & if\ (x,y) is\ on\ the\ border\ of\ I \\ 0 & otherwise \end{cases} \quad (3.14)$$

Then,

$$H = [\, R_{I^c}(F)]^c \quad (3.15)$$

where H is a binary image equal to I with all holes are filled.

Its syntax can be found in MATLAB toolbox function to perform this computation automatically when the optional argument 'holes' is used:

$$g = \text{imfill}(f,\ 'holes') \tag{3.16}$$

where g is the result of filling holes in the binary image f. A hole is a set of background pixels which is surrounded by object pixels.

CHAPTER 4

OPTIC DISC DETECTION AND EXTRACTION

Normal eye fundus structures, such as blood vessels, optic disc, macula and fovea, are essential parts in automatic diabetic retinopathy screening system. This is important to successfully find abnormal structures in a retinal image and mask out the normal anatomy from the analysis. An example is the optic disc, an anatomical structure with a bright appearance, which should be ignored when detecting bright lesions. In this chapter, a simple fast and robust OD detection method is presented. This method can detect the OD based on category of thresholding methods and it is composed of the following steps as shown in Fig. 4.1.

Preprocessing step is used to discuss on the problem of variable intensity in fundus image. It is discussed on section 4.1. Two differences methods are applied in section 4.2 to convert the image to binary image. After binarization the obtained object are all bright pixels which include all noises, OD and exudates. Therefore in section 4.3, the ROI based segmentation is used to select only the interesting object which is known as OD. The result from ROI based segmentation cannot detect all ODs correctly when the level of thresholding is too big or too small so the area of OD is estimated in section 4.4. Finally the area of OD detection is extracted in section 4.5.

4.1 Preprocessing

Abnormality detection in fundus images is very complicated with the differences in luminosity, brightness and contrast inside the images. Preprocessing step is the first step and important to solve these problems. The fundus images database from hospital are stored in RGB color space which consists of three channels (red, green and blue). The first task in image processing is to choose an appropriate representation using a color space definition. There are several different color spaces in the literature and all color spaces have their own advantages. Indeed, there are no color spaces that better than the others and suitable for all kinds of images. However from the literature reviews, it has been observed that the OD is more easily discriminated in red channel [28-31] because its intensity is brighter. Fig 4.2 shows the original image with its red, green and blue channels.

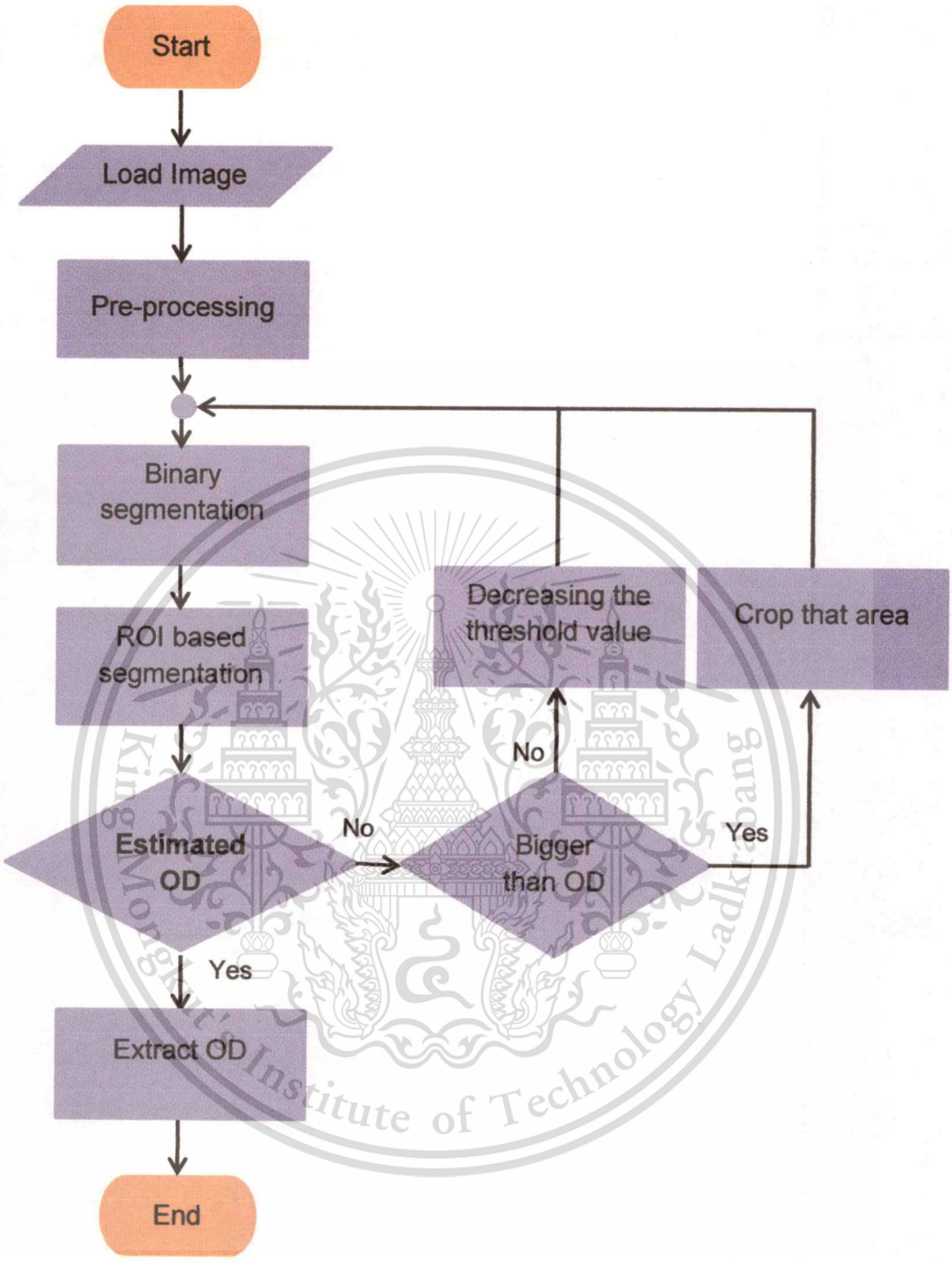

Figure 4.1 The flowchart of OD detection and extraction.

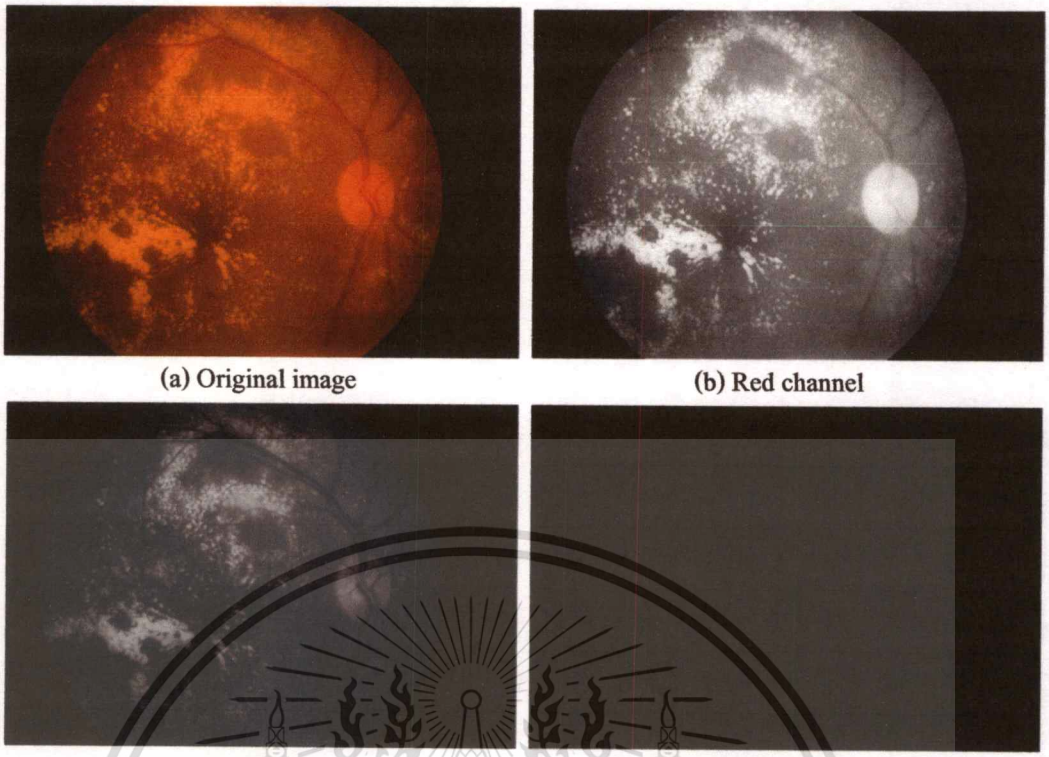

(a) Original image (b) Red channel

(c) Green channel (d) Blue channel

Figure 4.2 Conversion to grayscale.

Fig. 4.2 illustrates that in green channel, the OD is separated by blood vessel, and in the blue channel, we cannot find the any information about OD. Therefore it is difficult to define the shape of OD when the image is converted to binary image. But in the red channel, the OD is more easily defined with the characteristic of the most circular region after binary segmentation.

To make sure that the detection of OD is really should be done on red channel, we try to test on different channels of RGB color space to find the suitable thresholding value. For analysis using RGB color space, first the original image is converted into red, green and blue channels respectively. Next the Contrast-Limited Adaptive Histogram Equalization (CLAHE) and median filtering are respectively applied to red, green and blue channels in order to improve the quality of these channels. Then pixel counting is calculated and tested on histogram of all channels before and after applied CLAHE and median filtering. Finally the result of testing indicated that the best performance is 0.5% of the brightest pixels on red channel.

4.2 Image Binarization

In clinical environment, the variable intensity in retinal images is considered as one of the main obstacles for exudate detection as well as OD detection because the range of intensity value varies from one image to the others. To take these differences into account, we try to measure the maximization of the information between object and background. In this section, two methods are analyzed and compared.

Firstly is the pixel counting which is calculated the level of intensity in the image to find the thresholding level for converting it into binary image. As explain in section 3.1, 0.5 % of the brightest pixel is used as thresholding level to convert the red channel into binary image. Fig. 4.3 shows the histogram of 0.5% of the brightest pixels on red channel.

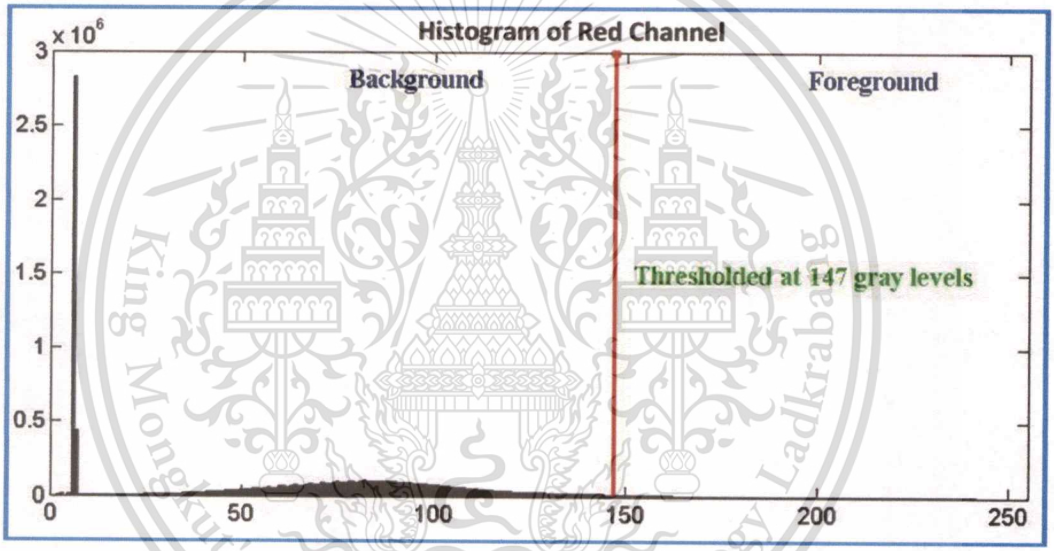

Figure 4.3 The histogram of red channel.

Secondly is the maximum entropy thresholding described in [32, 33]. This technique is based on Shannon entropy. For a random variable X with values in a finite set N, Shannon entropy is defined as:

$$H(X) = -\sum_{x=0}^{N-1} P_x \log_2 P_x \tag{4.1}$$

where

$$\sum_{x=0}^{N-1} P_x = 1, \qquad 0 \leq P_x \geq 1 \tag{4.2}$$

where $x = 1, 2, \ldots, N$, is a set of possible outcomes or states of a discrete information source modeled. Shannon's measurement is used as a measurement of information gain, choice and uncertainty. In particular, the minimum $H(X) = 0$ is if only if $P_{x_0} = 1, \forall x_0 \neq x, P_x = 1$, where x can indicate any positions in the distribution. At the opposite, $H(X)$ is maximal, when all the P_x are equal, for example $P_x = \frac{1}{N}$ for all $x = 1, 2, \ldots, N$.

In this research the entropy function is studied on 1D histogram of the gray level image. Suppose i is the gray-level value of an image so $i = [0, 1 \ldots t-1, t, t+1 \ldots 255]$, and the probability of the pixel being i can be defined as:

$$P_i = \frac{n_i}{n} \tag{4.3}$$

where n is the total number of pixels in the image and n_i is the number of pixels that have gray level i.

Let b and o represent the background and object respectively thus the probabilities of b and o can be calculated as:

$$P_b = \sum_{i=0}^{t-1} P_i \tag{4.4}$$

$$P_o = \sum_{i=t}^{255} P_i \tag{4.5}$$

So the entropies of object and background's probability distributions are given as:

$$H_b(t) = -\sum_{i=0}^{t-1} \frac{P_i}{P_b} \log_2 \frac{P_i}{P_b} \tag{4.6}$$

$$H_o(t) = -\sum_{i=t}^{255} \frac{P_i}{P_o} \log_2 \frac{P_i}{P_o} \tag{4.7}$$

Thus the entropy of the gray level image segmented by threshold t is:

$$H(t) = H_b(t) + H_o(t) \tag{4.8}$$

The theory of maximum entropy is used to select t which makes H be maximum. So, the optimal threshold t can be selected by maximizing the entropy of $H(t)$ which can be defined as:

$$t = \text{Arg Max}(H(t)) \tag{4.9}$$

where $0 \leq t \leq 255$, and Arg Max is stand for the argument of the maximum.

The object is detected as the bright pixels after apply the level of threshold t on the red channel of the fundus image.

4.3 ROI Based Segmentation

After binarization the obtained objects are all bright pixels which include all noises, OD and Exudates. Therefore the ROI based segmentation is used to select only the interesting object which is known as optic disc. The interesting region can be found based on two processes; neighborhood connecting pixels and compactness measurement, respectively. There are more than one candidate region identified from the result of binarization. So, first we applied neighborhood connecting pixels to label all group pixels then all small holes of the group pixels is filled up to make them smooth. Finally, compactness measurement in [34] is used to find the most circular region which is considered as OD. The maximum value of compactness will be 1 if the region is a circle. This value will decrease depend on its shape, for example elliptical-shaped regions, and irregular-shaped regions, as well as the other complicated boundaries regions. The equation of compactness measurement is defined as:

$$C(\mathcal{R}) = \frac{4\pi A(\mathcal{R})}{l_p^2(\mathcal{R})} \tag{4.10}$$

where $\mathcal{R}$ is the connected region with the pixels more than twenty thousands, as all connected regions with the pixels less than twenty thousands are considered as noise and are eliminated. $A(\mathcal{R})$ is the number of pixels in region $\mathcal{R}$ and $l_p(\mathcal{R})$ is the length of boundary region $\mathcal{R}$.

4.4 OD Localization

The result from ROI based segmentation cannot detect correctly when the level of threshold value is too small or too big. So the area of the OD is estimated. From the past research in [35],

the area of OD is enclosed in a square box which the inside pixels are about 27 times smaller than the total pixels in the fundus image. The other researcher [36] shows the range of OD area from 21 to 56 times smaller than the total pixels in the fundus image. Therefore the discussion is done on our database. The suitable range of OD area is analyzed by counting the pixels on the result of OD detection correctly. The maximum and minimum of OD area, 299860 pixels and 100780 pixels, are obtained respectively. This amount is about 33 times to 99 times smaller than the total of 10036224 pixels in our fundus images. When the area of OD detection is bigger than the maximum pixels value detection, it will be cropped and then the same process from image binarization has been redone until the OD detection is in the suitable range. In case the OD detection is smaller than the minimum pixels value detection, the same process will be repeatedly redone by decreasing the threshold value.

4.5 OD Extraction

After the OD is detected correctly, we obtain only the OD mask so it is needed to extract the real color of OD for verifying the result. Therefore the Morphological Reconstruction (MR) is used in the process. The process of MR is based on dilation on two images, a marker and a mask. All the pixels in OD mask are inverted first before they are used as a marker image. The original fundus image is used as a mask. All the pixels in the marker image are overlaid on the mask image by the dilation of the marker image repeatedly until the contour of the marker image fits under the mask image. The expression is defined as:

$$OD_g = R_B(F) \tag{4.11}$$

where B is the original fundus image, F is the inverted OD mask, and OD_g is the reconstruction of B from F, which is the result of OD region extraction. The processes of OD detection and extraction are shown in Fig. 4.4.

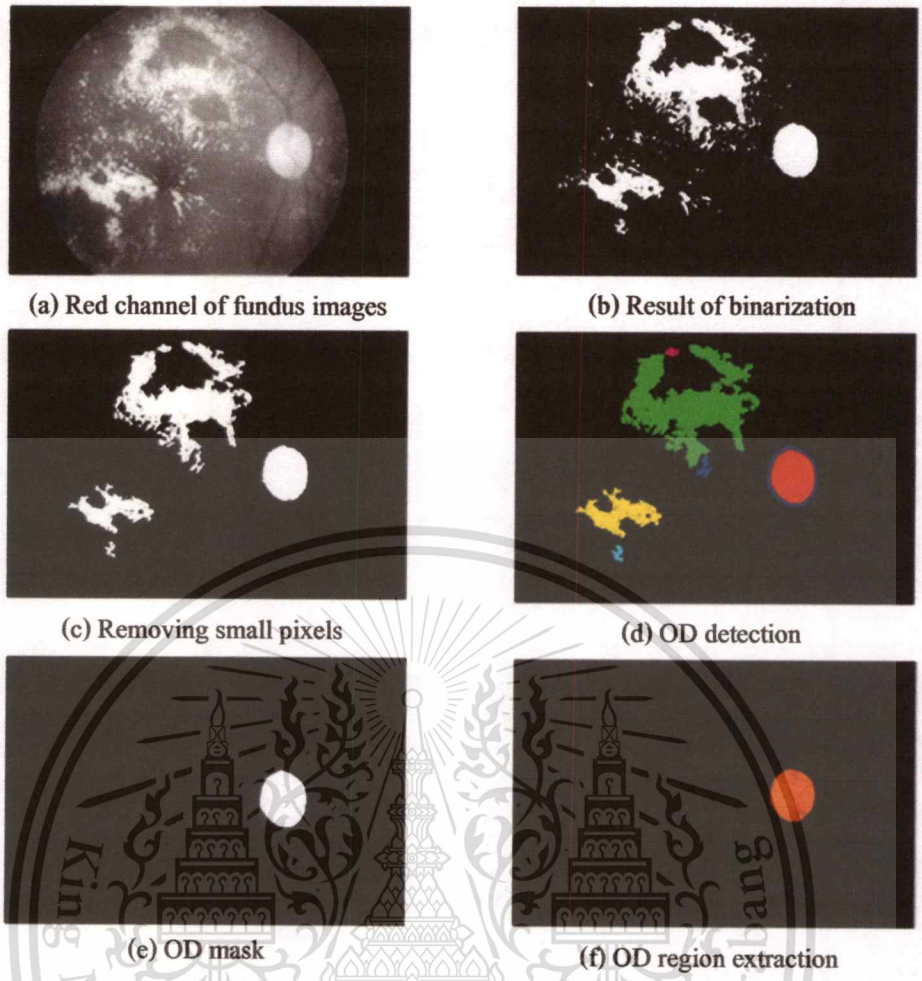

(a) Red channel of fundus images

(b) Result of binarization

(c) Removing small pixels

(d) OD detection

(e) OD mask

(f) OD region extraction

Figure 4.4 OD extraction.

CHAPTER 5

EXUDATE EXTRACTION

In this chapter the proposed method consists of four main steps. Preprocessing step is discussed in section 5.1. Section 5.2, exudate segmentation, is analyzed on two suitable methods based on category of thresholding. After exudate segmentation, the results still contain some noises in some fundus images which we can consider as poor quality images. There are two kinds of quality problems in the fundus images used in this research: The first is noise pixels whose colors are distorted. The second is noise from cotton wool spots, and artifacts in the papillary region that are characterized by the high gray-level intensity. To solve the problems, two methods are proposed in section 5.3. Finally exudates are extracted in section 5.4. Fig. 5.1 illustrates the flowchart of the method.

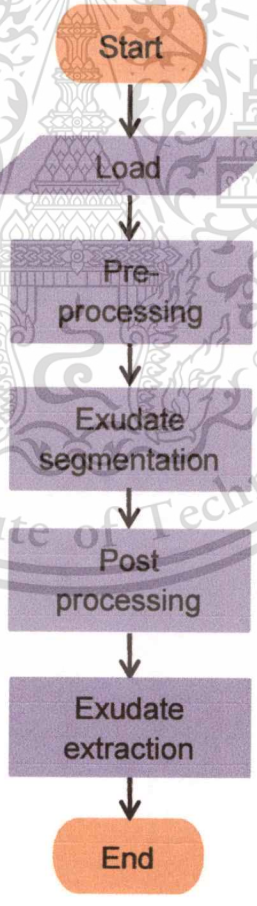

Figure 5.1 The flowchart of exudate extraction.

5.1 Preprocessing

As discussed in chapter 4, the variable intensities from one image to the others in fundus images are very complicated so the quality of the image is needed to be improved first before the next process. For OD, because its characteristic is the injection of the blood vessel therefore it is needed to be used in red channel which the intensity inside is brighter. For exudate, from the past researches in the literature review, it has been observed that green channel of RGB color space is used in the analysis because it has higher contrast and more energy [37-38]. So the green channel of fundus image is used in this chapter.

Exudates appear as bright lesions with the random yellowish deposits of varying size, shape and location in fundus images. OD in the process of exudate detection is considered as noise because of its characteristic similar with the exudate bright yellowish. The green channel of RGB color space is chosen to be applied, so the OD of this channel should be removed for marking it out from the process of exudates detection.

The same technique in section 4.5 is deployed on the green channel to eliminate its OD. The OD mask from OD estimation is used as a marker and the green channel of retinal image is used as a mask. All the pixels in the marker image are overlaid on the mask image by the dilation of the marker image repeatedly until the contour of the marker image fits under the mask image. The result from this process is shown in Fig. 5.2.

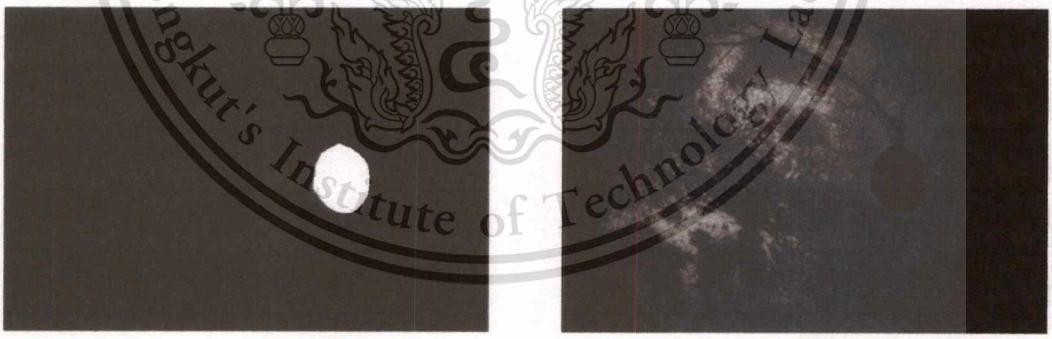

(a) OD mask (b) Eliminating OD

Figure 5.2 OD elimination.

5.2 Exudate Segmentation

After OD is eliminated, all bright pixels in fundus image can be considered as exudates. The same techniques in chapter 4, pixel counting and maximum entropy thresholding, are used to

filter out all of these bright pixels. The first method is pixel counting which is applied to filter out all 0.5 % of the brightest pixels for converting the image into binary image. The second method is the maximum entropy thresholding which is an automatic thresholding method that uses the theory of entropy to measure the maximization of the information between object and background. The second technique works well with all fundus images which contain only exudates but it fails in some non-exudate images. When we apply the maximum entropy thresholding method with non-exudate images which contain cotton-wool spots or artifact, this method will detect these false positives as exudates so it is needed to be prevented. The maximum entropy thresholding method used in this case is a bit different from applying for OD detection. The different is that we have to find the maximization of the information between object and background in the original green channel of fundus image and then apply that threshold value to the green channel which the OD inside is eliminated. When we do like this, the level of threshold value will be set at the highest level (OD and exudates) so that the result will not be affected when we apply it to the result images from OD elimination. Figure 5.3 shows the process of this key technique.

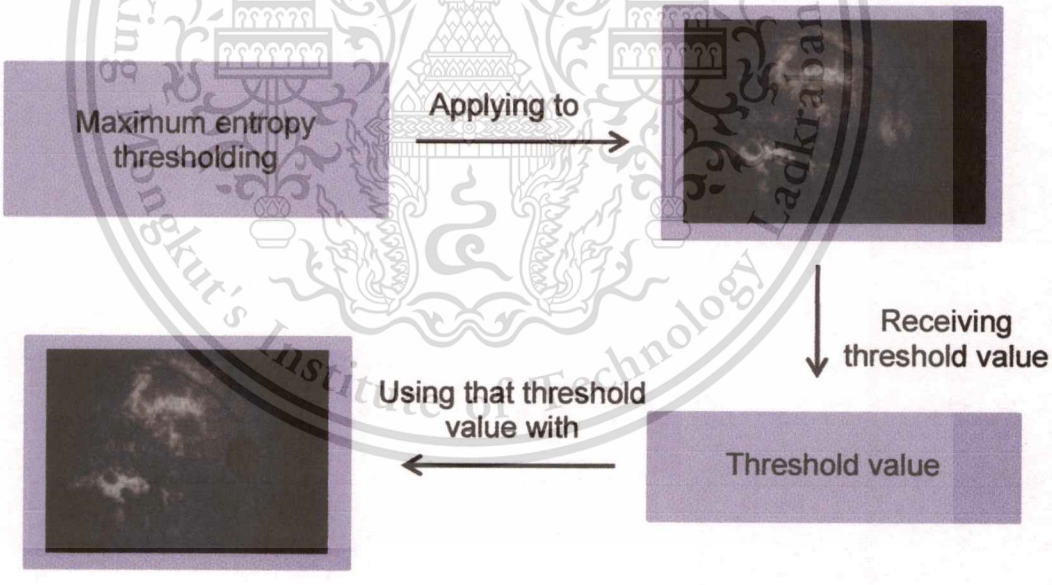

Figure 5.3 The process of key technique.

The result after applying the key technique on green channel of retinal image is illustrated in Fig. 5.4.

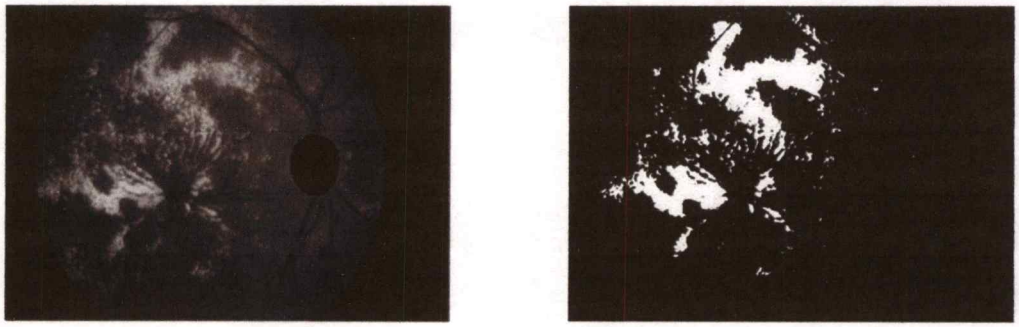

(a) OD elimination of green channel (b) The result after exudate segmentation

Figure 5.4 The result after exudate segmentation.

5.3 Post Processing

There are two kinds of quality problems in the fundus images used in this research. The first is noise pixels whose colors are distorted. This case seems to exist in regions where illumination has been inadequate. The illumination is usually adequate in the center of the image, but for poor quality images the illumination is located near the edge of the fundus area. The second is noise from cotton wool spots, and artifacts in the papillary region that are characterized by the high-gray level intensity.

There are two methods to solve image quality problems. The first is clearing illumination at the edge of fundus area. The second is using the sharp edges detection to find the sharpness of the edges which are the characteristic of exudate in addition to the high intensity. This characteristic is not representative of other elements such as cotton wool spots or artifacts in the papillary regions. So, we use the edge strength of the exudates to eliminate these false positives. We combine the thresholding image with the result images from sharp edges detection by using the Boolean operator.

5.3.1 Clearing the Illumination at the Edge of Fundus Area

Although the result obtained from exudate segmentation can detection almost all kinds of quality images, the poor image quality regions from the illumination at the edge of fundus image may cause errors in abnormality detection. Fig. 5.5 shows these kinds of poor quality images which are also included in the database.

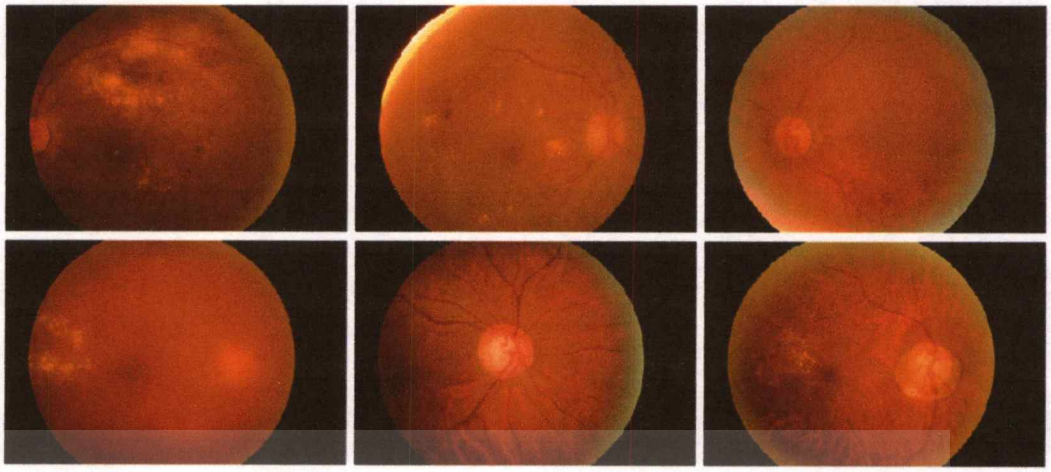

Figure 5.5 Fundus images which illumination affect at the edge of their fundus area.

The fundus image obtained from the hospital consists of a circular fundus area and a dark background surrounding the fundus area. In order to detect the illumination affect at the edge of fundus area first we have to make that affect becomes the edge of fundus image by cropping the result image after OD elimination. To crop the fundus image, it is important to separate the fundus area from its background. The method for creating a binary fundus mask is described. In a fundus mask, pixels belonging to the fundus are marked with 1's and the background of the fundus with 0's. This process is done by using Otsu's thresholding. Then all pixels with the value 1 in the first column, the last column, the first row and the last row are computed respectively in order to find two start points and two end points of a square box. After that the distances from each start point and end point are calculated and finally those points are used for cropping the fundus image. The cropped image is shown in Fig 5.6.

The effect of illumination at the edge of fundus area now is become the effect of the fundus image so that the effect can be eliminated by using clearing border objects. It is a syntax in MATLAB toolbox function which is used in the application of morphological reconstruction to remove objects that touch the border of the image.

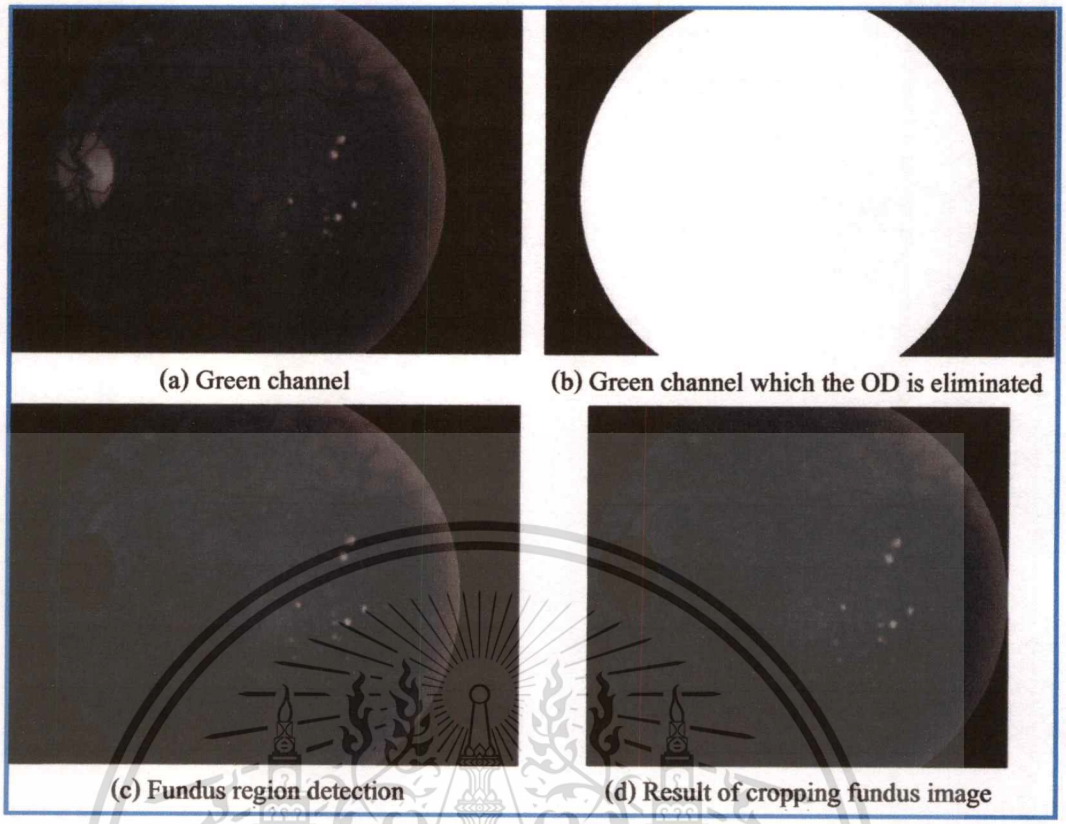

Figure 5.6 Cropping fundus area.

The key task is to select the appropriate marker to achieve the desired effect. Suppose we define the marker image, F, as

$$F(x,y) = \begin{cases} I(x,y) & if\ (x,y) is\ on\ the\ border\ of\ I \\ 0 & otherwise \end{cases} \quad (5.1)$$

where I is the original image. Then, using I as the mask image, the reconstruction

$$H = R_I(F) \quad (5.2)$$

The image, H, contains only the objects touching the border so the difference, 1 - H, contains only the objects from the original image that do not touch the border. Its syntax can be found in MATLAB toolbox function [39]:

$$C_b = \text{imclearborder}(C_r, \text{conn}) \quad (5.3)$$

where C_r is the cropping result of OD region elimination and C_b is the result of exudates mask. The value of conn is 8 because 8-connected neighborhood is used.

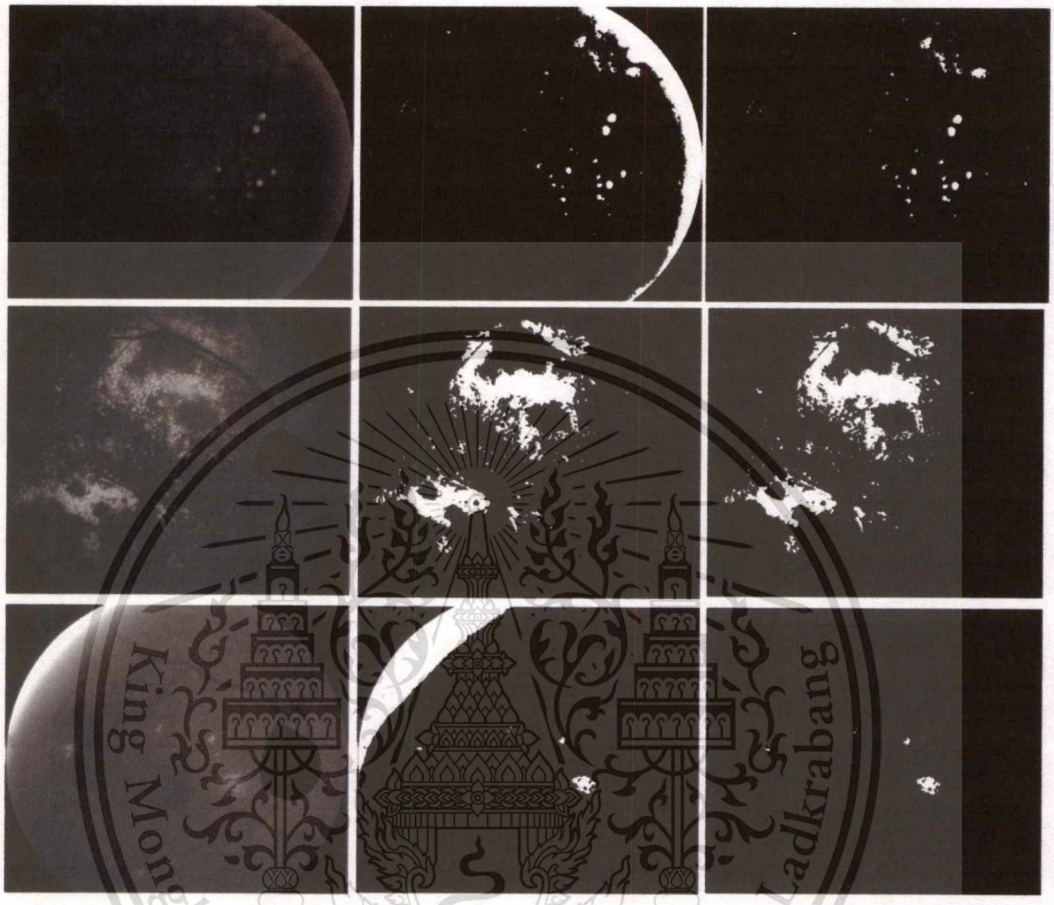

(a) Cropping the results of OD elimination

(b) Exudate segmentation after cropping

(c) Exudates mask after removing the bordered objects

Figure 5.7 Removing the illumination at the edge of fundus area from the result of exudates detection.

Since this technique, the clearing border object, is done on binary images, the threshold value from exudate segmentation in section 5.2 is applied to convert the cropping result into the binary image first. The result of exudates detection after removing the illumination at the edge of fundus area are shown in Fig. 5.7.

5.3.2 Sharp Edges Detection

As we mentioned in section 5.2, cotton wool spots and artifacts are carefully avoid from detection by using key technique but 100 percents of these false positive still not yet avoid. So after exudate segmentation, other bright lesions, such as cotton wool spots, and artifacts in the papillary region as well as OD that are characterized by a high grey level may be erroneously detected as exudate in some fundus images. Therefore, they must be removed from the final result. A significant attribute of exudates, in addition to high intensity, is the sharpness of their edges. This characteristic is not representative of other elements such as cotton wool spots or artifacts in the papillary regions. So, we use the edge strength of exudates to eliminate these false positives.

In our work, the Kirsch mask [40] and its different rotations were applied to the green channel of the retinal image, and the maximum response was selected to detect the edges in the image. The Kirsch mask and its rotation of 8 major compass orientations: N, NW, W, SW, S, SE, E, and NE are shown in Fig. 5.8.

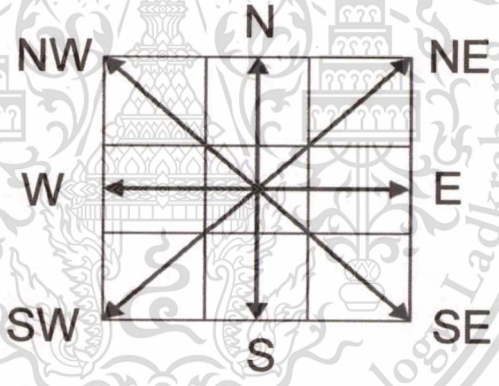

Figure 5.8 The compass orientations of Kirsch mask.

The different rotations of Kirsch mask can be defined as:

$$N=\begin{bmatrix} \frac{-3}{15} & \frac{-3}{15} & \frac{5}{15} \\ \frac{-3}{15} & 0 & \frac{5}{15} \\ \frac{-3}{15} & \frac{-3}{15} & \frac{5}{15} \end{bmatrix} \quad W=\begin{bmatrix} \frac{-3}{15} & \frac{5}{15} & \frac{5}{15} \\ \frac{-3}{15} & 0 & \frac{5}{15} \\ \frac{-3}{15} & \frac{-3}{15} & \frac{-3}{15} \end{bmatrix} \quad S=\begin{bmatrix} \frac{5}{15} & \frac{5}{15} & \frac{5}{15} \\ \frac{-3}{15} & 0 & \frac{-3}{15} \\ \frac{-3}{15} & \frac{-3}{15} & \frac{-3}{15} \end{bmatrix} \quad E=\begin{bmatrix} \frac{5}{15} & \frac{5}{15} & \frac{-3}{15} \\ \frac{5}{15} & 0 & \frac{-3}{15} \\ \frac{-3}{15} & \frac{-3}{15} & \frac{-3}{15} \end{bmatrix}$$

$$NW=\begin{bmatrix} \frac{5}{15} & \frac{-3}{15} & \frac{-3}{15} \\ \frac{5}{15} & 0 & \frac{-3}{15} \\ \frac{5}{15} & \frac{-3}{15} & \frac{-3}{15} \end{bmatrix} \quad SW=\begin{bmatrix} \frac{-3}{15} & \frac{-3}{15} & \frac{-3}{15} \\ \frac{5}{15} & 0 & \frac{-3}{15} \\ \frac{5}{15} & \frac{5}{15} & \frac{-3}{15} \end{bmatrix} \quad SE=\begin{bmatrix} \frac{-3}{15} & \frac{-3}{15} & \frac{-3}{15} \\ \frac{-3}{15} & 0 & \frac{-3}{15} \\ \frac{5}{15} & \frac{5}{15} & \frac{5}{15} \end{bmatrix} \quad NE=\begin{bmatrix} \frac{-3}{15} & \frac{-3}{15} & \frac{5}{15} \\ \frac{-3}{15} & 0 & \frac{5}{15} \\ \frac{-3}{15} & \frac{5}{15} & \frac{5}{15} \end{bmatrix}$$

The edge magnitude is selected from the maximum value found by the convolution of each mask with the image. The edge direction is defined by the mask that produces the maximum magnitude. For example if NE produces the maximum value, then the edge direction is northeast. We combined the result images from exudate segmentation with the result images from edges detection by using a Boolean operator. Finally exudates mask is obtained. Fig. 5.9 illustrates the results before and after post processing.

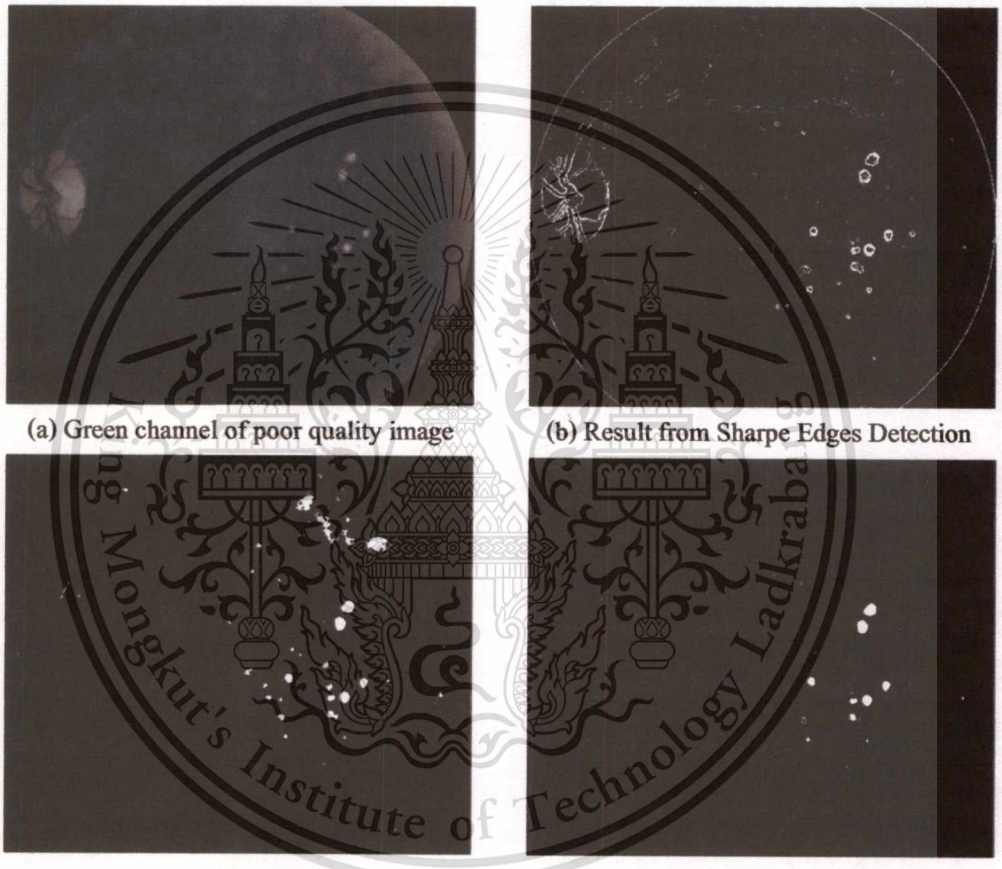

(a) Green channel of poor quality image

(b) Result from Sharpe Edges Detection

(c) Result from removing the bordered objects

(d) Result from applying post processing

Figure 5.9 The result before and after applying post processing.

5.4 Exudate Extraction

The final result of exudates mask is obtained after the post processing in subsection 5.3. To verify that our result is the real exudate or not, the real color of exudates is needed to be shown.

Therefore morphological reconstruction is used for this process. The exudates mask obtained is inverted before they are overlaid on the original retinal image to extract the lesions by utilizing Eq. (3.9), which the inverted exudate mask is used as the marker image, and the original image is used as the mask image. Fig. 5.10 shows the final result of exudate extraction.

Figure 5.10 The final result of exudate extraction.

CHAPTER 6

RESULTS AND DISCUSSION

In this chapter, the performance of the proposed algorithms result is demonstrated. The fundus images were obtained from Bhumibol Adulyadej Hospital with the resolution of 3872 x 2592 pixels in 24 bit JPEG format. These images contain all lesions related to DR (microaneurysms, hemorrhages, cotton-wool spots, exudate, etc.) and healthy images. 1579 fundus images with variable color, brightness and quality are used. These fundus images are classified into 3 groups by the ophthalmologists.

1. The first group is healthy fundus images which contain 218 images.
2. The second group has a little bit effect of exudate which contain contains 1059 images.
3. The third group has strong effect of exudate which contains 320 images.

In this thesis, because the ground truth information of lesions in the images is not made so the performance evaluation has been done over all the images by the verification of an ophthalmologist. The ophthalmologist verifies the exudate detection results for all test image sets based on the values of sensitivity and specificity. Sensitivity is used to measure the proportion of actual positives (exudate) which are correctly identified as exudate. Specificity is used to measures the proportion of negatives (non-exudate) which is correctly identified as non-exudate. The accuracy is the overall correctness of the system and is calculated as the sum of correct classifications divided by the total number of classifications.

Table 6.1 Result of exudate detection.

Methods	Pixel Counting	Maximum Entropy Thresholding
Accuracy from ophthalmologists	73%	85%
Average processing time per image	39.50 seconds	37.95 seconds

The results in Table 6.1 show that using the pixel counting and maximum entropy thresholding for binarization, 73% and 85% of exudate detection is obtained, respectively.

The reason that the proposed method cannot achieve 100% results because of presence of random noises and artifacts in some images as well as the quality of fundus images. The examples of the noises and artifacts that we cannot detect correctly are shown in Fig. 6.1 and Fig. 6.2.

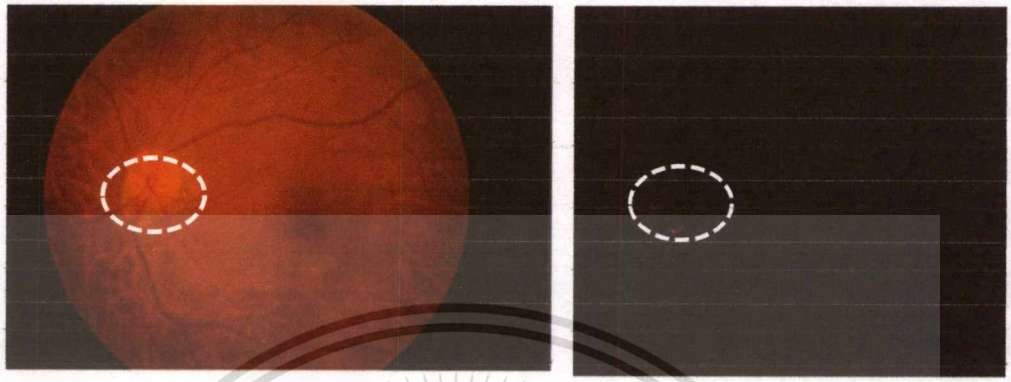

(a) The healthy fundus image affected by noises (b) The result of exudate extraction

Figure 6.1 An example of healthy fundus image affected by random noises.

Actually the result from healthy fundus image should contain nothing since the noises effect near the OD area have similar characteristic with the exudate, so the proposed method cannot discriminate for the real exudate in this case. The other effect is shown is Fig. 6.2. This effect is caused by the artifacts in some images.

(a) The healthy fundus image affected by artifacts (b) The result of exudate extraction

Figure 6.2 An example of healthy fundus image affected by artifacts.

Fig. 6.3 shows the other reason which can be occurred when the areas of noises or exudates wrongly detected as the OD area. To solve this problem, the area of OD should be more clearly

determined and discussed with the specialist on this field, or the more suitable method should be investigated.

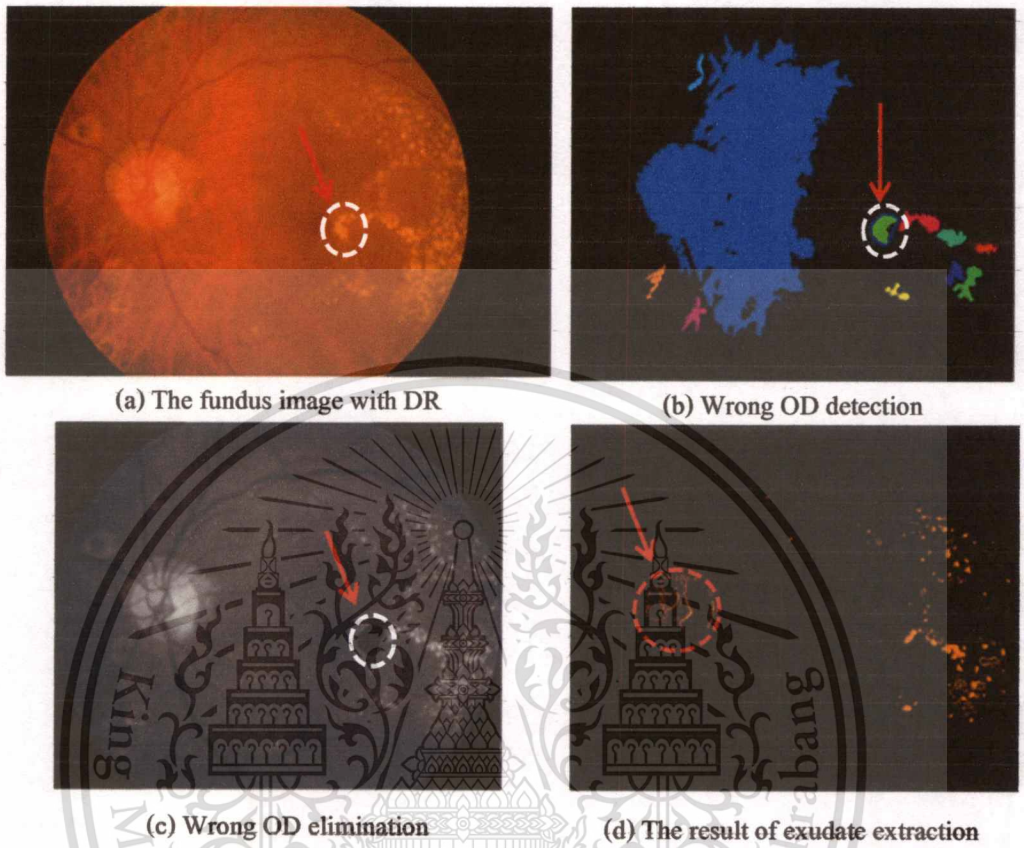

(a) The fundus image with DR (b) Wrong OD detection

(c) Wrong OD elimination (d) The result of exudate extraction

Figure 6.3 An example of wronging OD detection.

The results in Table 6.1 can be improved by choosing a better algorithm to discriminate the result of exudate detection with the seldom noises which appear as false positive. However, the proposed method does not require any training set which can make common issues with human segmentation inconsistencies. The training sets method requires large amounts of data and training process. Therefore it can be difficult to obtain in the practical use. Although this result is not achieve 100%, the average process time of this research takes only 37.95 second per image so it can be used to help the ophthalmologists if a better algorithm is investigated to improve the false positive.

Fig. 6.4, Fig. 6.5 and Fig. 6.6 show 100 fundus images which are randomly used with their results in this thesis.

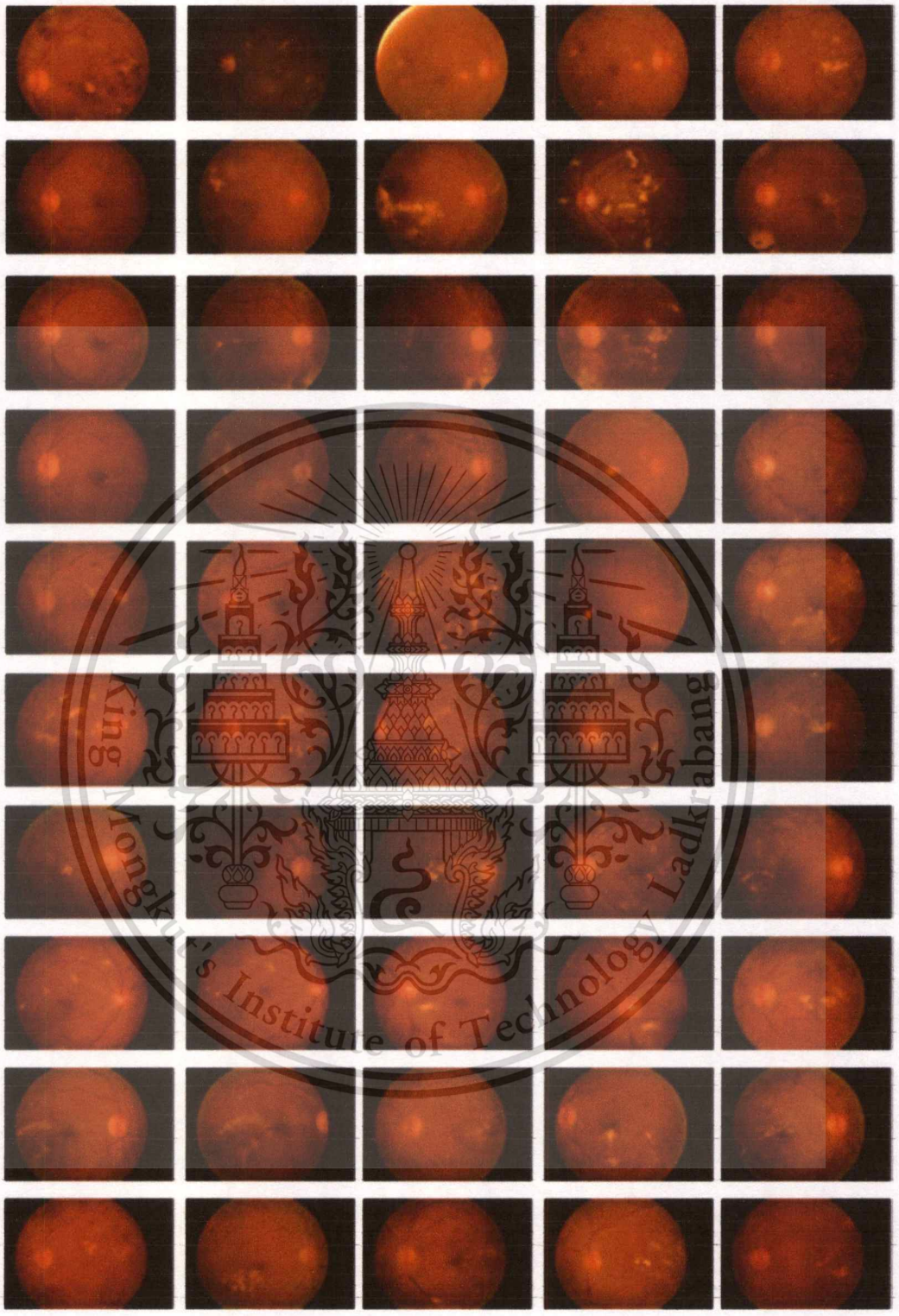

Figure 6.4 Fundus images which are used in this research (1).

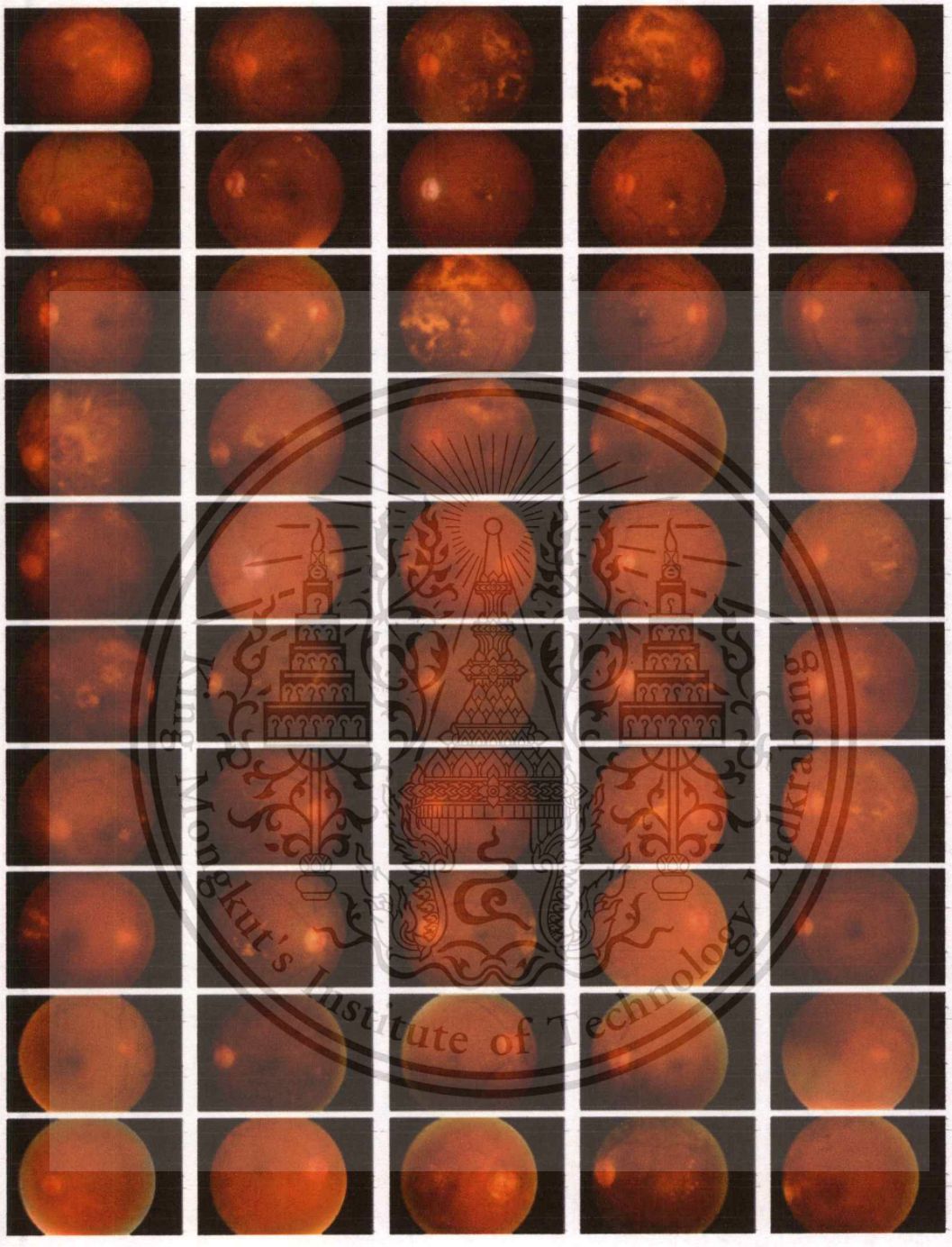

Figure 6.4 Fundus images which are used in this research (2).

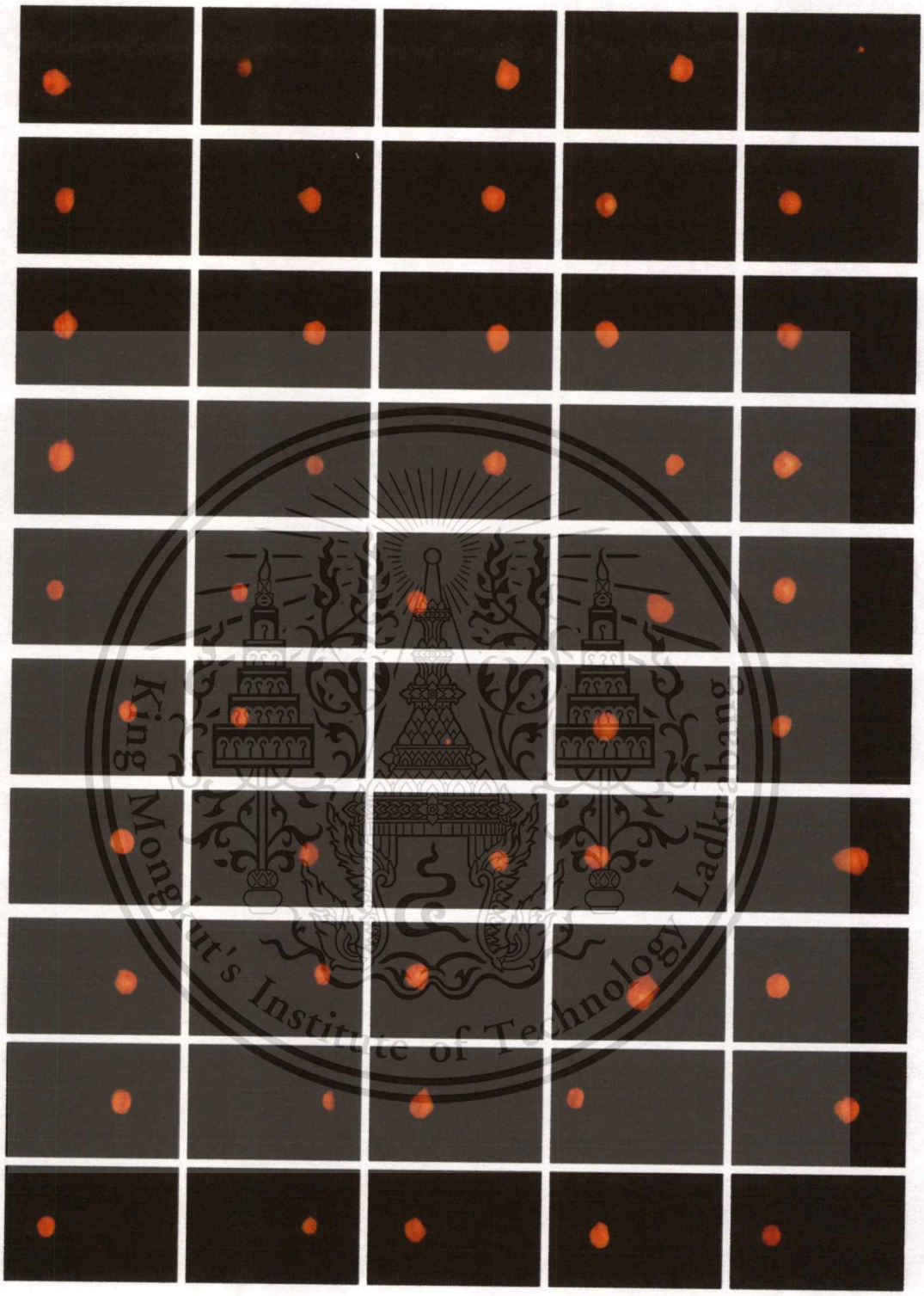

Figure 6.5 Results of OD extraction (1).

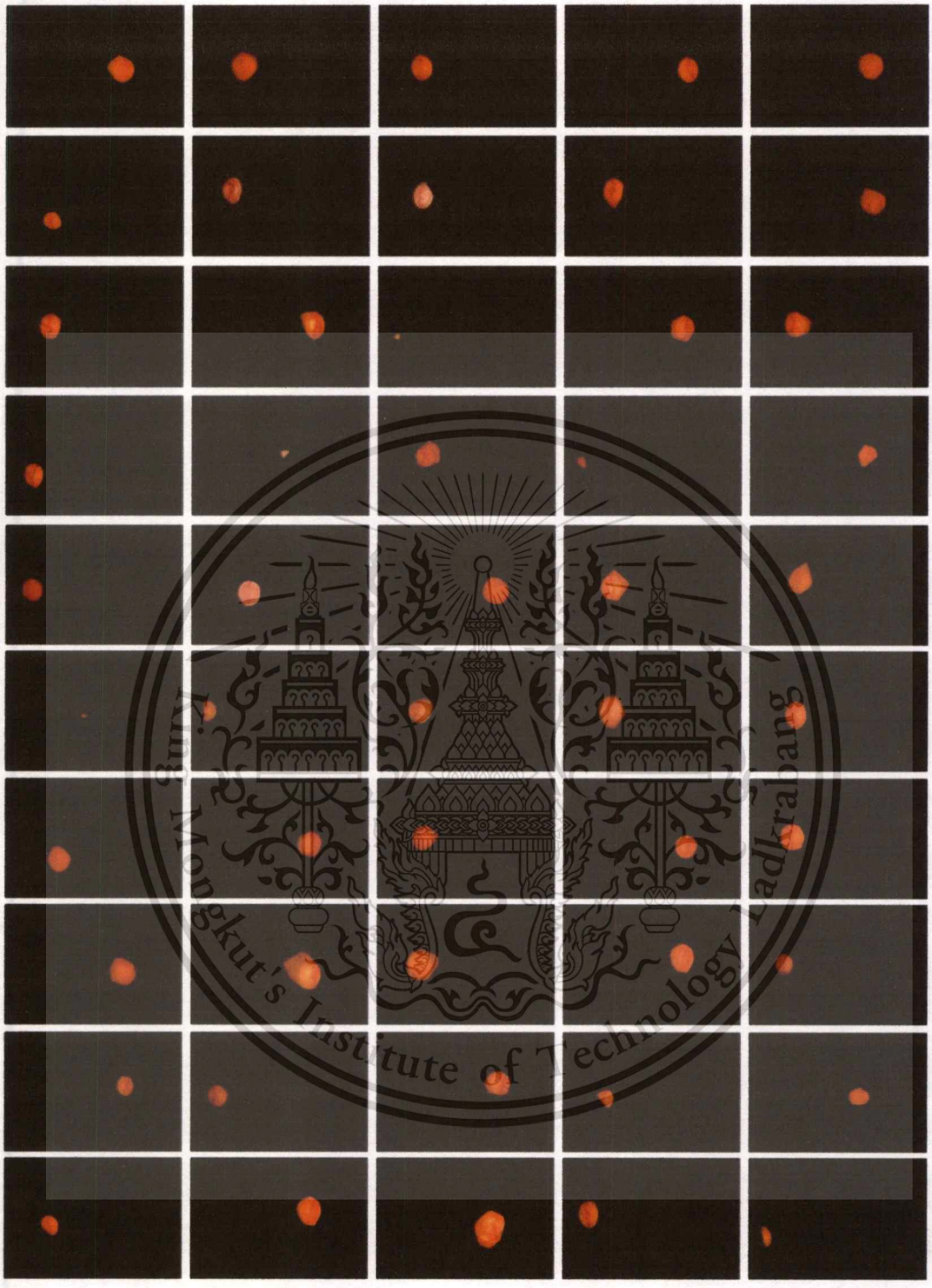

Figure 6.5 Results of OD extraction (2).

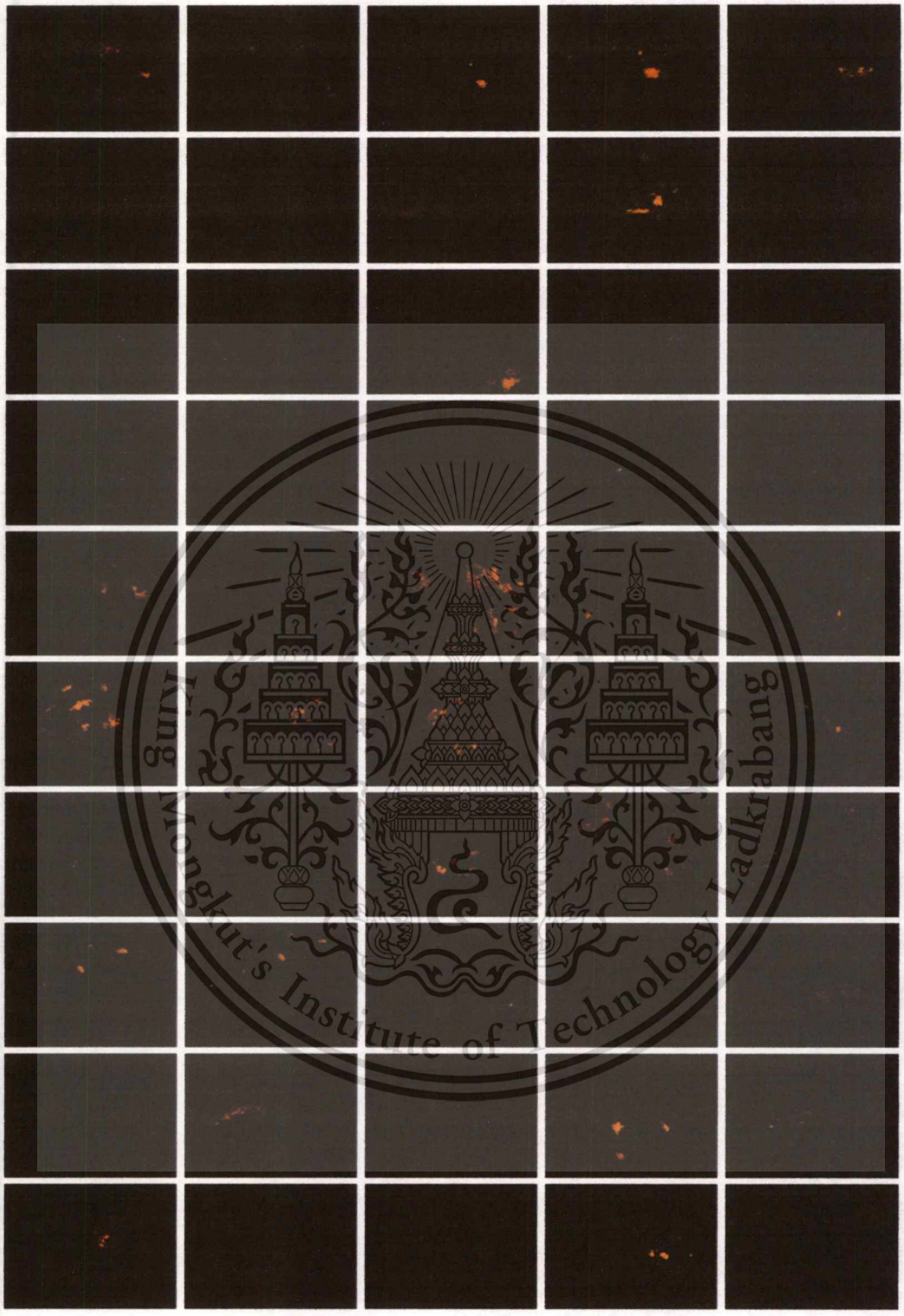

Figure 6.5 Results of exudate extraction (1).

Figure 6.5 Results of exudate extraction (2).

It is difficult to compare our algorithm with the other reported works in the literature because there are many methods which have been published throughout the years using variety of datasets, and the lack of databases with their ground truth for retinal structures. This is the reason that many researchers only show their methods and results, but do not compare with the past researches [13, 14, 19, 33, 41, 42, 43, 44]. However some methods of [13, 15, 19, 21, 26, 32, 33, 43, 44] did not report the average processing time per image and the other methods of [20, 45, 46] reported the lower performances to our approach with the same average processing time of 3 minutes.

CHAPTER 7

CONCLUSION

This thesis proposes methods to extract exudates for the automatic exudate detection. The proposed method is based on category of thresholding methods. We based our work on thresholding methods because it does not require high computing power and takes short time for processing. Computing power and processing time is very important for application in rural area in developing country where both expert ophthalmologists and high performance computers are rarely available.

There were four main issues that were addressed in this thesis:

1) How to improve the quality of the image by using the preprocessing step. We found that the red and green channels of RGB color space are suitable for using with the detection of OD and exudate respectively.

2) How to remove the OD which is known as the main interference of exudate detection. For removing the OD our proposed method is composed of 5 stages. First, preprocessing step is used to discuss on the problem of variable intensity in fundus image. Then two differences methods, pixel counting and maximum entropy thresholding, are applied to convert the image to binary image. After binarization the obtained object are all bright pixels which include all noises, OD and Exudates. Therefore the ROI based segmentation is used to select only the interesting object which is known as optic disc. The result from ROI based segmentation cannot detect all ODs correctly when the level of thresholding is too big or too small so the area of OD is estimated.

3) How to choose the suitable method for the measurement of the maximization information of the image to find the thresholding value automatically. We found that maximum entropy thresholding perform well for this issue.

4) How to solve the problem of poor quality image. There are two kinds of quality problems in the fundus images used in this research. The first is noise pixels whose colors are distorted. The second is noise from cotton wool spots, and artifacts in the papillary region that are characterized by high gray-level intensity. To solve these two problems, two methods are proposed. The first is clearing the illumination at the edge of fundus area, and the second is using the sharp edges detection to find the sharpness of the edges which are the characteristic of exudate in addition to high intensity.

The results show that by using the pixel counting and maximum entropy thresholding for exudate segmentation, the best performances are 73% and 85% of exudate detection obtained, respectively.

For the future work, the reason of the failure in some images should be more carefully examined, so that a new algorithm can be investigated to improve the present work as real application software for detection of diabetic retinopathy screening system.

References

[1] P. H. Scanlon, C. P. Wilkinson, S. J. Aldington and D. R. Matthews, A Practical Manual of Diabetic Retinopathy Management. Wiley-Blackwell, Oxford, UK, 2009.

[2] D.J. Withey, and Z.J. Koles, "Medical Image Segmentation: Methods and Software," Noninvasive Functional Source Imaging of the Brain and Heart and the International Conference on Functional Biomedical Imaging, 2007. NFSI-ICFBI 2007. Joint Meeting of the 6th International Symposium on, pp. 140-143, IEEE, 2007.

[3] Edited by Okechukwu Felix Erondu. Medical Imaging, 1th published, printed in Croatia, December 2006. ISBN 978-953-307-774-1.

[4] T. Chetthakul, C. Deerochanawong, S. Suwanwalaikorn, N. Kosachunhanun, C. Ngarmukos, P. Rawdaree, et al., "Thailand diabetes registry project: prevalence of diabetic retinopathy and associated factors in type 2 diabetes mellitus," J Med Assoc Thai 89, no. Suppl 1, S27-36, 2006.

[5] http://vspblog.com/camera-vs-the-human-eye.

[6] Laurelee Sherwood. Human Physiology-From Cell to Systems. Jack Carey, 2001.

[7] Gyuton, A. C., and Hall, J. E. Textbook of medical physiology, 11th edition. Elsevier Saunders, 2006.

[8] V. V. Kumari, and N. SuriyaNarayanan, "Detection of Optic Disk in Retinal Images-A Comparison," International Journal on Computer Science and Engineering, vol. 1, no. 3, pp. 192-195, 2009].

[9] David, J., , Krishnan, R., and Kumar, A. S. Neural network based retinal image analysis. In Proceedings of the International Congress on Image and Signal Processing (CISP2008) (2008), vol. 2, pp. 49 – 53.

[10] Foracchia, M., Grisan, E., and Ruggeri, A. Detection of optic disc in retinal images by means of a geometrical model of vessel structure. IEEE Transactions On Medical Imaging 23, 10 (October 2004), 1189–1195.

[11] Hutchinson A, McIntosh A, Peters J, Home P, Feder G, Baker R, Forrester J, Alexander W, Eltringham-Cox A, Greenwood R, Grimshaw G, Hine C, Khunti K, Wilson A, Woodward G, (2001) "Clinical guidelines and evidence review for Type 2 diabetes: Diabetic retinopathy: early management and screening" Sheffield: ScHARR, University of Sheffield.

[12] Thesis: Tomi Kauppi "Eye Fundus Image Analysis For Automatic Detection Of Diabetic Retinopathy", ISBN 978-952-265-016-0, December 12, 2010, Lappeenranta University of Technology, Lappeenranta, Finland.

[13] C. I. Sánchez, M. García, A. Mayo, M. I. López, and R. Hornero, "Retinal image analysis based on mixture models to detect hard exudates," Medical Image Analysis 13, vol. 4, pp. 650-568, 2009.

[14] L. Giancardo, F. Meriaudeau, T. P. Karnowski, Y. Li, K. W. Tobin, and E. Chaum, "Automatic retina exudates segmentation without a manually labelled training set," In Biomedical Imaging: From Nano to Macro, 2011 IEEE International Symposium, pp. 1396-1400, IEEE, 2011.

[15] B. Venkatalakshmi, V. Saravanan, and G. Niveditha, "Graphical user interface for enhanced retinal image analysis for diagnosing diabetic retinopathy," Communication Software and Networks (ICCSN), 2011 IEEE 3rd International Conference, pp. 610-613, IEEE, 2011.

[16] A. Sopharak, B. Uyyanonvara, S. Barman, and T. H. Williamson, "Automatic detection of diabetic retinopathy exudates from non-dilated retinal images using mathematical morphology methods," Computerized Medical Imaging and Graphics 32, no. 8, pp. 720-727, 2008.

[17] H. Li, and O. Chutatape, "Automated feature extraction in color retinal images by a model based approach," Biomedical Engineering, IEEE Transactions, vol. 51, no. 2, pp. 246-254, 2004.

[18] C. Sinthanayothin, J. F. Boyce, T. H. Williamson, H. L. Cook, E. Mensah, S. Lal, and D. Usher, "Automated detection of diabetic retinopathy on digital fundus images," Diabetic Medicine, vol. 19, no. 2, pp. 105-112, 2002.

[19] A. Sopharak, K. T. Nwe, Y. A. Moe, M. N. Dailey, and B. Uyyanonvara, "Automatic exudate detection with a naive Bayes classifier," Proceedings of the 2008 International Conference on Embedded Systems and Intelligent Technology, pp. 139-142, 2008.

[20] A. Osareh, B. Shadgar, and R. Markham, "A computational-intelligence-based approach for detection of exudates in diabetic retinopathy images," Information Technology in Biomedicine, IEEE Transactions on, vol. 13, no. 4, pp. 535-545, 2009.

[21] M. Garciaa, C. I. Sáncheza, M. I. Lópezb, D. Abásoloa, and R. Horneroa, "Neural network based detection of hard exudates in retinal images," Computer methods and programs in biomedicine, vol. 93, no. 1, pp. 9-19, 2009.

[22] A. Sopharak, K. T. Nwe, Y. A. Moe, M. N. Dailey, and B. Uyyanonvara, "Automatic exudate detection with a naive Bayes classifier," Proceedings of the 2008 International Conference on Embedded Systems and Intelligent Technology, pp. 139-142, 2008.

[23] K. Wisaeng, N. Hiransakolwong, and E. Pothiruk, "Automatic Detection of Exudates in Diabetic Retinopathy Images," Journal of Computer Science, vol. 8, no. 8, pp 1304-1313, 2012.

[24] B. Venkatalakshmi, V. Saravanan, and G. Niveditha, "Graphical user interface for enhanced retinal image analysis for diagnosing diabetic retinopathy," Communication Software and Networks (ICCSN), 2011 IEEE 3rd International Conference on, pp. 610-613, IEEE, 2011.

[25] Bankman, Isaac, ed. Handbook of medical image processing and analysis. Access Online via Elsevier, 2008.

[26] McAndrew, Alasdair. "An introduction to digital image processing with matlab", notes for SCM2511 image processing, School of Computer Science and Mathematics, Victoria University of Technology, 2004.

[27] Rafael C. Gonzalez and Richard E. Woods. Digital Image Processing, 2nd edition. Prentice Hall, 2002. ISBN 0-201-18075-8.

[28] H. F. Jaafar, A. K. Nandi, and W. Al-Nuaimy, "Detection of exudates from digital fundus images using a region-based segmentation technique," In 19th European Signal Processing Conference EUSIPCO, 2011.

[29] M. Esnaashari, S. A. Monadjemi, and G. Naderian, "A content-based retinal image retrieval method for diabetes-related eye diseases diagnosis," International Journal of Research and Reviews in Computer Science (IJRRCS), vol. 2, no. 6, 2012.

[30] K. Saranya, B. Ramasubramanian, and S. Kaja Mohideen, "A novel approach for the detection of new vessels in the retinal images for screening Diabetic Retinopathy," Communications and Signal Processing (ICCSP), 2012 International Conference, pp. 57-61, IEEE, 2012.

[31] A. Feroui, M. Messadi, I. Hadjidj, and A. Bessaid, "New segmentation methodology for exudate detection in color fundus images," Journal of Mechanics in Medicine and Biology, vol. 13, no. 01, 2013.

[32] M. Azarbad, A. Ebrahimzade, and V. Izadian, "Segmentation of Infrared Images and Objectives Detection Using Maximum Entropy Method Based on the Bee Algorithm," International Journal of Computer Information Systems and Industrial Management Applications (IJCISIM), vol.3, pp. 026-033, 2011

[33] Shannon, C.E. and W. Weaver (1949), "The Mathematical Theory of Communication (Urbana, lL." University of Illinois Press 19, no. 7, 1949.

[34] N. Jamil, and Z. A. Bakar, "Shape-Based Image Retrieval of Songket Motifs," In 19th Annual Conference of the NACCQ, pp. 213-219, 2006.

[35] J. Nayak, R. Acharya, P. S. Bhat, N. Shetty, and T. C. Lim, "Automated diagnosis of glaucoma using digital fundus images," Journal of medical systems, vol. 33, no. 5, pp 337-346, 2009.

[36] S. Kavitha, S. Karthikeyan, and K. Duraiswamy, "Neuroretinal rim Quantification in Fundus Images to Detect Glaucoma,". IJCSNS, vol. 10, no. 6, pp 134, 2010.

[37] V. Thongnuch, and B. Uyyanonvara, "Automatic optic disk detection from low contrast retinal images of ROP infant using GVF snake," Suranaree J. Sci. Technol, vol. 14, no. 3, pp. 223-226, 2007.

[38] M. Azarbad, A. Ebrahimzade, and V. Izadian, "Segmentation of Infrared Images and Objectives Detection Using Maximum Entropy Method Based on the Bee Algorithm," International Journal of Computer Information Systems and Industrial Management Applications (IJCISIM), vol.3, 026-033, 2011.

[39] http://www.mathworks.com.

[40] Gian cardo L, Meriaudeau F, Karnowski TP, Li Y, Tobin KW, Jr., Chaum E, Automatic retina exudates segmentation without a manually labelled training set, IEEE Int Symp Biomedical Imaging: From Nano to Micro, 2011.

[41] S. Sreng, N. Maneerat, D. Isarakorn, R. Varakulsiripunth, B. Pasaya, J. Takada, and R. Panjaphongse, "Feature Extraction from Retinal Fundus Image for Early Detection of Diabetic Retinopathy," IEEE Region 10 Humanitarian Technology Conference 2013, pp. 69-72, August 26-29, Sendai, Japan.

[42] K. Wisaeng, N. Hiransakolwong, and E. Pothiruk, "Automatic Detection of Exudates in Diabetic Retinopathy Images," Journal of Computer Science, vol. 8, no. 8, pp 1304-1313, 2012.

[43] A. Sopharak, B. Uyyanonvara, and S. Barman, "Automatic exudate detection from non-dilated diabetic retinopathy retinal images using fuzzy C-means clustering," Sensors 9, no. 3, pp. 2148-2161, 2009.

[44] R. SriRanjini, and M. Devaki, "Detection of Exudates in Retinal Images Based on Computational Intelligence Approach," International Journal of Computer Science and Network Security, vol.13, no. 3, pp. 86, march 2013.

[45] A. Sopharak, B. Uyyanonvara, S. Barman, and T. H. Williamson, "Automatic detection of diabetic retinopathy exudates from non-dilated retinal images using mathematical morphology methods," Computerized Medical Imaging and Graphics 32, no. 8, pp. 720-727, 2008.

[46] A. Sopharak, B. Uyyanonvara, and S. Barman, S. Vongkittirux, and N. Wongkamchang, "Fine exudate detection using morphological reconstruction enhancement," International Journal of Applied Biomedical Engineering vol.1, no.1, pp. 45-50, 2010.

Appendix A

Author Biography

Personal Information

Name	SYNA SRENG
Nationality	Cambodian
Date of birth	March 10, 1988
Place of birth	Kompong Popil Commune, Peal Raing District, Prey Veng Province, Cambodia

Education

Bachelor degree

Field	Electronics, Automation and Telecommunication
Duration	2006-2011
Department	Department of Electrical and Energy Engineering
University	Institute of Technology of Cambodia

Master degree

Field	Computer Engineering
Duration	2011-2013
Department	Instrumentation and Control Engineering
Faculty	International College
University	King Mongkut's Institute of Technology Ladkrabang (KMITL), Thailand

Research Interests

Application of digital image processing such as automatic diabetic retinopathy screening system, system matching and pattern recognition

Appendix B

List of Publications

[1] Syna Sreng, Noppadol Maneerat, Jun-ichi Takada, Don Isarakorn, Ruttikorn Varakulsiripunth, Bundit Pasaya, and Ronakorn Panjaphongse M.D, *"Automatic Exudate Extraction for Early Detection of Diabetic Retinopathy,"* The 5th International Conference on Information Technology and Electrical Engineering, October 7-8, 2013, Yogyakarta, Indonesia.

[2] Syna Sreng, Noppadol Maneerat, Jun-ichi Takada, Don Isarakorn, Ruttikorn Varakulsiripunth, Bundit Pasaya, and Ronakorn Panjaphongse M.D, *"Feature Extraction from Retinal Fundus Image for Early Detection of Diabetic Retinopathy,"* IEEE Region 10 Humanitarian Technology Conference 2013, pp. 69-72, August 26-29, Sendai, Japan.

[3] Sreng Syna, Santikon Amnuayphol, Purachai Chongsomchai, Nattapong Chawalitsakulchai, Noppadol Maneerat, Ruttikorn Varakulsiripunth, Suwannee Junyapoon, *"Automatic Colony Counter based on Image Processing,"* 5th AUN/SEED-Net Regional Conference on Information and Communications Technology, pp. 11-14, October 18-19, 2012, Manila, Philippines.

ISSN: 2088-6578
ISBN: 978-1-4799-0423-5

50th ANNIVERSARY
DEPARTMENT OF ELECTRICAL ENGINEERING AND INFORMATION TECHNOLOGY UGM

IEEE
Advancing Technology for Humanity

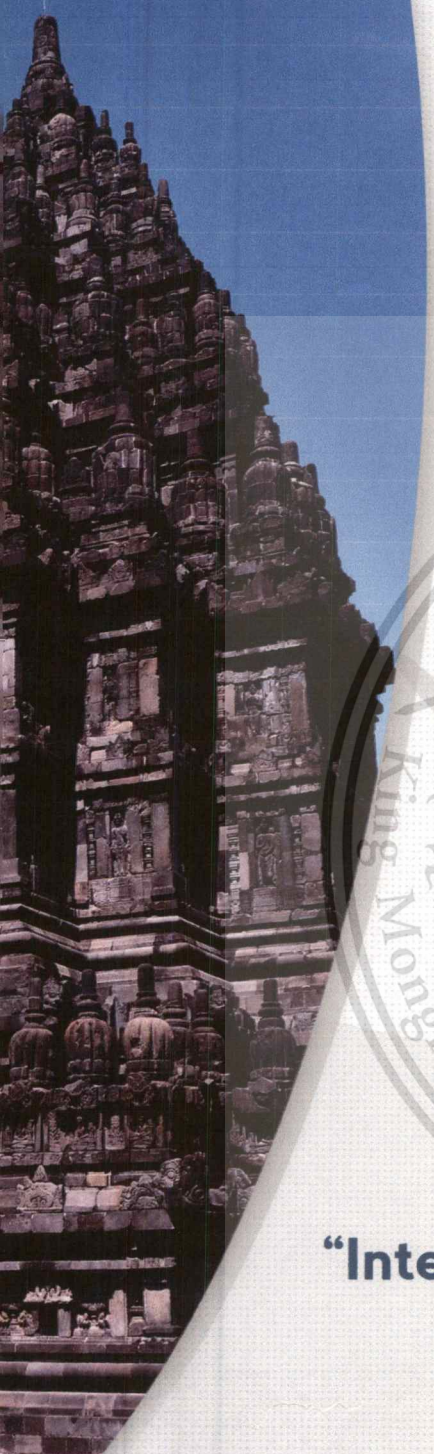

ICITEE 2013

Proceedings of

2013 International Conference on Information Technology and Electrical Engineering

7-8 October 2013
The Sahid Rich Jogja Hotel
Yogyakarta, Indonesia

"Intelligent and Green Technologies for Sustainable Development"

Organized by
Department of Electrical Engineering and Information Technology
Universitas Gadjah Mada, Indonesia

ICITEE 2013 Sponsorships

Technically Co-Sponsored by

IEEE
INDONESIA SECTION

Supported by

Indonesian
Society For Soft-Computing

LPPM UGM

Automatic Exudate Extraction for Early Detection of Diabetic Retinopathy

Syna Sreng
International College
King Mongkut's Institute of Technology Ladkrabang
Bangkok, Thailand
srengsina@yahoo.com
s4601152@kmitl.ac.th

Noppadol Maneerat, Don Isarakorn,
Bundit Pasaya
Faculty of Engineering
King Mongkut's Institute of Technology Ladkrabang
Bangkok, Thailand
kmnoppad@kmitl.ac.th

Jun-ichi Takada
Graduate School of Science and Engineering
Tokyo Institute of Technology
Tokyo, Japan
takada@ide.titech.ac.jp

Ronakorn Panjaphongse M.D
Ophthalology Department
Bhumibol Adulyadej Hospital
Royal Thai Air Force
Bangkok, Thailand
ronakorn_p@rtaf.mi.th

Ruttikorn Varakulsiripunth
Faculty of Information Technology
Thai-Nichi Institute of Technology
Bangkok, Thailand
kvruttik@hotmail.com

***Abstract*—Diabetic Retinopathy (DR) is the most common cause of blindness in diabetic patients, but early detection and timely treatment can prevent this problem. Exudates have been found to be one of the signs and serious DR anomalies so the proper detection of these lesions and the treatment should be done immediately to prevent loss of vision. The aim of this study is to automatically detect these lesions in fundus images. To achieve this goal, the proposed method first preprocesses to improve the quality of fundus image, and then Optic Disc (OD) is detected and eliminated to prevent the interference to the result of exudate detection by combination of 3 methods; image binarization, Region Of Interest (ROI) based segmentation and Morphological Reconstruction (MR). Next, exudates are detected by applying the maximum entropy thresholding to filter out the bright pixels from the result of OD region eliminated. Since the result contains some noises which appear as bright light at the edge of fundus area in some images, that affect is considered and eliminated to improve the result of false positive. Finally, exudates are extracted by using MR. The proposed technique has been tested on 100 fundus images from hospital. Experimental results show that 91 % of exudate is extracted correctly with the average process of 3.92 second per image.**

Keywords— optic disc; exudate; diabetic retinopathy; maximum entropy thresholding; morphological reconstruction

I. INTRODUCTION

Diabetes mellitus is a group of diseases characterized as the chronic condition in which there is an excess of glucose circulating in the bloodstream [1]. The effect of diabetic mellitus on the eye is called DR. It is a visual complication and becomes the most common cause of visual loss and blindness. Early detection and timely treatment can prevent the problem. For this reason, all diabetic patients should get their both eyes examined quit often (at least once every year). Ophthalmologists play a most important role to help diabetic patients for an eye examination. However, the number of ophthalmologists is limited in Thailand. The study of Thailand diabetic project shows that about one thousand ophthalmologists have to work with six million diabetic patients. Among all of them about 30 percent of patients are effected by DR [2]. Therefore, automatic retinal image analysis is very useful to help ophthalmologists in detection and diagnosis of DR. DR clinical signs includes microaneurysms, microvascular abnormalities, hemorrhages, cotton-wool spots and exudate. Exudate is among the signs of DR so the proper detection of these lesions is an essential task. It appears as bright lesions with the random yellowish deposits of varying size, shapes and location in retinal images. On the research work leading to automatic analysis of exudate detection, the knowledge of OD location is very useful. OD is known as the bright circular region which appears with similar features as exudates. So, in order to prevent the result of exudate detection from the interference of OD, it should be removed out first.

In the past researches, exudate detection was presented in different categories. Thresholding methods base on intensity levels and color image [3-5]. A combination of region growing and edge detection was used in [6, 7]. The classification methods build a feature vector for each pixel classification by

This work is financial supported by AUN SEED-Net program under the Research collaboration scheme, Coordinating Center for Thai Government Science and Technology Scholarship students (CSTS) and National Science and Technology Development Agency (NSTDA).

using a naive Bayes classifier [8] and color images clustering [9], as well as a neural network classifier was used in [10].

The aim of this study is to automatically detect exudates in fundus images. To achieve the goal, this paper proposes a new algorithm to extract exudates based on maximum entropy thresholding and morphological reconstruction, which falls into the category of thresholding method. This proposed method does not require any training set which can make common issue to be processed. In addition, training sets method requires large amounts of data therefore it takes long time for processing and can be difficult to obtain in the real application. Thresholding method is used in this work because it does not require high computing power and takes short time for processing. Computing power and processing time are very important for application in rural area in developing country where both expert ophthalmologists and high performance computers are rarely available.

In the previous work, we proposed the method for detection of exudate by calculating the pixel count for estimating the histogram of the gray level image and blob boundary detection as well as MR for elimination of OD first. Then maximum entropy thresholding was applied for exudate detection [11]. On verification the result from the ophthalmologists, the accuracy of 89% was obtained. Since this result is limited by variable intensity in retinal images, we perform a new method to measure the maximization of information by using maximum entropy threshold. Next ROI based segmentation and MR are used for the step of OD detection and elimination. Then maximum entropy thresholding is applied again on result of OD region eliminated. After that the bright light which appears at the edges of retinal area in some images is also considered and eliminated to improve the result of false positive. Finally, exudates are extracted by using MR. Overall accuracy of 91% is successful.

The rest of paper is organized as follows: section II briefly summarizes the different stages of the proposed algorithm. Section III describes the results and discussions, and finally section IV is conclusion.

II. METHODOLOGY

The proposed method for exudate detection is composed of three main stages: *A.* preprocessing, *B.* OD elimination and *C.* exudate extraction.

A. Preprocessing

Abnormality detection in fundus image is very complicated with the differences in luminosity, brightness and contrast inside fundus images. Preprocessing step is very important to solve these problems. The fundus images database from hospital are stored in RGB color space which consists of three components (red, green and blue). Since the process of this proposed method has two main steps (OD and Exudate detections) so the preprocessing step has to consider in both cases. From the analysis of RGB component of the images, we found that the exudate is more easily discriminated in green component because it has higher contrast and more energy [12-13], but the OD is more easily discriminated in red component [14-17] because it is brighter in intensity. Fig. 1 shows the original image with its red, green and blue components. This figure illustrates that in green component, the OD is separated by blood vessel. Therefore it is difficult to define the shape of OD when the image is converted to binary image, but in the red component, the OD is easily defined with the characteristic of the most circular region after binary segmentation.

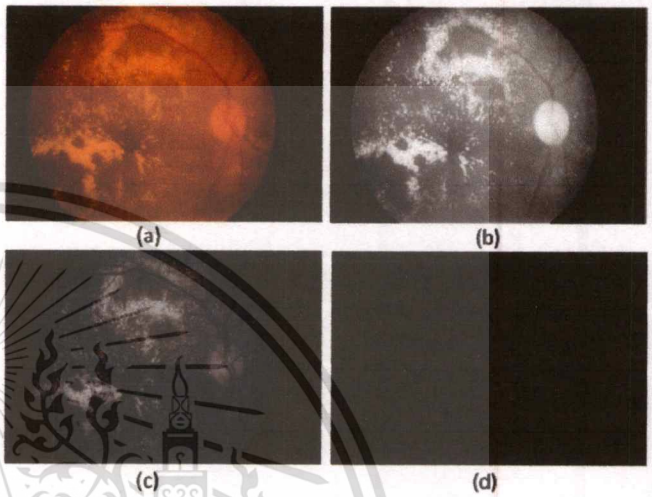

Figure 1. (a) Original Image (b) Red Component (c) Green Component (d) Blue Component

For analysis using both green and red components, first the original image is converted into the red component (for OD detection) then into the green component (for exudate detection), and finally median filtering is applied to reduce noise on the green component.

B. OD Elimination

The OD is referred to the optic nerve inside our eye. It appears as a bright circular region which is similar characteristic to the exudate. In order to prevent the result of exudate detection from the interference of OD, it should be removed out first [5, 8, 18]. In this paper, OD elimination detection involves three steps as shown in following:

- Image binarization
- ROI based segmentation
- Morphological reconstruction

1) Image binarization

In clinical environment, the variable intensity in fundus images is considered as one of the main obstacles for exudate detection as well as OD detection because the range of intensity value varies from one image to another. To take these differences into account, we measure the maximization of the information between object and background by using maximum entropy thresholding described in [19, 20]. In this research the entropy function is studied on 1D histogram of the

gray level image. Suppose i is the gray level value of an image so $i = [0, 1 \dots t-1, t, t+1 \dots 255]$, and the probability of the pixel being i can be defined as:

$$P_i = \frac{n_i}{n} \quad (1)$$

where n is the total number of pixels in the image and n_i is the number of pixels that have gray level i.

Let o and b represent the object and background respectively thus the probabilities of o and b can be calculated as:

$$P_o = \sum_{i=0}^{t-1} P_i \quad (2)$$

$$P_b = \sum_{i=t}^{255} P_i \quad (3)$$

So the entropies of object and background's probability distributions are given as:

$$H_o(t) = -\sum_{i=0}^{t-1} \frac{P_i}{P_o} \log_2 \frac{P_i}{P_o} \quad (4)$$

$$H_b(t) = -\sum_{i=t}^{255} \frac{P_i}{P_b} \log_2 \frac{P_i}{P_b} \quad (5)$$

Thus the entropy of the gray level image segmented by threshold t is:

$$H(t) = H_o(t) + H_b(t) \quad (6)$$

The theory of maximum entropy is used to select t which makes H becomes maximum value. So, the optimal threshold t can be selected by maximizing the entropy of $H(t)$ which can be defined as:

$$t = \text{Arg Max}(H(t)) \quad (7)$$

where $0 \leq t \leq 255$

The object is detected as the bright pixels after apply the level of threshold t on the red component of fundus image.

2) ROI based segmentation

In this method the OD is extracted by finding the region of interest based on two processes; neighborhood connecting pixels and compactness measurement, respectively. After binarization, there are more than one candidate regions identified. So, first we applied neighborhood connecting pixels to label all group pixels then all small holes of the group pixels is filled to make them smooth. Finally, compactness measurement in [21] is used to find the most circular region which is considered as OD. The maximum value of compactness will be 1 if the region is a circle. This value will decrease depend on its shape. For example elliptical-shaped regions, and irregular-shaped regions, as well as the other complicated boundaries regions. The equation of compactness measurement is defined as:

$$C(\mathcal{R}) = \frac{4\pi A(\mathcal{R})}{l_p^2(\mathcal{R})} \quad (8)$$

where $\mathcal{R}$ is the connected region with the pixels more than twenty thousands, as all connected region with the pixels less than twenty thousands are considered as noise and are eliminated. $A(\mathcal{R})$ is the number of pixels in region $\mathcal{R}$ and $l_p(\mathcal{R})$ is the length of boundary region $\mathcal{R}$.

3) Morphological reconstruction

The process of MR is based on dilation on two images, a marker and a mask. The resulting image from ROI based segmentation is used as a marker and the result of green component from the preprocessing is used as a mask. All the pixels in the marker image are overlaid on the mask image by the dilation of the marker image repeatedly until the contour of the marker image fits under the mask image. The expression is defined as:

$$\text{OD}_g = R_B(\text{F}) \quad (9)$$

where B is the mask image, F is the marker image, and OD_g is the reconstruction of B from F, which is the result of OD region eliminated. The process and result of OD elimination is shown in Fig. 2.

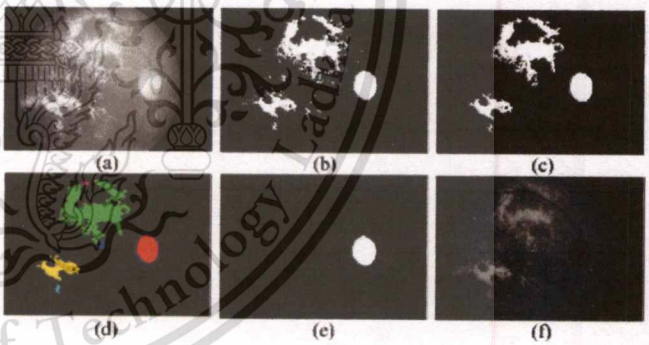

Figure 2. OD Elimination. (a) Red Component of Retinal Images (b) Result of Binarization (c) Removing Small Pixels (d) OD Detection (e) OD Mask (d) Result of OD Region Eliminated

C. Exudate Extraction

In some cases the interference of the exudates detection is not only the OD, but also the bright light which appears at the edge of fundus area depending on the quality of the images. Fig. 3 shows these kinds of poor quality images which are also included in this database.

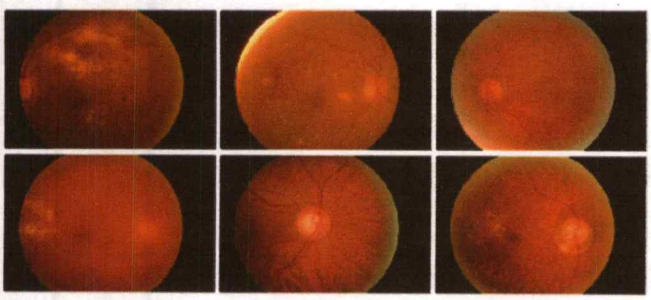

Figure 3. Fundus Images which Bright Light Appears at the Edge of Its Fundus Area

The fundus images obtained from a hospital consist of a circular fundus and a dark background surrounding the fundus area so in order to detect the bright light affect first we have to make that affect becomes the edge of fundus image by cropping the result image after OD elimination. Then, maximum entropy thresholding apply in image binarization is used to filter out the left bright objects that are considered as the exudate mask. Since the result of this work not contains only exudates but also some noises from the effect of light at the edge of retinal area in some cases so clearing border objects [22] which is a part of morphological image processing is used. Its syntax is:

$$C_b = \text{imclearborder}(C_r, \text{conn}) \quad (10)$$

where C_r is the cropping result of OD region elimination and C_b is the result of exudates mask. The value of conn is 8 because 8-connected neighborhood is used.

Finally exudates mask which obtained is inverted before they are overlaid on the original retinal image to extract the lesions by utilizing Eq. (9), where the inverted exudate mask is used as the marker image, and the original image is used as the mask image. Fig. 4 illustrates the result of this process.

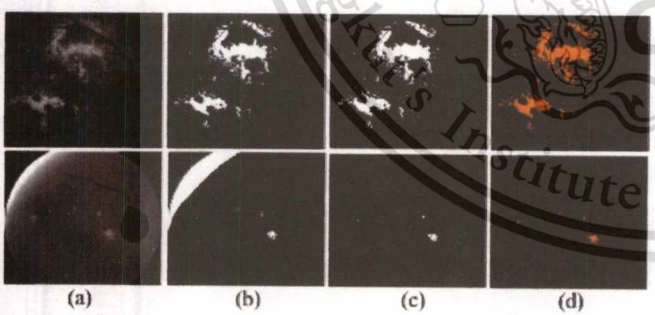

Figure 4. Exudates Extraction. (a) Cropping the Results of OD Elimination (b) Binarization after Cropping (c) Exudates Mask after Removing the Bordered Objects (d) Results of Exudates Extraction

III. RESULTS AND DISCUSSIONS

In this study, 100 fundus images with variable color, brightness and quality are used. The images were obtained from Bhumibol Adulyadej Hospital with the resolution of 3872x2592 pixels in 24 bit JPEG format. These images contain all lesions related to DR (microaneurysms, microvascular abnormalities, hemorrhages, cotton-wool spots, exudate, etc.) and healthy images. The accuracy is the overall correctness of the system and is calculated as the sum of correct classifications divided by the total number of classifications as define in Eq. (11).

$$\text{Accuracy} = \frac{TP+TN}{TP+TN+FN+FP} \quad (11)$$

From Eq. (11), TP, TN, FP and FN are numbers of classifications. TP is when all exudates are correctly identified as exudate. FN is when some exudates are incorrectly identified as non-exudate. TN is when all non-exudates are correctly identified as non-exudate and FP is when some non-exudates are incorrectly identified as exudate. Performance evaluation has been done over all the images by the verification of ophthalmologists. The result shows that 91 % of exudates detection was successful. The reason that the proposed method cannot achieve 100% results because of presence of noise and artifacts in some images as well as the quality of retinal images. This result can be improved by choosing a better algorithm to discriminate the result of exudate detection with the seldom noises which appear as false positive. However, the proposed method does not require any training set which can make common issues with human segmentation inconsistencies. The training sets method requires large amounts of data and training process. Therefore it can be difficult to obtain in the real application. Although this result is not achieve 100%, the average process of this research takes only 3.92 second per image so it can be used to help the Ophthalmologists for the real application if a better algorithm is investigated to improve the false positive.

Because of many methods have been published throughout the years using a variety of datasets, and the lack of a database with their ground truth for retinal structures, so it is difficult to compare our algorithm with the other reported work in the literature. This is the reason that many researchers only show their methods and results, but do not compare with the past researches [3, 4, 8, 11, 17, 18, 23, 24]. However some methods of [3, 5, 8, 10, 13, 16, 17, 23, 24] do not report the average processing time per image and the other methods of [9, 25, 26] report the lower performances to our approach with the same average processing time of 3 minutes.

IV. CONCLUSION

This paper proposed the method to extract exudates for early detection of DR. First, preprocessing is performed to improve the quality of fundus image, and then OD is detected and eliminated to prevent the interference to the result of exudate detection by combination of 3 methods; image binarization, ROI based segmentation and MR. Next the maximum entropy threshold is applied on result of OD region eliminated to filter out the exudate mask. Since the result contains some noises which appear as bright light at the edge of retinal area in some images, that affect is considered and eliminated to improve the result of false positive. Finally, exudates are extracted by using MR. Overall accuracy of 91%

was successful with the average process of 3.92 second per image.

For the future work, the reason of the failure in some images should be more carefully examined, so that a new algorithm can be investigated to improve the present work as real application software for early detection of diabetic retinopathy screening system.

ACKNOWLEDGMENT

This research is supported by Coordinating Center for Thai Government Science and Technology Scholarship students (CSTS) National Science and Technology Development Agency (NSTDA). The authors also would like to thank AUN/SEED-Net for financial support of one of the authors (Mr. Syna Sreng) for his study at King Mongkut's Institute of Technology Ladkrabang (KMITL), THAILAND.

REFERENCES

[1] P. H. Scanlon, C. P. Wilkinson, S. J. Aldington and D. R. Matthews, A Practical Manual of Diabetic Retinopathy Management. Wiley-Blackwell, Oxford, UK, 2009.

[2] T. Chetthakul, C. Deerochanawong, S. Suwanwalaikorn, N. Kosachunhanun, C. Ngarmukos, P. Rawdaree, et al., "Thailand diabetes registry project: prevalence of diabetic retinopathy and associated factors in type 2 diabetes mellitus," J Med Assoc Thai 89, no. Suppl 1, S27-36, 2006.

[3] C. I. Sánchez, M. García, A. Mayo, M. I. López, and R. Hornero, "Retinal image analysis based on mixture models to detect hard exudates," Medical Image Analysis 13, vol. 4, pp. 650-568, 2009.

[4] L. Giancardo, F. Meriaudeau, T. P. Karnowski, Y. Li, K. W. Tobin, and E. Chaum, "Automatic retina exudates segmentation without a manually labelled training set," In Biomedical Imaging: From Nano to Macro, 2011 IEEE International Symposium, pp. 1396-1400, IEEE, 2011.

[5] B. Venkatalakshmi, V. Saravanan, and G. Niveditha, "Graphical user interface for enhanced retinal image analysis for diagnosing diabetic retinopathy," Communication Software and Networks (ICCSN), 2011 IEEE 3rd International Conference, pp. 610-613, IEEE, 2011.

[6] H. Li, and O. Chutatape, "Automated feature extraction in color retinal images by a model based approach," Biomedical Engineering, IEEE Transactions, vol. 51, no. 2, pp. 246-254, 2004.

[7] C. Sinthanayothin, J. F. Boyce, T. H. Williamson, H. L. Cook, E. Mensah, S. Lal, and D. Usher, "Automated detection of diabetic retinopathy on digital fundus images," Diabetic Medicine, vol. 19, no. 2, pp. 105-112, 2002.

[8] A. Sopharak, K. T. Nwe, Y. A. Moe, M. N. Dailey, and B. Uyyanonvara, "Automatic exudate detection with a naive Bayes classifier," Proceedings of the 2008 International Conference on Embedded Systems and Intelligent Technology, pp. 139-142, 2008.

[9] A. Osareh, B. Shadgar, and R. Markham, "A computational-intelligence-based approach for detection of exudates in diabetic retinopathy images," Information Technology in Biomedicine, IEEE Transactions on, vol. 13, no. 4, pp. 535-545, 2009.

[10] M. Garciaa, C. I. Sáncheza, M. I. Lópezb, D. Abásoloa, and R. Horneroa, "Neural network based detection of hard exudates in retinal images," Computer methods and programs in biomedicine, vol. 93, no. 1, pp. 9-19, 2009.

[11] S. Sreng, N. Maneerat, D. Isarakorn, R. Varakulsiripunth, B. Pasaya, J. Takada, and R. Panjaphongse, "Feature extraction from retinal fundus image for early detection of diabetic retinopathy", unpublished.

[12] J. Nayak, R. Acharya, P. S. Bhat, N. Shetty, and T. C. Lim, "Automated diagnosis of glaucoma using digital fundus images," Journal of medical systems, vol. 33, no. 5, pp 337-346, 2009.

[13] S. Kavitha, S. Karthikeyan, and K. Duraiswamy, "Neuroretinal rim Quantification in Fundus Images to Detect Glaucoma,". IJCSNS, vol. 10, no. 6, pp 134, 2010.

[14] H. F. Jaafar, A. K. Nandi, and W. Al-Nuaimy, "Detection of exudates from digital fundus images using a region-based segmentation technique," In 19th European Signal Processing Conference EUSIPCO, 2011.

[15] M. Esnaashari, S. A. Monadjemi, and G. Naderian, "A content-based retinal image retrieval method for diabetes-related eye diseases diagnosis," International Journal of Research and Reviews in Computer Science (IJRRCS), vol. 2, no. 6, 2012.

[16] K. Saranya, B. Ramasubramanian, and S. Kaja Mohideen, "A novel approach for the detection of new vessels in the retinal images for screening Diabetic Retinopathy," Communications and Signal Processing (ICCSP), 2012 International Conference, pp. 57-61, IEEE, 2012.

[17] A. Feroui, M. Messadi, I. Hadjidj, and A. Bessaid, "New segmentation methodology for exudate detection in color fundus images," Journal of Mechanics in Medicine and Biology, vol. 13, no. 01, 2013.

[18] K. Wisaeng, N. Hiransakolwong, and E. Pothiruk, "Automatic Detection of Exudates in Diabetic Retinopathy Images," Journal of Computer Science, vol. 8, no. 8, pp 1304-1313, 2012.

[19] M. Azarbad, A. Ebrahimzade, and V. Izadian, "Segmentation of Infrared Images and Objectives Detection Using Maximum Entropy Method Based on the Bee Algorithm," International Journal of Computer Information Systems and Industrial Management Applications (IJCISIM), vol.3, pp. 026-033, 2011

[20] Shannon, C.E. and W. Weaver (1949), "The Mathematical Theory of Communication (Urbana, lL." University of Illinois Press 19, no. 7, 1949.

[21] N. Jamil, and Z. A. Bakar, "Shape-Based Image Retrieval of Songket Motifs," In 19th Annual Conference of the NACCQ, pp. 213-219, 2006.

[22] http://www.mathworks.com.

[23] R. SriRanjini, and M. Devaki, "Detection of Exudates in Retinal Images Based on Computational Intelligence Approach," International Journal of Computer Science and Network Security, vol.13, no. 3, pp. 86, march 2013.

[24] A. Sopharak, B. Uyyanonvara, and S. Barman, "Automatic exudate detection from non-dilated diabetic retinopathy retinal images using fuzzy C-means clustering," Sensors 9, no. 3, pp. 2148-2161, 2009.

[25] A. Sopharak, B. Uyyanonvara, S. Barman, and T. H. Williamson, "Automatic detection of diabetic retinopathy exudates from non-dilated retinal images using mathematical morphology methods," Computerized Medical Imaging and Graphics 32, no. 8, pp. 720-727, 2008.

[26] A. Sopharak, B. Uyyanonvara, and S. Barman, S. Vongkittirux, and N. Wongkamchang, "Fine exudate detection using morphological reconstruction enhancement," International Journal of Applied Biomedical Engineering vol.1, no.1, pp. 45-50, 2010.

Feature Extraction from Retinal Fundus Image for Early Detection of Diabetic Retinopathy

Syna Sreng
International College
King Mongkut's Institute of Technology Ladkrabang
Bangkok, Thailand
srengsina@yahoo.com
s4601152@kmitl.ac.th

Noppadol Maneerat, Don Isarakorn,
Ruttikorn Varakulsiripunth, Bundit Pasaya
Faculty of Engineering
King Mongkut's Institute of Technology Ladkrabang
Bangkok, Thailand
kmnoppad@kmitl.ac.th

Jun-ichi Takada
Graduate School of Science and Engineering
Tokyo Institute of Technology
Tokyo, Japan
takada@ide.titech.ac.jp

Ronakorn Panjaphongse M.D
Ophthalology Department
Bhumibol Adulyadej Hospital
Royal Thai Air Force
Bangkok, Thailand
ronakorn_p@rtaf.mi.th

***Abstract*—Automated detection of lesions in retinal fundus image can be aid in the detection of diabetic retinopathy. Exudates are the early sign of diabetic retinopathy so the proper detection of these lesions is an essential task in an automatic retinal screening. On the research work leading to automatic analysis of exudate detection, the knowledge of Optic Disk (OD) location is very useful. An efficient algorithm is presented to detect the OD and exudate which are the most important features for early detection of diabetic retinopathy. From a retinal fundus image, the proposed method first preprocesses and estimates the histogram of retinal background, then filters out the bright pixels in intensity image. They include OD, and non-OD (exudates and noise). Next, an OD boundary is determined and eliminated after applying blob boundary measurement and morphological reconstruction. Finally, exudates are extracted by applying the maximum entropy thresholding to filter out the bright pixels from the green component of retinal image which OD region inside is eliminated. The proposed technique has been tested first on 100 images from hospital. Experimental results show that 93% and 89% of OD and exudate were detected correctly, respectively.**

Keywords— optic disc; exudate; diabetic retinopathy; blob boundary measurement; maximum entropy thresholding

I. INTRODUCTION

Diabetic retinopathy is a common cause of visual loss and blindness in diabetic patients. Ophthalmologists play a most important role to help diabetic patients for an eye examination. However, the number of ophthalmologists is limited in Thailand. The study of Thailand diabetic project [1] shows that about one thousand ophthalmologists have to work with six million diabetic patients. Among all of them one million and a half of patients are effected by diabetic retinopathy. Therefore, automatic retinal image analysis is very essential to help ophthalmologists in detection and diagnosis of diabetic retinopathy. Exudates appear as bright lesions with the random yellowish deposits of varying size, shapes and location in retinal images. OD is known as the bright circular region which appears with similar features as exudates. Fig. 1 illustrates the position of OD and exudates in retinal image.

Figure 1. OD and Exudates Region in Retinal Image

In order to prevent the result of exudate detection from the interference of optic disc, many researchers try to report different techniques to remove it out first as you can see some in [2-4]. Sopharak et al. [2] apply entropy filtering operator and Otsu's binarization algorithm to separate the complex regions from the smooth regions, and then they use compactness measurement and binary dilation to detect the OD. Next Naïve Bayes classifier was employed to select the features of exudates. Wisaeng et al. [3] combine mathematical morphology and Otsu's algorithms to eliminate OD first and then use Fuzzy C-Means (FCM) clustering and morphological methods to extract exudates. Venkatalakshmi et al. [4] detect OD by applying perfect blob measurement, and then AND operation is performed to removes all false positive such as OD to detect exudates.

This paper proposes a new algorithm to extract the important features which are known as OD and exudates for early detection of diabetic retinopathy. First, preprocessing and

This work is financial supported by AUN SEED-Net program under the Research collaboration scheme.

estimating the histogram of retinal background are applied, and then the bright pixels are filtered out in intensity image. Next, an OD boundary is determined and eliminated after applying blob boundary measurement and morphological reconstruction. Finally, exudates are extracted by using maximum entropy thresholding. The rest of paper is organized as follows: section II presents OD detection and elimination. Exudates detection is presented in section III. Section IV describes the results and discussions, and finally section V is conclusion.

II. Optic Disc Detection and Elimination

The optic disc is referred to optic nerve inside our eye. It appears as a bright circular region which is similar characteristic to the exudate. In order to prevent the result of exudate detection from the interference of OD, it should be removed out first [2-4]. In this paper, OD detection involves two steps as shown in following:

- Preprocessing and estimating histogram of retinal image.
- Blob boundary detection and morphological reconstruction

A. *Preprocessing and Estimating Histogram of Retinal Image*

Abnormality detection in retinal image is very complicated with the differences in luminosity, brightness and contrast inside retinal images. Preprocessing step is very important to solve these problems. The retinal fundus images database from hospital are stored in RGB color space which consists of three components (red green and blue). From the previous researches, it has been observed that green component of image is used in the analysis because it has higher contrast and more energy [5-8], but in this research both red and green components are used for analysis. Although green component has higher contrast, red component is brighter in intensity. Fig. 2 shows the original image with its red, green and blue components.

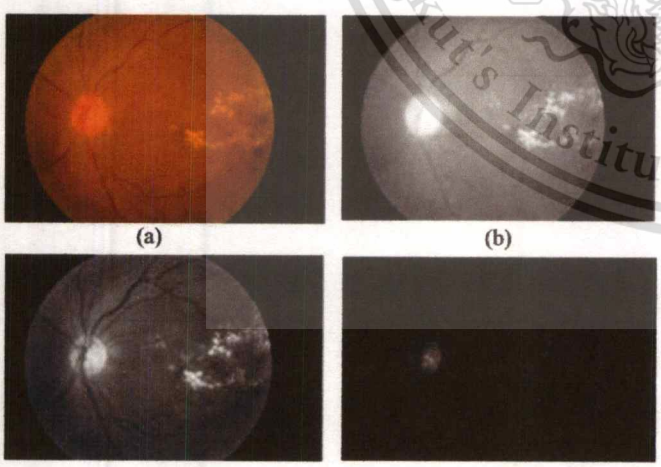

Figure 2. (a) Original Image (b) Red Component (c) Green Component (d) Blue Component

In this research, both green and red components are analyzed to estimate the suitable threshold level. For analysis using both green and red components, first the original image is converted into green and red component respectively then the Contrast-Limited Adaptive Histogram Equalization (CLAHE) is applied to the green component in order to improve the contrast of this component. Next pixel count is calculated and tested on histogram of green component, CLAHE of green component and red component respectively in order to determine the suitable threshold value. The results indicated that the best performance is 0.5% of the brightest pixels level on red component. Finally, this threshold value is applied to convert the red component into binary image. Fig. 3 shows the estimation histogram of red component.

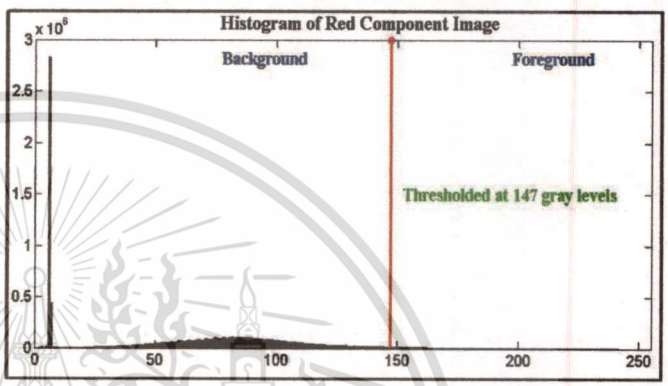

Figure 3. The Estimated Histogram of Red Component

B. *Blob Boundary Measurement and Morphological Reconstruction*

After binarization, there are more than one candidate regions identified. So, we applied the blob boundary measurement to find the most circular region by using the compactness measurement in [9]. The maximum value of compactness will be 1 if the region is a circle. This value will decrease depend on its shape. For example elliptical-shaped regions, and irregular-shaped regions, as well as the other complicated boundaries regions. The equation of compactness measurement is defined as:

$$C(\mathcal{R}) = \frac{4\pi A(\mathcal{R})}{l_p^2(\mathcal{R})} \quad (1)$$

Where $\mathcal{R}$ is the connected region with the pixels more than twenty thousands, as all connected region with the pixels less than twenty thousands are considered as noise and are eliminated. $A(\mathcal{R})$ is the number of pixels in region $\mathcal{R}$ and $l_p(\mathcal{R})$ is the length of boundary region $\mathcal{R}$. The result from blob boundary measurement cannot detect correctly when the level of threshold value is too small or too big. So, the area of the OD is estimated. From the past research in [10], the area of OD is enclosed in a square box which the pixels are inside is about 27 times smaller than the total pixels in the retinal image. Another researcher [11] show the range of OD area is from 21 to 56 times smaller than the total pixels in the retinal image. Therefore the discussion is done on our database. The suitable range of OD area is analyzed by counting the pixels on the

result of OD detection correctly. The maximum and minimum of OD area, 299860 pixels and 100780 pixels, are obtained respectively. When the area of OD detection is bigger than the maximum pixels value detection, it will be cropped and then the same process from estimating histogram of retinal background has been redone until the OD detection is in the suitable range. In case the OD detection is smaller than the minimum pixels value detection, the same process will be repeatedly redone by increasing the threshold value.

OD mask is obtained after the processing and then morphological reconstruction is applied to remove candidate OD region. The process of morphological reconstruction is based on dilation on two images, OD mask and the green component of retinal image. All the pixels in OD mask are overlaid on the green component image by the dilation of the OD mask repeatedly until the contour of the OD mask fits under the green component image. The expression is defined as:

$$\mathrm{OD_g} = R_B(\mathrm{F}) \tag{2}$$

Where B is the green component image, F is the OD mask, and $\mathrm{OD_g}$ is the reconstruction of B from F, which is the result of OD region eliminated. The process and result of OD elimination is shown in Fig 4.

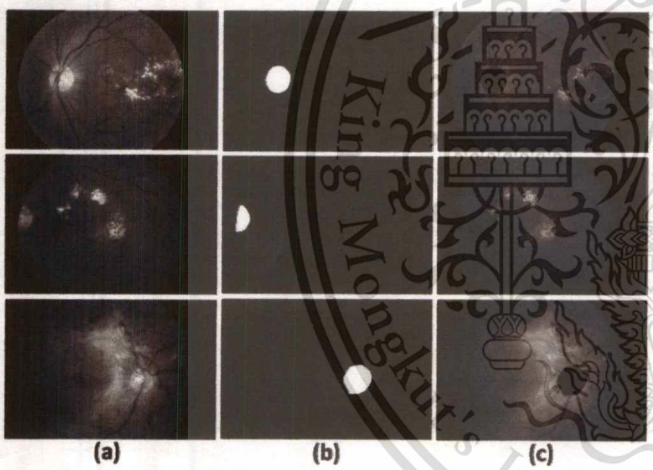

Figure 4. (a) Green Component of Retinal Images (b) Mask of ODs (c) ODs Region Eliminated from (a)

III. EXUDATES DETECTION

Exudates are the primary sign of diabetic retinopathy. They appear as bright lesions with the random yellowish deposits of varying size, shape and location in retinal images. OD in the process of exudate detection is considered as noise because of its characteristic. So, after OD is removed all bright objects can be detected as exudates. Maximum entropy thresholding describe in [12] is applied for filtering out these bright objects. In this research the entropy function is studied on 1D histogram of the gray level image. Suppose i is the gray level valve of an image so $i = [0, 1 \ldots t-1, t, t+1 \ldots 255]$, and the probability of the pixel being i can be defined as:

$$P_i = \frac{n_i}{n} \tag{3}$$

Where n is the total number of pixels in the image and n_i is the number of pixels that have gray level i.

Let o and b represent the object and background respectively thus the probabilities of o and b can be calculated as:

$$P_{\mathrm{o}} = \sum_{i=0}^{t-1} P_i \tag{4}$$

$$P_{\mathrm{b}} = \sum_{i=t}^{255} P_i \tag{5}$$

So the entropies of object and background's probability distributions are given as:

$$H_{\mathrm{o}}(t) = -\sum_{i=0}^{t-1} \frac{P_i}{P_{\mathrm{o}}} \log_2 \frac{P_i}{P_{\mathrm{o}}} \tag{6}$$

$$H_{\mathrm{b}}(t) = -\sum_{i=t}^{255} \frac{P_i}{P_{\mathrm{b}}} \log_2 \frac{P_i}{P_{\mathrm{b}}} \tag{7}$$

Thus the entropy of the gray level image segmented by threshold t is:

$$H(t) = H\mathrm{o}\,(t) + H\mathrm{b}\,(t) \tag{8}$$

The theory of maximum entropy is used to select t which makes H be maximum. So, the optimal threshold t can be selected by maximizing the entropy of $H(t)$ which can be defined as:

$$t = \mathrm{Arg\,Max}(H(t)) \tag{9}$$

Where $0 \leq t \leq 255$

Exudates are detected as the bright pixels after apply the level of threshold t. The result of exudates detection is illustrated in Fig. 5.

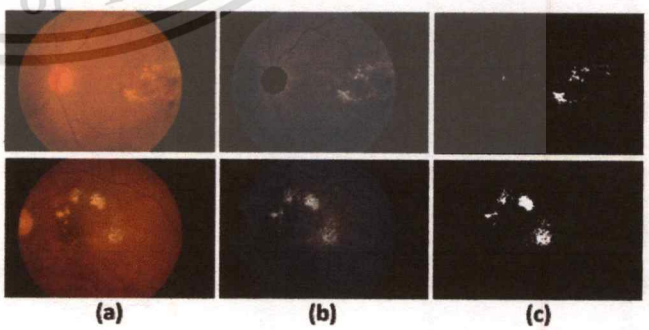

Figure 5. (a) Original Retinal Images (b) Eliminated ODs Region (c) Exudates Detection Images

IV. Results and Discussions

100 retinal fundus images from Bhumibol Adulyadej Hospital with the resolution of 3872x2592 pixels in 24 bit JPEG format are used for this research. The accuracy is the overall correctness of the system and is calculated as the sum of correct classifications divided by the total number of classifications as define in Eq. (10).

$$\text{Accuracy} = \frac{TP+TN}{TP+TN+FN+FP} \quad (10)$$

In Eq. (10), TP, TN, FN and FP show, the number of true positive, number of true negative, number of false negative and number of false positive samples respectively. Performance evaluation has been done over all the images by verification of the ophthalmologists. The results show that 93% and 89% of detections OD and exudate were successful, respectively. As the minimum success rate of 90% is required for the real application in the hospital, this proposed method is sufficient for the OD detection, but the improvement is expected for exudate detection. The reason for low success rate of detecting exudates is the variable intensity from one image to another and the presence of noise as well as artifacts in some retinal images in databases, which may be classified as low quality images. These results can be improved by choosing a better algorithm in preprocessing of OD detection to increase the number of OD detection correctly, and apply a suitable method to discriminate the result of exudates detection with the selfdom noises which appear as false positive. Given the more OD detection correctly and the better result of false positive, the more successful rate of exudates detection is obtained.

Because of many methods have been published throughout the years using a variety of datasets and evaluation methods, so it is difficult to compare our algorithm with the other reported work in the literature. This is the reason that many researchers only show their methods and results, but do not compare with the past researches [2, 3, 8, 13, 14, 15]. However our proposed method does not required any training sets which require large amounts of data and take time to be processed.

V. Conclusion

This paper proposed method to extract OD and exudates for early detection of diabetic retinopathy. First, preprocessing is applied and then the histogram of retinal background is estimated for filtering out the bright pixels in intensity image. Next, an OD boundary is determined and eliminated after applying blob boundary measurement and morphological reconstruction. Finally, exudates are extracted by applying the maximum entropy thresholding to filter out the bright pixels from the green component of retinal image which OD region inside is eliminated. Given success rate of 93 % and 89 % on OD and exudate detection, respectively, the proposed method is about to approach to the required value of 90 % for the real practical in hospital. For the future work, the reason of the failure should be more carefully examined, so that a new algorithm can be investigated to improve the present work as real application software for early detection of diabetic retinopathy screening system.

Acknowledgment

The authors would like to thank Asian University Network (AUN/SEED-Net) for financial support of one of the authors (Mr Syna Sreng) for his study at King Mongkut's Institute of Technology Ladkrabang (KMITL), THAILAND.

References

[1] T. Chetthakul, C. Deerochanawong, S. Suwanwalaikorn, N. Kosachunhanun, C. Ngarmukos, P. Rawdaree, et al., "Thailand diabetes registry project: prevalence of diabetic retinopathy and associated factors in type 2 diabetes mellitus," J Med Assoc Thai 89, n. Suppl 1, S27-36, 2006.

[2] A. Sopharak, K. T. Nwe, Y. A. Moe, M. N. Dailey, and B. Uyyanonvara, "Automatic exudate detection with a naive Bayes classifier," Proceedings of the 2008 International Conference on Embedded Systems and Intelligent Technology, pp. 139-142, 2008.

[3] K. Wisaeng, N. Hiransakolwong, and E. Pothiruk, "Automatic Detection of Exudates in Diabetic Retinopathy Images," Journal of Computer Science, vol. 8, no. 8, pp 1304-1313, 2012.

[4] B. Venkatalakshmi, V. Saravanan, and G. Niveditha, "Graphical user interface for enhanced retinal image analysis for diagnosing diabetic retinopathy," Communication Software and Networks (ICCSN), 2011 IEEE 3rd International Conference on, pp. 610-613, IEEE, 2011.

[5] H. F. Jaafar, A. K. Nandi, and W. Al-Nuaimy, "Detection of exudates from digital fundus images using a region-based segmentation technique," In 19th European Signal Processing Conference EUSIPCO, 2011.

[6] M. Esnaashari, S. A. Monadjemi, and G. Naderian, "A content-based retinal image retrieval method for diabetes-related eye diseases diagnosis," International Journal of Research and Reviews in Computer Science (IJRRCS), vol. 2, n. 6, 2012.

[7] K. Saranya, B. Ramasubramanian, and S. Kaja Mohideen, "A novel approach for the detection of new vessels in the retinal images for screening Diabetic Retinopathy," Communications and Signal Processing (ICCSP), 2012 International Conference, pp. 57-61, IEEE, 2012.

[8] A. Feroui, M. Messadi, I. Hadjidj, and A. Bessaid, "New segmentation methodology for exudate detection in color fundus images," Journal of Mechanics in Medicine and Biology, vol. 13, n. 01, 2013.

[9] N. Jamil, and Z. A. Bakar, "Shape-Based Image Retrieval of Songket Motifs," In 19th Annual Conference of the NACCQ, pp. 213-219, 2006.

[10] V. V. Kumari, and N. SuriyaNarayanan, "Detection of Optic Disk in Retinal Images-A Comparison," International Journal on Computer Science and Engineering, vol. 1, no. 3, pp. 192-195, 2009.

[11] V. Thongnuch, and B. Uyyanonvara, "Automatic optic disk detection from low contrast retinal images of ROP infant using GVF snake," Suranaree J. Sci. Technol, vol. 14, no. 3, pp. 223-226, 2007.

[12] M. Azarbad, A. Ebrahimzade, and V. Izadian, "Segmentation of Infrared Images and Objectives Detection Using Maximum Entropy Method Based on the Bee Algorithm," International Journal of Computer Information Systems and Industrial Management Applications (IJCISIM), vol.3, 026-033, 2011.

[13] R. SriRanjini, and M. Devaki, "Detection of Exudates in Retinal Images Based on Computational Intelligence Approach," International Journal of Computer Science and Network Security, vol.13, no.3, pp. 86, march 2013.

[14] L. Giancardo, F. Meriaudeau, T. P. Karnowski, Y. Li, K. W. Tobin, and E. Chaum, "Automatic retina exudates segmentation without a manually labelled training set," In Biomedical Imaging: From Nano to Macro, 2011 IEEE International Symposium, pp. 1396-1400, IEEE, 2011.

[15] C. I. Sánchez, M. García, A. Mayo, M. I. López, and R. Hornero, "Retinal image analysis based on mixture models to detect hard exudates" Medical Image Analysis, vol. 13, no. 4, pp. 650-658, 2009.

AUN/SEED-Net

5th AUN/SEED-Net Regional Conference on Information and Communications Technology

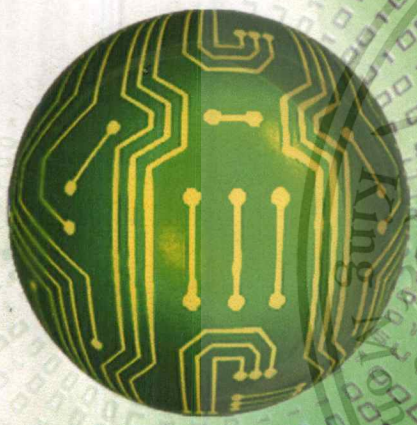

"Leveraging ICT Research to Meet the Challenges of Establishing Secure, Equitable and Sustainable Communities for the 21st Century"

October 18-19, 2012 - Traders Hotel, Manila, Philippines

AUN/SEED-Net

5th AUN/SEED-Net Regional Conference on Information and Communications Technology

"Leveraging ICT Research to Meet the Challenges of Establishing Secure, Equitable and Sustainable Communities for the 21st Century"

Traders Hotel
Manila, Philippines
October 18-19, 2012

Hosted by

De La Salle University
Gokongwei College of Engineering
Electronics and Communications Engineering Department

Automatic Colony Counter based on Image Processing

Sreng Syna[1] Santikon Amnuayphol[2] Purachai Chongsomchai[2] Nattapong Chawalitsakulchai[2]
Noppadol Maneerat[2] Ruttikorn Varakulsiripunth[3] Suwannee Junyapoon[4]

[1]International College, King Mongkut's Institute of Technology Ladkrabang (KMITL), Bangkok, Thailand 10520
Email: srengsina@yahoo.com
[2]Department of Instrumentation and Control Engineering, Faculty of Engineering, King Mongkut's Institute of Technology Ladkrabang (KMITL), Bangkok, Thailand 10520 Email: kmnoppad@kmitl.ac.th
[3]Department of Electronics Engineering, Faculty of Engineering, King Mongkut's Institute of Technology Ladkrabang (KMITL), Bangkok, Thailand 10520
[4]Department of Chemistry, Faculty of Science, King Mongkut's Institute of Technology Ladkrabang (KMITL), Bangkok, Thailand 10520

***Abstract*— Nowadays, the conventional colony counting method has to use an expert for manual counting which is difficult to get the results in a short time and accurately when there are many experimental samples. Although the automatic quantity colonies detector has been developed, it is still expensive and necessary to install and use in microbiological laboratory because of size and mass. It is not portable. This paper presents a developed colony counter that consists of a small incubator, temperature controller using PID (Proportional Integral Derivative), a webcam installed in incubator and automatic quantity colonies detection software using image processing technology. The developed colony counter based on image processing can count the number of colonies from bacteria are red stained in the agar plate. The experimental colonies counting results are similar to the expert's counting. The developed colony counter is small, portable and cheap.**

Keywords- colony counting method; image processing; PID; manual counting; incubator

I. INTRODUCTION

At present cleanness is important in many industries such as food, medicine, cosmetics and so on. The food quality control is a part of the cleanliness because it affects health directly. Food quality is also an indicator of each industry. Therefore the colonies counting in the food takes part in the food quality measurement.

The manual counting method known as ordinary nutrient agar pour method is commonly used to count inoculation colony number [1]. This method is complex, time-consuming, and low efficiency. Therefore, there are many researchers studied on the use of computer image processing technology to develop a set of detection system and find an approach of colony identification and rapid counting [2-8].

In this research, the automatically colony counting equipment is developed by the software uses two main algorithms: Edge Detection [9] and Blob Detection algorithm [10] with Visual Basic 6.0 to count the number of colony including small incubator and webcam connected with developed image processing software. This method can be applied in field work without taking sampling plates back to the microbiological laboratory.

This paper is structured as follows: section 2 presents the related works. The system structure is presented in section 3. Section 4 describes the experimental results, while section 5 presents conclusion.

II. RELATED WORKS

A. Manual Counting Method

Colonies counting method is a basic method to quantify the amount of microorganisms. The conventional method is counting the number of bacteria on agar plates [11, 12] as following steps.

1. Sampling food onto the agar plate.
2. After an appropriate incubation period, examine the plates for colonial growth.
3. Colonies will form on the top and the bottom of agar plate.
4. Colonies counting by the experts that using a light box and marker pen for mark and count the colonies which have 30-300 colonies. This will become easier with practice.
5. Using a light box or colony counter (if one is available) and marker pen (put a dot above each colony as you count it), count the number of colonies which is having 30 - 300 colonies. This will become easier with practice.
6. Write the number of colonies on a note.

B. Temperature Control

PID controller is a part in the development of Automatic colony counter based on image processing to control the temperature at 37°c while incubating agar plate because bacteria grow well at this temperature. Ryckaert and his assistants proposed the temperature control of an oven cavity is found to be successful. The application also illustrates the use of advanced measurement and control hardware [13]. Block diagram of the PID controller is shown as Fig. 1.

This work is financial supported by AUN SEED-Net program under the Research collaboration scheme.

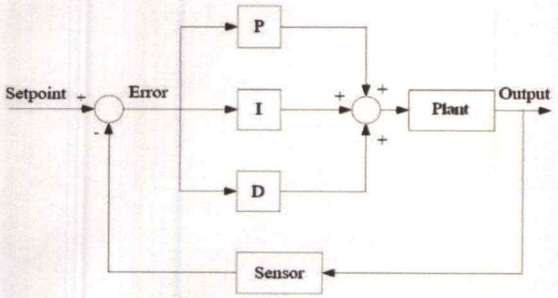

Figure 1. Block Diagram of the PID Controller

The PID controller consists of 3 actions:

1. Proportional Control Action (P-Action)

The output of P-Action is proportional to the error or a change in measurement.

2. Integral Control Action (I-Action)

I-Action eliminates offset to the Set Point which its output depends on initial integral time. If integral time setting is low value, the response will reach to the Set Point rapidly along with high overshoot conversely. If setting of integral time is high value, its overshoot is less according with longer setting time.

3. Derivative Control Action (D-Action)

The derivative term slows the rate of change of the controller output. It is used to reduce the magnitude of overshoot produced by the integral component and improves the combined controller-process stability.

C. *Image Processing*

1. Pixel Analysis

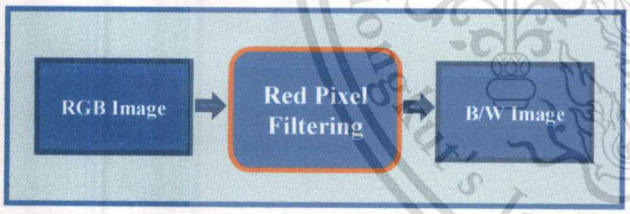

Figure 2. Pixel Analysis Diagram

Pixel Analysis is used for filter the red pixel of every pixel from RGB image. If it is red pixel in RGB image, it will be white pixel in Black and White image. If it is not red pixel in RGB image, it will be black pixel in Black and White image. Finally we will get the Black and White image for the next analysis process.

Figure 3. Colony image

In the Fig. 3, the format of captured image by webcam is the real color bitmap. In order to describe the characteristics of each pixel we use three values: R, G, B and then filter red pixel for detecting the colonies. The working steps are shown in Fig. 4.

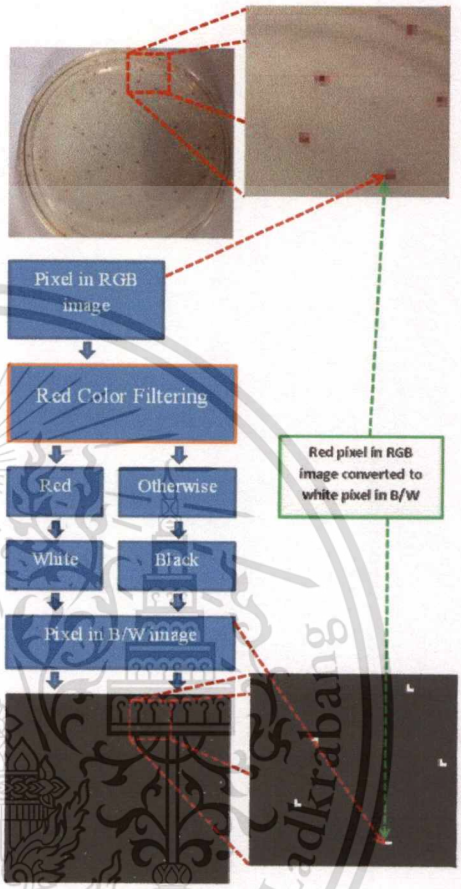

Figure 4. Steps Working of Pixel Analysis

2. Blob Detection Algorithm

In many typical image processing applications, blob analysis is widely used. The blob features usually calculates area and perimeter, blob shape, and location. This algorithm has been successful used in other automatic detectors.

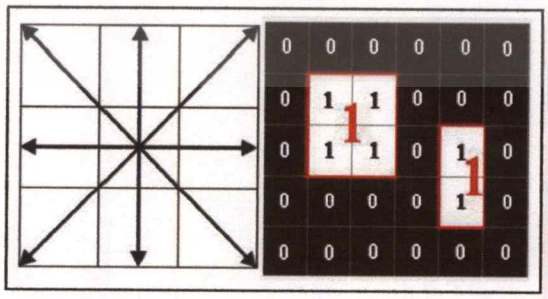

Figure 5. Blob Detection Method

In the Fig. 5, we define touching pixels as adjacent pixels along the vertical or horizontal axis as touching and include diagonally adjacent pixels to detect the same pixels

color and analyze the number of colonies. The procedure is concluded in Table. I.

TABLE I. BLOB DETECTION ALGORITHM

The input is a binary image (B/W colour).
The output is a blob image and the number of blob.
The blob labels (the integer values in the blob array) are given in the blob list as the index value. The index value for the first blob (not necessarily the largest, just the first one encountered in scan order) is 2. All reject blobs have a label of 1.
Blob Detection is done on a binary image, where pixels are either 'object' (1), or 'background', (0). Theoretically, intensity thresholds may be used with a gray scale image (or some other more complex scheme with a color image or with a group of registered images) to identify pixels as either object or background. For purposes of this Algorithm, we will talk in terms of a binary image as the 'original' image for input into the blob detection algorithm.

III. SYSTEM STRUCTURE OF AUTOMATIC COLONY COUNTER

Fig. 6 explains the principle of work and overview of the system. The system is divided into two main sections of the incubator and the computer.

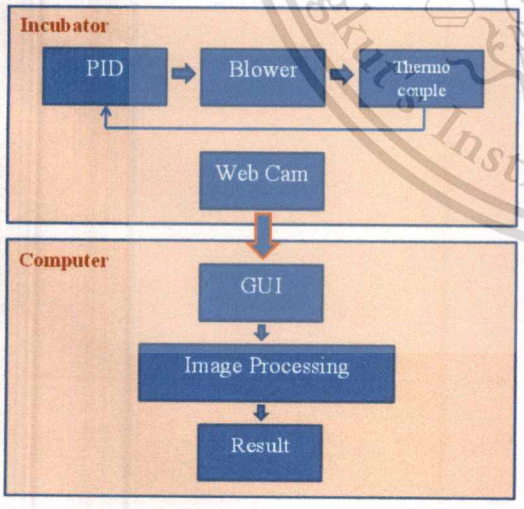

Figure 6. Overview of the automatic colony counter

Fig. 6 shows the incubator section, due the PID controller is used to control the temperature for its stability. Data feedback is input to PID controller by RTD thermocouple (Resistor Temperature Detector).

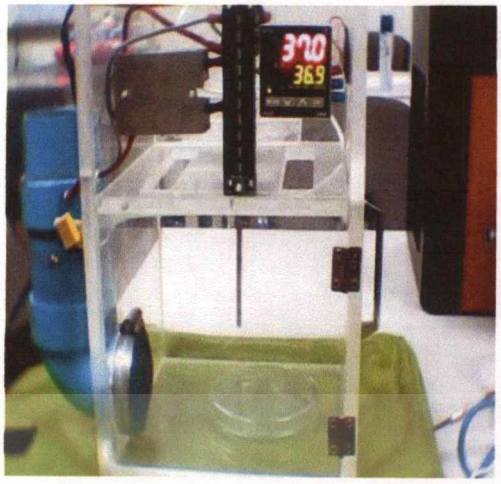

Figure 7. The Automatic Colony Counter

The process of automatic incubated colony counter has procedures as follow:

1. Prepare the agar plate.
2. Sampling food onto the agar plate.
3. Close plate and put it in the developed incubator for incubation at 37°c until it is ready.
4. Run the developed software and click start. The webcam will capture an image.
5. First step the software analyzes the captured image which is RGB color with Pixel Analysis.
6. The software counts number of colonies by using Blob Analysis.
7. The last step the software will show the result.

Figure 8. The Graphics User Interface of Developed Software

When the process is proceeding, the bacteria is on the agar plate is incubated. So counting colony with the automatic colony counter is easier than the manual counting because the manual counting has to take the plate outside the incubator to count colonies but the automatic colony counter is needless to take the plate out.

IV. RESULTS

We developed software for the automatic colony counting of bacteria. The experiment is done with the red stained colonies plates which are already incubated. We compared the counting efficiency between the developed automatic colony counter and the manual counting by the experts and calculated the error. The experimental results are shown in Table II.

TABLE II. EFFICIENCY OF THE AUTOMATIC COLONY COUNTER COMPARE WITH THE EXPERTS

Sample	Manual colony counting by the experts (colony)	Automatic colony counting (colony)	Error (%)
Sample 1st	65	68	4.6%
Sample 2nd	95	98	3.1%
Sample 3rd	124	129	4.0%
Sample 4th	173	185	6.9%
Sample 5th	214	228	6.5%
Result of average error			5.0%

From the experiment indicated the counting results of automatic colony counter are similar to the manual counting by the experts. There is a shadow and reflection in the automatic colony counter which may cause of error. Benefit comparison between colony counting by the experts and the automatic colony counter is shown in Table III.

TABLE III. BENEFIT COMPARISON BETWEEN THE EXPERT AND AUTOMATIC COLONY COUNTER

Variable	Manual colony counting by the expert	Automatic colony counter
Portable	Difficulty	Easily
Price	High	Low
Convenience	Difficulty	Easily
Materials Quality	Good	Fair
Bacteria Searching	Experts	Calculation Software
Efficiency	Very Good	Good
Durable	Good	Very Good

V. CONCLUSIONS

From the efficiency results and the benefit comparisons, the automatic colony counter can be used for the colony counting which does not need high accuracy. However the automatic colony counter has more durable counting than human counting. The average error of the automatic colony counting is 5.0% can be improved in the future research.

ACKNOWLEDGMENT

We would like to thank Asian University Network (AUN/SEED-Net) for financial support of one of the authors (Mr Sreng Syna) for his study at King Mongkut's Institute of Technology Ladkrabang (KMITL), THAILAND.

REFERENCES

[1] National Standard of the People's Republic of China [S]. Food hygiene inspection methods (Microbiology section). Beijing: China Standard Press, 1985. 194-196.
[2] SHEN Wei-zheng, WU Ya-chun, ZHAO lie, ZHENG Hui, "Experimental Study for Automatic Colony Counting System Based on Im age Processing" 2010 International Conference on Computer Application and System Modeling (ICCASM 2010).
[3] Mukherjee DP, Pal A, Sarma SE, et al. Bacterial colony counting using distance transform[J]. Int J Biomed Comput. 1995, 38(2): 131.
[4] Garcia-Armesto MR, Prieto M. Modern microbiological methods for foods:colony count and dirtect count methods[J]. A review Microbiologia, 1993,9(1): 1.
[5] Pickett DA, Welch OF. Evaluation of the automated Bactalert system for pediatric blood culturing[J]. Am J Clin Pathol, 1995,103(3) 320.
[6] Spadinger I, Palcic B. Cell survival measurements at low doses using an automated image cytometry device[J]. Int J Radiat, 1993, 63(2): 183.
[7] Ates, H.; Gerek, O.N. "An Image-Processing Based Automated Bacteria Colony Counter" Computer and Information Sciences, 2009. ISCIS 2009. 24th International Symposium on Digital Object Identifier: 10.1109/ISCIS.2009.5291926 Publication Year: 2009 , Page(s): 18 – 23
[8] Hong Men, Yujie Wu, Xiaoying Li, Zhen Kou, Shanrang Yang, "Counting Method of Heterotrophic Bacteria Based on Image Processing" IEEE Publication Year: 2008 , Page(s): 1238 – 1241.
[9] Xin Chen, Houjin "The Edge Detection Algorithm in RGB space" IEEE conference
[10] Jiamin Liu, Jacob M. White, Ronald M. Summers"AUTOMATED DETECTION OF BLOB STRUCTURES BY HESSIAN ANALYSIS AND OBJECT SCALE" Proceedings of 2010 IEEE 17th International Conference on Image Processing, September 26-29, 2010, Hong Kong
[11] ScottSutton,Ph.D, "Colonies counting " http://www.linkedin.com/
[12] SOP," Counting Bacterial Colonies - Pour Plate Method", http://toolboxes.flexiblelearning.net.au/demosites/series4/412/laboratory/methodsman/mmsopCountBacterialColonies.htm
[13] V.G. Ryckaert, J.E. Claes, J.F. Van Impe "Model-based temperature control in ovens"Journal of Food Engineering, Volume 39, Issue 1, January 1999, Pages 47-58
[14] Chuleewan Thunyasirinon, Pipat Sribenjalux, Paradee Chuaybamroong "Comparison of Six-Satage and Single-Stage Viable Anderson Impactor (N6) for Airborne Microbe sampling" KKU Res J 13 (1) : Jan. - Feb. 2008
[15] www.alsglobal.com/upload/environment/downloads/Asia/Technical Updates/ALS%20Thailand%20%20Enviromail%20010%20-%20Indoor%20Air%20Quality.pdf